

**WIND-INDUCED PRESSURES ON CANOPIES ATTACHED TO
THE WALLS OF LOW-RISE BUILDINGS**

José Daniel Candelario Suárez

A Thesis

In

The Department

Of

Building, Civil and Environmental Engineering

Presented in Partial Fulfillment of the Requirements
For the Degree of Master of Applied Science (Building Engineering) at
Concordia University
Montreal, Quebec, Canada

November 2012

© José Daniel Candelario Suárez, 2012

CONCORDIA UNIVERSITY
School of Graduate Studies

This is to certify that the thesis prepared

By: José Daniel Candelario Suárez

Entitled: Wind-induced pressures on canopies attached to the walls of low-rise buildings

and submitted in partial fulfillment of the requirements for the degree of

Master of Applied Science (Building Engineering)

complies with the regulations of the University and meets the accepted standards with respect to originality and quality.

Signed by the final examining committee:

_____ Chair
Dr. O. Pekau

_____ Examiner
Dr. S. Rakheja External (to program)

_____ Examiner
Dr. K. Galal

_____ Supervisor
Dr. T. Stathopoulos

Approved by _____
Dr. Maria Elektorowicz, GPD
Department of Building, Civil and Environmental Engineering

_____ Dr. R. Drew, Dean
Faculty of Engineering and Computer Science

Date _____

ABSTRACT

WIND-INDUCED PRESSURES ON CANOPIES ATTACHED TO THE WALLS OF LOW-RISE BUILDINGS

JOSE DANIEL CANDELARIO SUAREZ

Current knowledge regarding wind-induced pressures on attached canopies is restricted to a limited number of studies. As a result, most wind standards and codes of practice do not provide guidelines for the design of such components.

This thesis consists of a parametric study that expands current knowledge by providing a better understanding on the behavior of pressure coefficients acting on canopies attached to low rise buildings. All experimental results presented on this study have been carried out in the Building Aerodynamics Laboratory of Concordia University.

Two canopy models have been fabricated for the purpose of this study in the form of rectangular thin plates with pressure taps equally distributed along both upper and lower faces. These canopy models were attached at different locations on an acrylic glass building model with a gable roof of 4:12 slope. A total of 63 geometrically unique configurations were selected for this parametric study. The experiments were performed in the boundary layer wind tunnel for a simulated open terrain exposure. The 63 configurations, as well as the location of pressure taps on both faces of the canopy allow a detailed investigation of the different wind loading patterns exhibited as a function of the changes in the building geometry. A total number of 28 different wind directions have

been tested for every configuration. Local and area-averaged peak values of the induced pressures have been analyzed as a function of the different geometrical relationships, which are unique to each configuration.

The experimental results indicate that a slight difference in the geometry of the attached canopy and the parent building can result in an 80% difference of the peak net pressure coefficient. It has also been noted that the most critical uplift forces occur in canopies located above the intermediate regions of the parent wall. In contrast, downward forces exhibit less sensitivity to changes in geometry.

Following the analysis and observations of the experimental data, recommended design guidelines have been provided for implementation in wind standards and building codes of practice. Comparisons with previous experimental results and provisions of other international standards and codes of practice are provided.

ACKNOWLEDGMENTS

I would like to express my sincere gratitude to Dr. Theodore Stathopoulos for his guidance and supervision during the course of this study and for his undying willingness to pass his knowledge on to others. Special thanks are due to my friend and colleague Dr. Ioannis Zisis for his involvement in the study and for the revision of this thesis. I would also like to express my gratitude to my friends and colleagues at Concordia University for their company and support both inside and outside the office.

I wish to dedicate this work to my grandfather Gumersindo Suárez González and to my mother María Teresa Suárez Toro.

TABLE OF CONTENTS

LIST OF FIGURES	x
LIST OF TABLES	xvii
CHAPTER 1 INTRODUCTION	1
1.1 OVERVIEW	1
1.2 SCOPE AND OBJECTIVES	3
1.3 THESIS ORGANIZATION	4
CHAPTER 2 LITERATURE REVIEW	6
2.1 DESCRIPTION OF EXISTING WORK	6
2.2 JUSTIFICATION OF THE PRESENT STUDY	12
CHAPTER 3 EXPERIMENTAL METHODOLOGY	16
3.1 GENERAL	16
3.2 CONCEPT OF A BOUNDARY LAYER WIND TUNNEL	16
3.3 CHARACTERISTICS OF THE BLWT CONCORDIA UNIVERSITY BUILDING AERODYNAMICS LABORATORY	18
3.3.1 Physical characteristics.....	18
3.3.2 Instrumentation.....	21
3.3.3 Characteristics of the simulated flow	22
3.4 PRESSURE COEFFICIENTS	31

3.4.1 Definition of pressure coefficients	31
3.4.2 Pressure coefficients applied to this study	33
3.4.3 Pressure coefficients and velocity averaging periods	35
3.5 BUILDING MODELS AND CONFIGURATIONS TESTED	37
3.5.1 Selection of scale	37
3.5.2 Description of attached canopy and parent building model	38
3.5.3 Definition of Parameters and Configurations Tested	42
CHAPTER 4 PRESSURE COEFFICIENTS ON UPPER AND LOWER SURFACES SEPARATELY	45
4.1 GENERAL	45
4.2 EFFECT OF WIND DIRECTION ON SURFACE PRESSURES	47
4.3 PRESSURES ON UPPER AND LOWER SURFACE PRESSURES	49
Effect of h_c/h , h_c/w_c and e_d/l_c on the upper surface of the canopy	49
Effect of h_c/h , h_c/w_c and e_d/l_c on the lower surface of the canopy	52
4.4 LOCAL PRESSURE COEFFICIENTS ON REGIONS OF UPPER AND LOWER SURFACES	55
4.5 ENVELOPES OF PRESSURE COEFFICIENTS ON UPPER AND LOWER SURFACES	58
CHAPTER 5 NET PRESSURE COEFFICIENTS ON ATTACHED CANOPIES	63
5.1 GENERAL	63

5.2 EFFECT OF WIND DIRECTION ON CRITICAL NET PRESSURE COEFFICIENTS	64
5.3 VISUALIZATION OF FLOW AROUND THE CANOPY	67
5.4 NET PRESSURES AND CORRELATION COEFFICIENTS	69
5.5 EFFECT OF PARAMETERS ON NET PRESSURE COEFFICIENTS.....	77
5.5.1 Effect of $\frac{hc}{h}$	77
5.5.2 Effect of $\frac{hc}{wc}$	79
5.5.3 Effect of canopy length (lc) and location (ed).....	81
5.6 NET LOCAL PRESSURE COEFFICIENTS DIVIDED BY REGIONS.....	83
5.7 COMPARISONS WITH EXPERIMENTAL RESULTS OF PREVIOUS STUDIES	85
5.8 ENVELOPES OF NET PRESSURES	89
CHAPTER 6 TOWARDS CODIFICATION	93
6.1 GENERAL	93
6.2 RECOMMENDED DESIGN GUIDELINES FOR ATTACHED CANOPIES	94
6.2.1 Design guidelines for suctions on upper and lower surfaces	94
6.2.2 Design Guidelines for Net loads.....	96
6.3 COMPARISONS WITH CURRENT DESIGN PROVISIONS	99
6.3.1 AZ/NZS 1170.2:2002.....	99
6.3.2 DIN EN 1991-1-4/NA:2010-12.....	101

6.3.3 ASCE 7-10 overhangs and partially enclosed structure	102
CHAPTER 7 CONCLUSIONS AND RECOMMENDATIONS FOR FUTURE	
STUDIES	105
7.1 SUMMARY	105
7.2 CONCLUSIONS.....	106
7.3 LIMITATIONS AND RECOMMENDATIONS FOR FUTURE STUDIES	107
REFERENCES	109
BIBLIOGRAPHY.....	115
APPENDIX A.....	116
APPENDIX B.....	120
APPENDIX C	148

LIST OF FIGURES

Figure 1.1	Canopy attached to a low-rise residential building.....	2
Figure 1.2	Canopy destroyed by hurricane winds	2
Figure 2.1	Canopy model mounted on the force balance system, after Jancauskas and Holmes (1985)	7
Figure 2.2	Internal manifolding and pressure tap location of attached canopy surface used for pressure measurements, after Jancauskas and Holmes (1985)	8
Figure 2.3	Segment obtained from the provisions of the AS/NZS 1170.2:2002	9
Figure 2.4	Segment obtained from the provisions of the DIN EN 1991-1-4 2010-12	11
Figure 2.5	Illustration relating the attached canopy to the roof of a <i>Partially Enclosed Building</i>	13
Figure 2.6	Expected differences in flow patterns between a roof overhang and a canopy attached at a high and at an intermediate portion of the parent wall.....	13
Figure 2.7	Comparison of recommended local net pressure coefficients according to the five currently available design provisions	14
Figure 3.1	Construction plans of the Boundary Layer Wind Tunnel at Concordia University’s Building Aerodynamics Laboratory, after Stathopoulos (1984).....	19

Figure 3.2	Open terrain exposure at the BLWT in the Building Aerodynamics Laboratory at Concordia University	20
Figure 3.3	Schematic of the experimental setup at the boundary layer wind tunnel ..	22
Figure 3.4	Boundary layer flow and notation used for elevations and velocities	23
Figure 3.5	Wind velocity and turbulence intensity profiles for open-terrain exposure	24
Figure 3.6	Variation of C and m with roughness length, after Counihan (1975).....	27
Figure 3.7	Spectra of longitudinal turbulence component at $\frac{z}{z_G} = \frac{1}{6}$, after Stathopoulos (1984).....	30
Figure 3.8	Illustration of the generation of net pressure coefficients, $C_{p,net}$	34
Figure 3.9	Gust duration curve, after Durst (1960).....	36
Figure 3.10	Building configuration tested.....	39
Figure 3.11	Building model with different canopies in place	40
Figure 3.12	Top view of building and canopy model showing pressure tap locations	40
Figure 3.13	Ranges of the modifiable dimensions of the canopy and parent building model.....	42
Figure 4.1	Canopies with sheathing attached to the lower surface of the beam and joist system.....	46

Figure 4.2	Attached canopy (not to scale) with sheathing at both upper and lower surfaces highlighting components affected by upper and lower surface pressure coefficients.....	46
Figure 4.3	Wind directions tested for each of the 63 configurations, after Zisis (2010).....	47
Figure 4.4	Effect of wind direction on peak minimum, and peak maximum C_p on the upper surface of a canopy extending over the full length of the parent wall.....	48
Figure 4.5	Effect of wind direction on peak minimum, and peak maximum C_p on the lower surface of a canopy extending over the full length of the parent wall.....	48
Figure 4.6	Effect of hc/h on Peak Local, and Area-Averaged $C_{p,upper}$	50
Figure 4.7	Effect of hc/wc on peak local, and area-averaged $C_{p,upper}$	51
Figure 4.8	Effect of length and edge distances on local and area-averaged $C_{p,upper}$	52
Figure 4.9	Effect of hc/h on peak local, and area-averaged $C_{p,lower}$	54
Figure 4.10	Effect of hc/h on peak local, and area-averaged $C_{p,lower}$	54
Figure 4.11	Effect of length and edge distances on local and area-averaged $C_{p,lower}$	55

Figure 4.12	Division of regions on the attached canopy (adapted from ASCE 7-10 for flat low-pitch roofs)	57
Figure 4.13	Peak local Cp_{upper} at different regions of the canopy as a function of hc/h	57
Figure 4.14	Peak local Cp_{lower} at different regions of the canopy as a function of hc/h	58
Figure 4.15	Area-averaging effect and corresponding envelopes for the upper surface of the canopy on all configurations tested	60
Figure 4.16	Area-averaging effect and corresponding envelopes for the lower surface of the canopy on all configurations tested	61
Figure 4.17	Envelopes for pressure coefficients as a function of effective areas at upper and lower surfaces of all 63 configurations combined	62
Figure 5.1	Drawing of a conventional canopy attached to a low rise building (not to scale) indicating the components affected by net loads	64
Figure 5.2	Effect of wind direction on peak minimum, peak maximum and mean Cp_{net} for a canopy extending over the full length of the parent wall	66
Figure 5.3	Effect of wind direction on peak minimum, peak maximum and mean Cp_{net} for an eccentrically placed canopy extending over half of the length of the parent wall	66
Figure 5.4	Wind directions at the occurrence of minimum and maximum peak Cp, net	67

Figure 5.5	Flow visualization for a canopy attached at the mid height of the parent wall and a zero degree azimuth.....	68
Figure 5.6	Flow visualization for a canopy attached close to the eave height of the parent wall and a zero degree azimuth.....	69
Figure 5.7	Pressure and correlation coefficient contour plots for a canopy attached at the mid height of the parent wall and a zero degree azimuth	71
Figure 5.8	Pressure and correlation coefficient contour plots for a canopy attached close to the eave height of the parent wall and a zero degree azimuth.....	72
Figure 5.9	Pressure and correlation coefficient contour plots for a canopy attached at the mid height of the parent wall and the critical wind direction	75
Figure 5.10	Pressure and correlation coefficient contour plots for a canopy attached close to the eave height of the parent wall and the critical wind direction	76
Figure 5.11	Effect of hc/h on local, and area-averaged $Cp_{,net}$ for $wc = 3.65m$	78
Figure 5.12	Effect of $\frac{hc}{wc}$ on local and area-averaged $Cp_{,net}$ for $\frac{hc}{h} = 0.94$	80
Figure 5.13	Effect of $\frac{hc}{wc}$ ratio on local and area-averaged $Cp_{,net}$ for $\frac{hc}{h} = 0.34$	81
Figure 5.14	Effect of length and edge distances on local and area-averaged $Cp_{,nets}$...	82
Figure 5.15	Two and three dimensional contour plots displaying the distribution of the net pressure coefficients on attached canopy.....	83

Figure 5.16	Peak local Cps as a function of $\frac{hc}{h}$ at the different regions of the canopy.....	84
Figure 5.17	Comparison between results of the present study and Jancauskas and Holmes, 1985	87
Figure 5.18	Comparison between results of the present study and Hölscher et al. 2007.....	88
Figure 5.19	Area averaging effect and envelopes for the corresponding ranges of Cases I, II and III separately.....	91
Figure 5.20	Area-alleviation effect and corresponding envelopes for all 63 configurations combined.....	92
Figure 6.1	Proposed design values for $\min C_{p,upper}$ and $C_{p,lower}$ on attached canopies.....	94
Figure 6.2	Proposed design values for $GC_{p, net}$ on attached canopies.....	97
Figure 6.3	Comparisons between the recommended envelopes of the present study and AS/NZS provisions	100
Figure 6.4	Comparison between the recommended local net pressure coefficients of the present study and the DIN provisions for three different hc/h ratios.....	101
Figure 6.5	Comparisons between the recommended design values for a full length canopy and ASCE 7-10 for overhangs.....	103

Figure 6.6 Comparisons between the recommended design values for three different
hc/h ratios and ASCE 7-10 provisions for the roof of a partially enclosed
building104

LIST OF TABLES

Table 3.1	Configurations tested and definition of nomenclature used.....	44
Table 6.1	Geometrical reduction factors for min $GCp_{,upper}$ and $GCp_{,lower}$	95
Table 6.2	Geometrical reduction factor for the local $GCp_{,net}$	98

CHAPTER 1

INTRODUCTION

1.1 OVERVIEW

An attached canopy is a roof adjacent to a building not enclosed by walls and used for recreational purposes rather than as a storage space or carport (see Fig. 1.1). This kind of addition is of common use in low-rise housing because it provides an adequate space for many social and leisure activities with partial protection from the elements. Because their main function is to provide shelter from the rain and direct sunlight, attached canopies are generally lightweight and as a result wind loading is often the governing design consideration.

Under-designing an attached canopy can lead to its partial or complete destruction (see Fig. 1.2). In an extreme scenario the shattered canopy can generate projectiles that may cause further damage to neighboring buildings. With this in mind, members of industry and practitioners have been compelled to design attached canopies using highly conservative loads because of the lack of specific design provisions.

Currently there is only limited knowledge as of what the proper design loads should be for these types of structures. Neither the National Building Code of Canada 2010 (NBCC), nor the American Society of Civil Engineers Standard (ASCE 7-10) has established any provisions for the proper design of attached canopies. In North America,



Figure 1.1 Canopy attached to a low-rise residential building



Figure 1.2 Canopy destroyed by hurricane winds

only the International Building Code (IBC 2012) and the International Residential Code (IRC 2012) contain some provisions to address this issue. However, these provisions do not seem to result from a detailed study.

Several codes and standards from other parts of the world do provide wind loading design guidelines for attached canopies (sometimes referred to as awnings), however these have been found to present some limitations and inconsistencies within each other.

By expanding the knowledge regarding wind loading patterns on attached canopies, the selection of materials and the economical aspects related to its design and construction can be assessed more efficiently whilst ensuring the integrity of the canopy's structure and components and cladding elements.

1.2 SCOPE AND OBJECTIVES

This thesis consists of a parametric study which aims to expand current knowledge on the wind loading design of canopies attached to low-rise buildings. This is done by examining the sensitivity of the wind loads acting on the attached canopy to changes in the relative dimensions of the canopy and the parent building, i.e. the building to which the canopy is attached.

Pressures have been obtained from wind tunnel simulation at both upper and lower surfaces of the canopy for an array of geometrical configurations and wind directions. Separate upper and lower pressures are to be used in the design of components

and cladding elements, while simultaneous (net) pressures are to be used in the design of the principal structure of the attached canopy.

The principal objective of this study is to generate wind loading design guidelines for attached canopies. These guidelines could be considered for implementation on future wind standards and building codes of practice. Comparisons between the findings of the present study and the available international studies and design guidelines are presented to assess the possible discrepancies and limitations of each.

1.3 THESIS ORGANIZATION

Chapter 2 consists of the literature review. A discussion of the pertinent studies currently available is provided as well as a justification for the present study.

Chapter 3 presents the experimental methodology performed for the fulfilment of this thesis. The concept of a Boundary Layer Wind Tunnel (BLWT) and proper simulation of the boundary layer is explained. The features of the BLWT at Concordia University's Building Aerodynamics Laboratory and the flow properties used for experimentation are presented. Finally, the fabrication details of the building and attached canopy model as well as the parameters and configurations tested are described.

Chapter 4 presents the analyses of the experimental results for both peak local and area averaged suction on both upper and lower surfaces of the attached canopy

individually. The relationships between the peak pressures and the variation of critical parameters are presented. The area-averaging effect for the peak suction obtained for every configuration are summarized into one figure for the upper surface and one for the lower surface of the canopy.

Chapter 5 presents the analyses of the experimental results for both peak local and area averaged net pressure coefficients. The patterns observed are expanded upon by the use of contour plots, correlations coefficients between upper and lower surfaces, and flow visualization still frame photographs. The relationships between the peak pressures and the variation of each isolated parameter are observed and commented upon. Comparisons between the experimental data of the present study to previous studies are presented. Consequently, the peak net pressure coefficients obtained for every configuration are summarized into one figure.

In Chapter 6 the experimental findings are summarized into design recommendations to be considered for implementation in building codes and standards. Subsequently, comparisons between the recommended design guidelines of the present study and the other available provisions are made.

Finally, conclusions, limitations, and recommendations for future research on the subject are presented in Chapter 7.

CHAPTER 2

LITERATURE REVIEW

2.1 DESCRIPTION OF EXISTING WORK

The number of studies related to the effect of wind-induced pressures on attached canopies is presently limited. In addition, available studies have been found to present some limitations and inconsistencies with each other. All of the experimental studies comprised in this literature review are based on the results obtained from boundary layer wind tunnel experimentation.

The first available study is the work of Jancauskas and Holmes (1985). These experiments were performed in two different boundary layer wind tunnels an urban terrain exposure. The integrated peak loads exerted on the attached canopies were measured by different methods at each of the wind tunnels. One of the studies used a force-balance method whose experimental setup is shown in Figure 2.1. The other method considered pressure-based measurements. Figure 2.2 illustrates the array of the pressure taps used in the attached canopy model for this portion of the study. A total of 14 configurations were tested in this study by varying the height of the parent building, the height of the attached canopy, the length of the canopy, and its width. It must be noted that the configurations tested in this study do not consider the effect that the location of the canopy along the length of the adjacent building will generate on the

wind-induced pressures. Furthermore, it must be noted that only integrated peak loads are presented. This study is the basis of the provisions available on the Australian/New Zealand Standard as shown in Figure 2.3.

Paluch et al. (2003) carried out extensive work regarding wind loads on canopies attached to arched roofs. A total of 30 configurations of arched-roof buildings with attached canopies of different geometries were tested using a pressure based measuring system in a boundary layer wind tunnel. The focus of this study however, is more oriented towards the static wind loads on the arched roofs as a result of the presence of an attached canopy. In addition, pressures on the attached canopies have not been measured in upper and lower surfaces simultaneously.

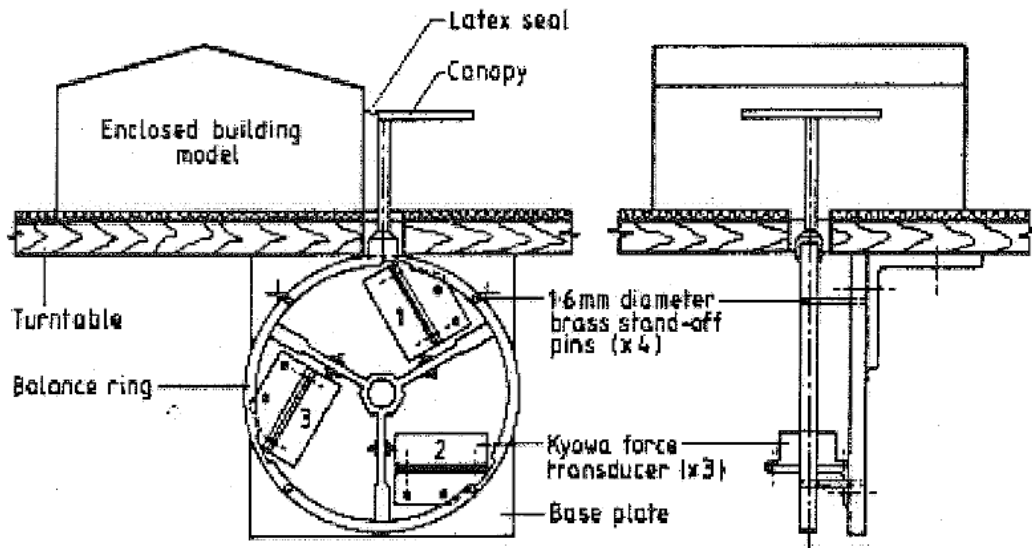


Figure 2.1 Canopy model mounted on the force balance system, after Jancauskas and Holmes (1985)

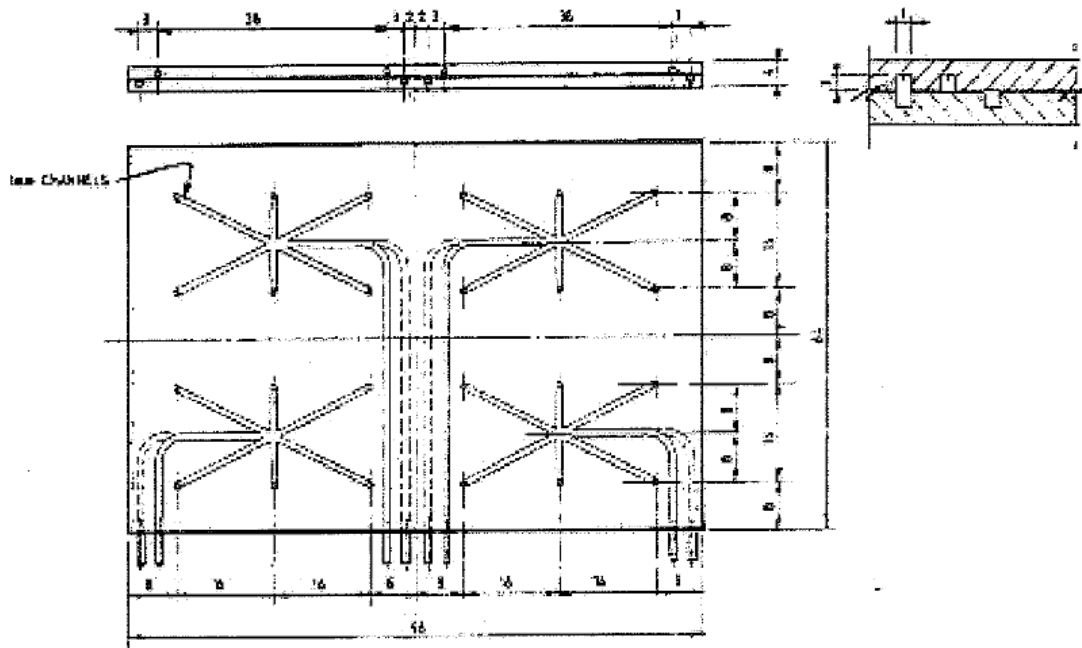


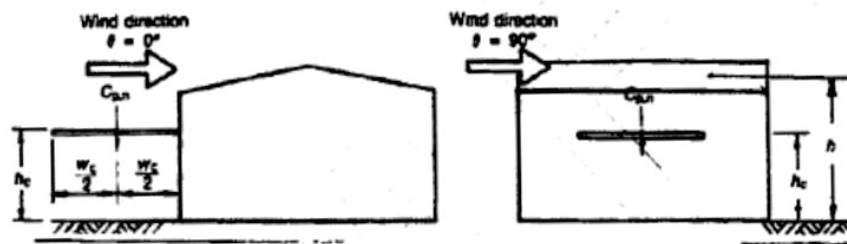
Figure 2.2 Internal manifolding and pressure tap location of attached canopy surface used for pressure measurements, after Jancauskas and Holmes (1985)

TABLE D8
NET PRESSURE COEFFICIENTS, $C_{p,n}$, FOR CANOPIES AND AWNINGS
ATTACHED TO BUILDINGS (refer to Figure D6(a)) FOR $\theta = 0^\circ$

Design case	Ratio** h_c/h	Net pressure coefficients, $C_{p,n}$
$h_c/h < 0.5$	0.1	1.2, -0.2
	0.2	0.7, -0.2
	0.5	0.4, -0.2
$h_c/h \geq 0.5$	0.5	0.5, -0.3
	0.75	0.4, $[-0.3 - 0.2(h_c/w_c)]$ or -1.5^*
	1.0	0.2, $[-0.3 - 0.6(h_c/w_c)]$ or -1.5^*

* Whichever is the lower magnitude

** For intermediate values of h_c/h , use linear interpolation.



(a) Open canopy or awning

FIGURE D6 NET PRESSURE COEFFICIENTS, $C_{p,n}$, FOR CANOPIES, AWNINGS AND
CARPORTS ATTACHED TO BUILDINGS

Figure 2.3 Segment obtained from the provisions of the AS/NZS 1170.2:2002

Hölscher et al. (2007) performed an extensive study on wind-induced pressures on attached canopies. Experiments were carried out on a boundary layer wind tunnel and the loads were recorded using a pressure-based measuring technique. Experiments were performed for a suburban terrain exposure for canopies attached to a flat roof building.

For each configuration 24 wind directions were tested. Both local and area integrated peak loads have been analyzed. The results and analysis resulting from this study form the basis of the design guidelines provided in Eurocode 1 for Wind Actions (DIN EN 1991-1-4:2010-12) shown in Figure 2.4.

Goyal et al. (2007) carried out a critical review in which the latest research being done in the subject is discussed. Comparisons between the provisions on the AZ/NZS 1170.2:2002 and the IS: 875 (Part-3)-1987 are also provided. It is concluded that currently available codes of practice provide insufficient information regarding the wind pressure coefficients on buildings with attached canopies, and thus states the need for further investigation on the subject.

Zisis and Stathopoulos (2010) carried out a detailed study on wind-induced pressures on attached canopies. The experiments were performed on a boundary layer wind tunnel for a roughness simulating an open terrain exposure. The loads were determined using a system of pressure sensitive scanners. For each configuration a total of 28 wind directions were tested. This study presents both local and area averaged peak loads, as well as pressure and correlation coefficient contour plots so as to give a better understanding of the loading patterns on attached canopies. Some comparisons are also made with the corresponding design guidelines provided by the AZ/NZS 1170.2:2002. It must be noted, however that this study was limited to 3 different configurations.

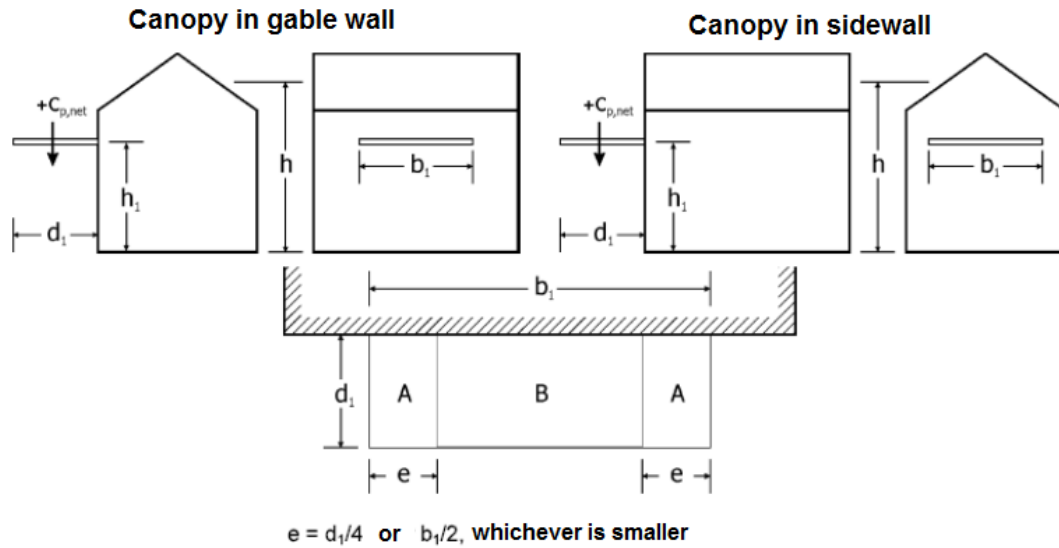


FIGURE NA.V.1 — Dimensions and classification of surfaces for canopies

height ratio h_1/h	Area					
	Downward Load	A Upward Load		Downward Load	B Upward Load	
		$h_1/d_1 \leq 1,0$	$h_1/d_1 \geq 3,5$		$h_1/d_1 \leq 1,0$	$h_1/d_1 \geq 3,5$
$\leq 0,1$	1,1	-0,9	-1,4	0,9	-0,2	-0,5
0,2	0,8	-0,9	-1,4	0,5	-0,2	-0,5
0,3	0,7	-0,9	-1,4	0,4	-0,2	-0,5
0,4	0,7	-1,0	-1,5	0,3	-0,2	-0,5
0,5	0,7	-1,0	-1,5	0,3	-0,2	-0,5
0,6	0,7	-1,1	-1,6	0,3	-0,4	-0,7
0,7	0,7	-1,2	-1,7	0,3	-0,7	-1,0
0,8	0,7	-1,4	-1,9	0,3	-1,0	-1,3
0,9	0,7	-1,7	-2,2	0,3	-1,3	-1,6
1,0	0,7	-2,0	-2,5	0,3	-1,6	-1,9

For intermediate $1,0 << h_1/d_1 < 3,5$ use linear interpolation, For intermediate h_1/h linear interpolation may be used.

Figure 2.4 Segment obtained from the provisions of the DIN EN 1991-1-4 2010-12

In addition to the *AZ/NZS 1170.2:2002* and the *DIN EN 1991-1-4/NA:2010-12*, provisions for the wind load design of attached canopies are also available on the Austrian Standard (ÖNORM B 4014-1), the Swiss Standard (Schweizerische Norm, SIA 261), and the Indian Standard code of practice for design loads (IS: 875 (Part-3)-1987). However, it is unclear if these provisions are the result of other wind tunnel studies or if they are just adaptations of other design provisions.

2.2 JUSTIFICATION OF THE PRESENT STUDY

The National Building Code of Canada (NBCC) and the American Society of Civil Engineering Minimum Design Loads of Buildings and Other Structures (ASCE 7-10) both lack provisions for the design of attached canopies. As a result, many practitioners in North America have resolved to design such elements by adapting currently available provisions so as to obtain an idea of an adequate pressure coefficient. One of these approaches is to consider the attached canopy as if it were the roof of a *Partially Enclosed Building* (ASCE 7-10) or a *Building with Large Openings* (NBCC) as shown in in Figure 2.5. Another approach is to consider the canopy as an extension of the roof overhang, thus designing it with the corresponding provisions. As it can be seen in Figure 2.6, this results in significant geometrical differences which are in turn expected to have a substantial impact on the flow patterns about the attached canopy.

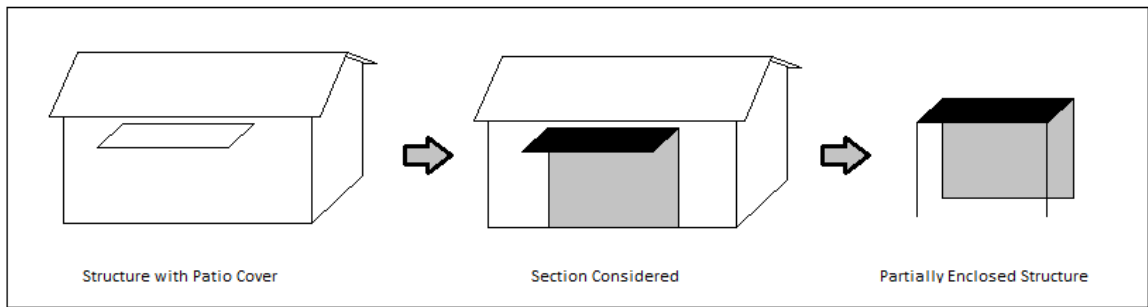


Figure 2.5 Illustration relating the attached canopy to the roof of a *Partially Enclosed Building*

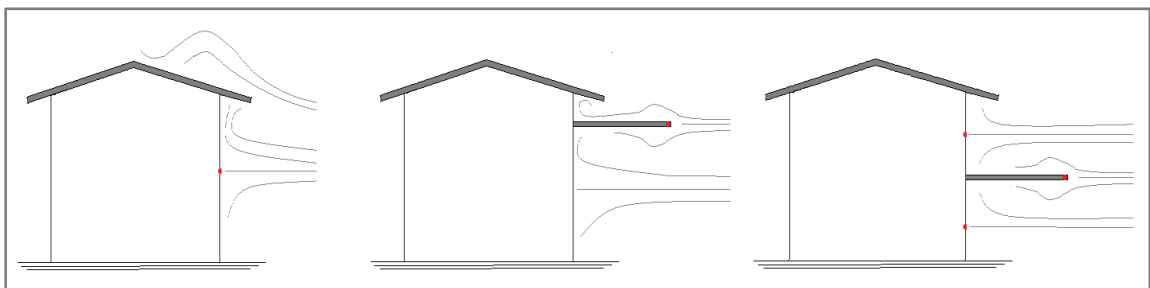


Figure 2.6 Expected differences in flow patterns between a roof overhang and a canopy attached at a high and at an intermediate portion of the parent wall

In addition to this, the several Wind Standards and Codes of practice that do provide design guidelines for wind-induced pressures on attached canopies, exhibit several limitations and inconsistencies as expressed by Zisis and Stathopoulos (2010), and Goyal et al. (2007). It has been seen for many cases that these guidelines do not seem to yield consistent results with each another. This is illustrated in Figure 2.7 where the design values suggested by each of the aforementioned standards are plotted for three identical configurations.

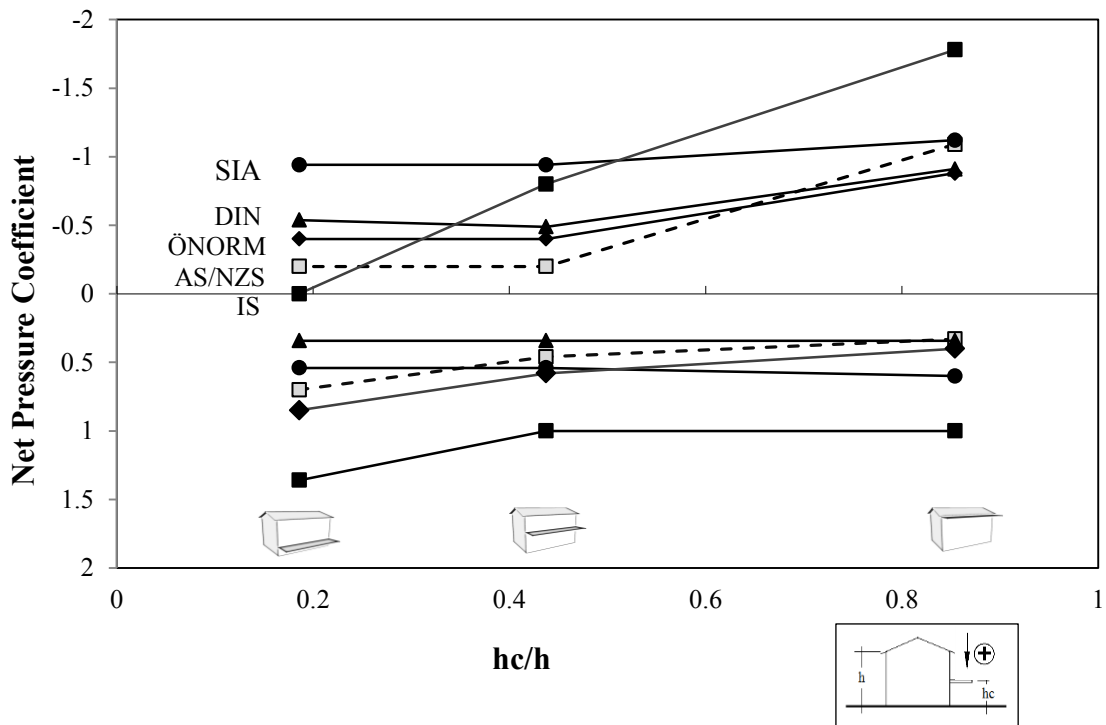


Figure 2.7 Comparison of recommended local net pressure coefficients according to the five currently available design provisions (all pressure coefficient values are referenced to the dynamic velocity pressure based on a 3-sec averaging wind speed measured at the mean roof height)

The objective of this thesis is to attend to these demands and inconsistencies by providing a more extensive parametric study so as to produce more reliable design guidelines for the design of attached canopies. As it has been previously stated by Goyal et al. (2007):

“Codes of practice of different countries dealing with design of structures for wind load, including Indian Standard on Wind Loads, do not give enough information regarding wind pressure coefficients on the buildings with projections (...) very little experimental research work has been done so far on buildings with projections, particularly attached canopies (...) it is, therefore, required to carryout further studies to investigate the effects of attached canopies on wind loads on buildings.”

CHAPTER 3

EXPERIMENTAL METHODOLOGY

3.1 GENERAL

A parametric study has been carried out to assess the impact that changing the dimensions of an attached canopy and its geometry relative to the parent building will have on the wind-induced loading. A modifiable model of a low rise structure with an attached canopy has been constructed and examined in a Boundary Layer Wind Tunnel while monitored by pressure sensitive scanners placed along both surfaces of the canopy model. In this chapter the pertinent aspects regarding the aforementioned process are explained in greater detail.

3.2 CONCEPT OF A BOUNDARY LAYER WIND TUNNEL

The boundary layer phenomenon results from the interaction of a free flow and a submerged body. Friction forces occurring at the interaction between the particles of air and the surface of the submerged body result in interruptions of the free flow. These interruptions can be seen as marked deviations between velocities measured over small periods of time (e.g. 3-sec gusts) and the average wind velocity. The magnitude of the variation in the wind velocity with respect to the arithmetic mean is generally used to

define the turbulence of a flow. The higher the surface roughness the higher the turbulence is expected to be and thus the properties of the boundary layer flow are altered. The atmospheric boundary layer is the result of the interaction of the wind and the surface of the earth. A boundary layer wind tunnel (BLWT), as opposed to a conventional wind tunnel, recreates the interaction between the wind and the terrain so as to simulate the natural characteristics of the wind at a defined scale. Most BLWTs today are based on the contributions of Danish engineer Martin Jensen (Jensen 1958). He observed that by building very long wind tunnels and by modelling the surface roughness, proper simulation of the wind could be achieved. Jensen (1958) formulated scaling laws for proper wind tunnel simulations by comparing pressures on a full scale low rise structure to a model in a boundary layer wind tunnel.

Presently, in order to assess proper simulation, the mean velocity and turbulence intensity profiles, the longitudinal scale of turbulence, and the power spectra of the longitudinal velocity are considered fundamental.

3.3 CHARACTERISTICS OF THE BLWT AT THE CONCORDIA UNIVERSITY BUILDING AERODYNAMICS LABORATORY

3.3.1 Physical characteristics

The BLWT in the Building Aerodynamics Laboratory (BAL) at Concordia University is of the open circuit return type and consists of a 1.8m x 1.8m (6ft x 6ft) cross section and a working section of about 12m (39.4ft) long. Top, side, and front views retrieved from the original construction plans are provided in Figure 3.1. The flow is

generated by a MARK HOT double inlet centrifugal blower with a capability of providing $40 \text{ m}^3/\text{s}$ (86400 cfm). As a result, a maximum testing wind speed of 14.0 m/sec can be attained. The wind speed can be reduced to 3 m/sec by manually adjusting the outlet control.

The floor is covered with a polypropylene carpet and the ceiling consists of wooden panels of adjustable height. Different terrain exposures may be simulated by the addition of floor panels with specific roughness elements and by adjusting the ceiling to achieve a zero longitudinal pressure gradient. In this way, the proper simulation of the atmospheric flow for any exposure category can be ensured. It must be noted, however, that every experiment comprised in this study has been conducted for an open terrain exposure (low roughness) as shown in Figure 3.2.

At the test section a turntable of a 1.20m diameter has been placed to allow for the testing of models for any desired wind direction. Additionally, an acrylic glass window has been placed at the wind tunnel wall to facilitate flow visualization experimentation without having the equipment interfere with the flow.

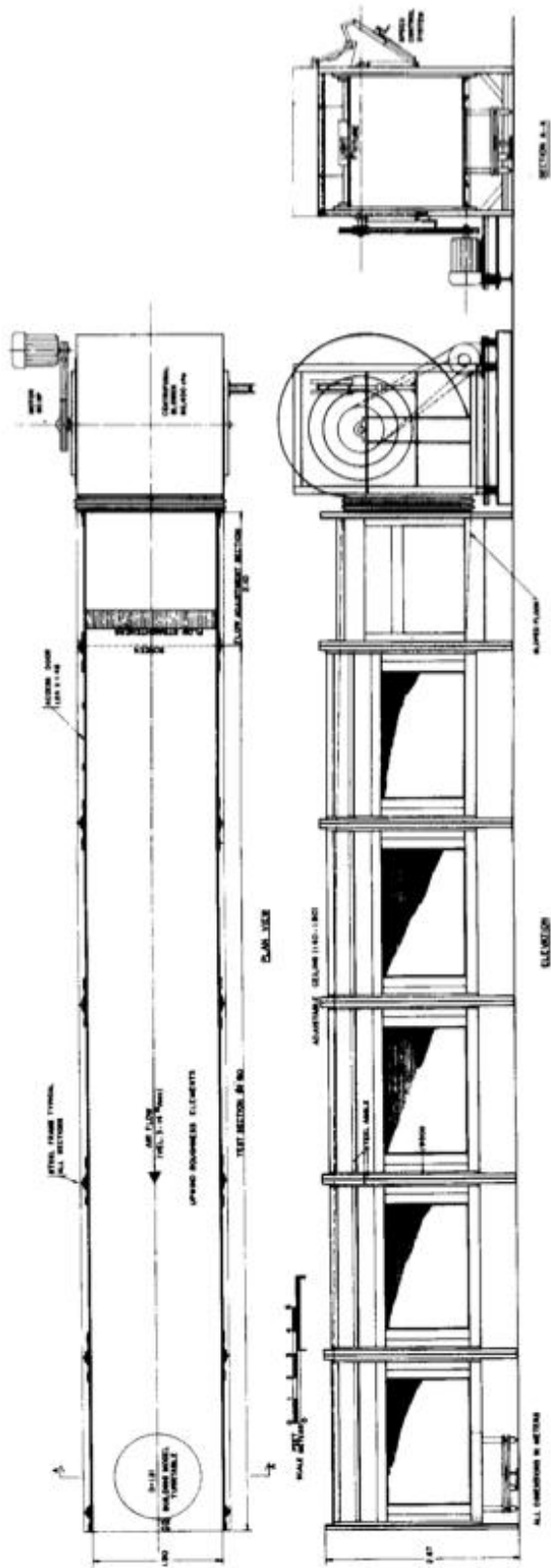


Figure 3.1 Construction plans of the Boundary Layer Wind Tunnel at Concordia University's Building Aerodynamics Laboratory, after Stathopoulos (1984)



Figure 3.2 Open terrain exposure at the BLWT in the Building Aerodynamics Laboratory at Concordia University

3.3.2 Instrumentation

Instrumentation used for the measurement of flow phenomena in the BLWT at the Building Aerodynamics Laboratory consisted of two major independent systems for velocity and for pressure measurements. Velocity related measurements, such as wind speed and turbulence intensity profiles, were performed using a 4-hole Cobra Probe (Turbulent Flow Instrumentation) in combination with an automated traverse system (Rotalec). Measurements were conducted at a sampling rate of 1000Hz for a duration of approximately 30 seconds. The gradient mean wind velocity was set at approximately 13.4 m/s.

Pressure measurements were conducted using a Digital Service Module DSM 3400 as the Data Acquisition System (DAS) in combination with a ZOC33/64Px pressure scanner and Thermal Control Unit (TCU) system all from Scanivalve Corp. The pressure taps in the building models are connected to the ZOC33/64Px scanners using urethane flexible tubing. Compressed air is connected to the system for purging and calibration purposes. The DAS was operated by a second computer connected to the DSM 3400 through an Ethernet network connection. A schematic of the experimental setup is shown in Figure 3.3.

The scanning period was set at 50 microseconds for 64 channels resulting in a sampling frequency of 312.5 Hz. A total of 8200 frames are thus scanned in approximately 26.2 seconds, corresponding to a full-scale storm of approximately 1 hour.

In addition, a fog generator (Dantec) and a high speed camera were used for the flow visualisation portion of the study.

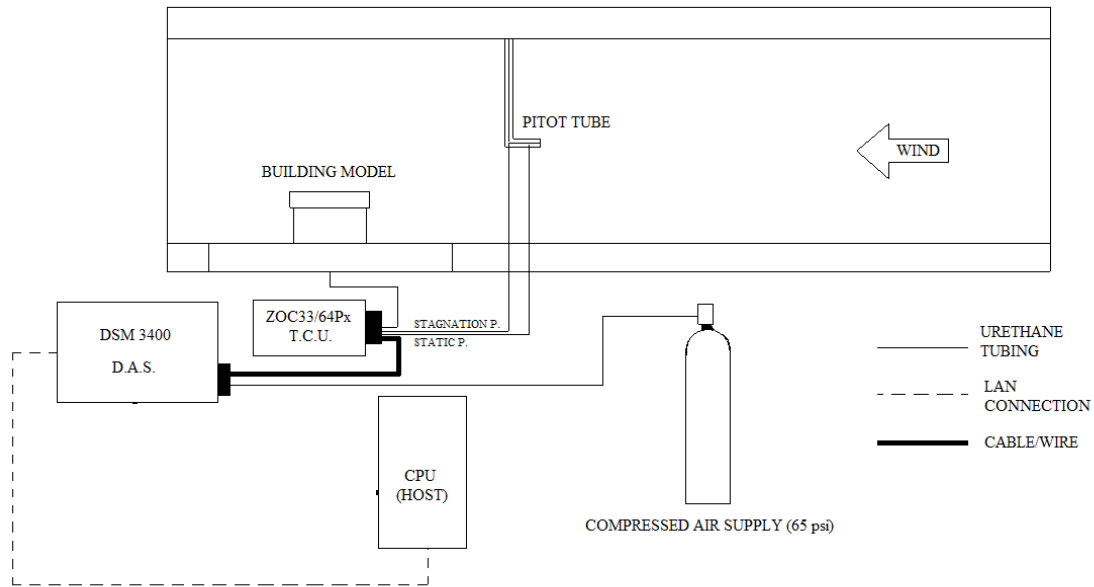


Figure 3.3 Schematic of the experimental setup at the boundary layer wind tunnel

3.3.3 Characteristics of the simulated flow

In order for the pressure measurements obtained in the wind tunnel to have a physical meaning one must first be assured that the flow generated at the testing section adequately simulates the properties of the atmospheric wind. Comparisons between theoretical and experimental velocity profiles, turbulence intensity, integral scale of turbulence, and spectra of the velocity fluctuations are defined and evaluated in this section to assess the validity of the experimentation.

The variation of the mean velocity as a function of elevation (\bar{V}_z) and the location of the gradient height (Z_G) after which the mean wind velocity is constant (\bar{V}_G) are

instrumental for the modelling of the atmospheric boundary layer. Figure 3.4 provides a schematic illustrating the boundary layer flow and the aforementioned parameters.

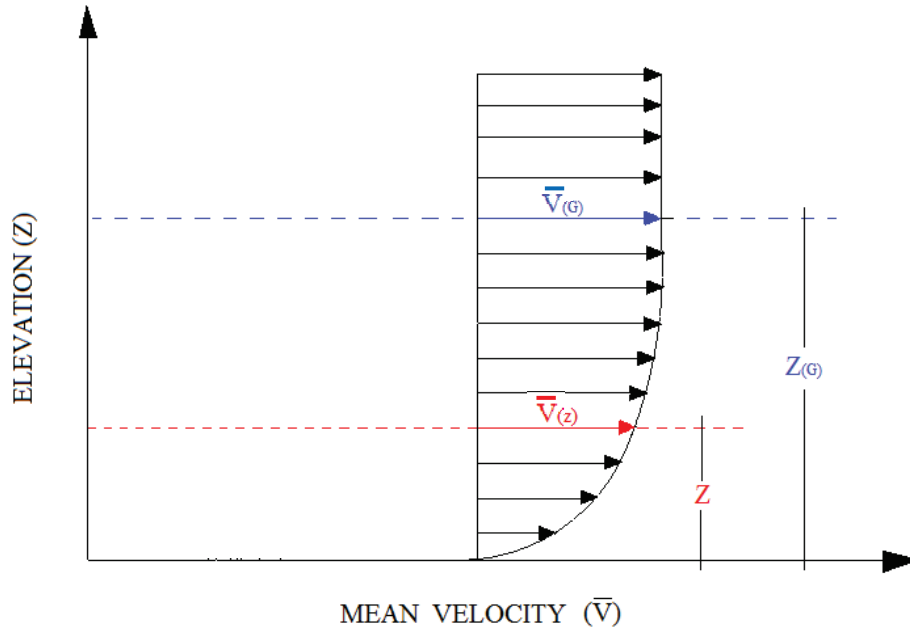


Figure 3.4 Boundary layer flow and notation used for elevations and velocities

The average and root mean square longitudinal wind velocities (\bar{V}_z and V_{rms}) were measured at different heights at the center of the wind tunnel test section without the model in place. The corresponding average velocity (\bar{V}_z) and longitudinal turbulence intensity (V_{rms} / \bar{V}_z) profiles are shown in Figure 3.5 as a function of Z/Z_G . The experimental values are compared to the theoretical values in accordance with the power law equation of the form:

$$\frac{\bar{V}_z}{\bar{V}_G} = \left(\frac{Z}{Z_G}\right)^\alpha \quad (3.1)$$

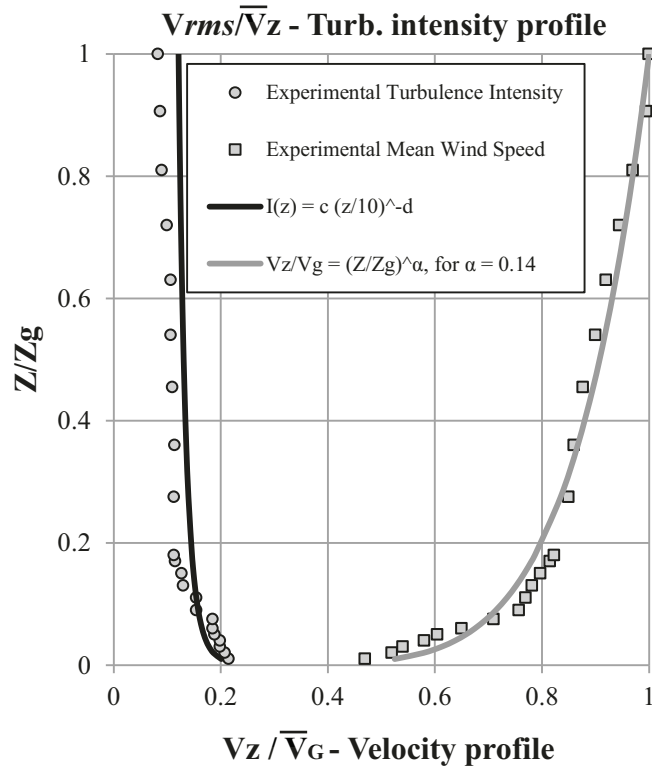


Figure 3.5 Wind velocity and turbulence intensity profiles for open-terrain exposure

where α is a the power law exponent which depends on the type of exposure. It has been observed that a power law exponent of $\alpha = 0.14$ provides the best agreement with the measured values, which conforms to full scale measurements of an open terrain exposure (Liu, 1991). The experimental turbulence intensity is compared to the theoretical values as given by:

$$I_{(z)} = c \cdot \left(\frac{z}{10}\right)^{-d} \quad (3.2)$$

where c and d are terrain-dependant coefficients (Zhou and Kareem, 2002) taken as 0.15 and 0.11, respectively, for an open terrain exposure.

In general, it can be seen that the experimental values obtained for the velocity and turbulence intensity profiles show a good agreement with the theoretical properties of an atmospheric flow at an open terrain exposure.

Velocity fluctuations at a certain height inside the atmospheric boundary layer can be defined as a sequence of eddies being transported by the mean wind velocity in a periodic fluctuation with a circular frequency $\omega = 2\pi n$, where n is the frequency. The integral scales of turbulence measure the average size of these eddies. The length of an eddy can be measured in three dimensions for three different components of the fluctuating wind (longitudinal, transverse, and vertical). As a result, nine integral length scales of turbulence have been defined (Simiu and Scanlan, 1996).

For wind tunnel experimentation, it has been found that the most important to simulate amongst the nine integral scales of turbulence is the longitudinal size of the eddy in the longitudinal direction of the velocity fluctuations.

Mathematically the integral length scale of turbulence in the longitudinal direction is defined as:

$$L_v^x = \frac{V}{v^2} \int_0^{\infty} R_v(\tau) d\tau \quad (3.9)$$

where $R_v(\tau)$ is the autocovariance function of the fluctuation $v(x_1, t)$ which relates the similarity of the wind signal to itself at a certain time lag. An experimental value of $L_v^x = 112\text{m}$ has been estimated at one sixth of the boundary layer depth for an open terrain exposure (Stathopoulos, 1984).

In addition, the following empirical expression has been proposed (Counihan, 1975) for estimation of length scale of turbulence in the longitudinal direction:

$$L_v^x = Cz^m \quad (3.10)$$

where z is the height in meters, and C and m can be determined from Figure 3.6 as a function of the roughness length z_o . Evaluating the expression at an elevation of one sixth the gradient height and using the experimental roughness length $z_o = 0.01\text{cm}$ an approximated value of $L_u^x = 122\text{m}$ is obtained.

It can be noted that both values obtained for the approximation of the integral length scale of turbulence in the longitudinal direction fall within the ranges of the experimental values measured for an open terrain exposure (Shiotani, 1971).

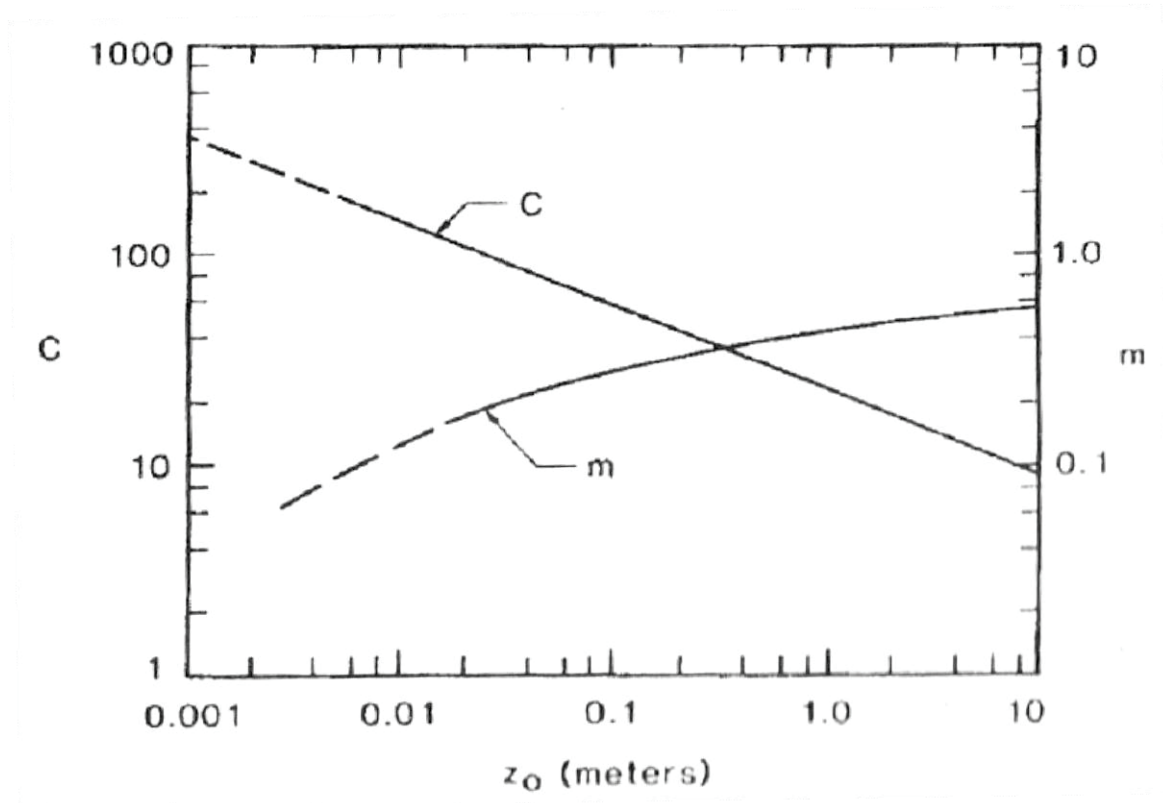


Figure 3.6 Variation of C and m with roughness length, after Counihan (1975)

It is well known that variations in velocity at a certain height can be defined as a sequence of eddies being transported by the mean wind velocity in a periodic fluctuation with a circular frequency. These turbulent fluctuations determine the total kinetic energy of the flow. If the fluctuations of the wind with respect to time are analyzed as signals, then the sequence can be decomposed into different frequencies. The signal can thus be represented in the frequency domain instead of the time domain. This is useful to describe the total amount of kinetic energy generated by the eddies. The mathematical definition for the spectrum of the wind at a given height z is:

$$\sigma^2 = \int_0^\infty S_z(n) dn \quad (3.11)$$

where σ^2 is the variance of the longitudinal wind speed, n is the frequency and $S_z(n)$ is the power spectral density of the longitudinal turbulence component at a given height z .

Two principal analytical and empirical spectral representations have been regarded to closely approximate the behavior of the atmospheric flow. The first is the analytical expression known as Von Karman's equation:

$$\frac{n S(n)}{\sigma^2} = \frac{4 n'}{(1+70.8 n'^2)^{5/6}} \quad (3.12)$$

where,

$$n' = \frac{nL_x^v}{\bar{V}_z} \quad (3.13)$$

and,

$$L_x^v = \frac{25(Z-d)^{0.35}}{Z_o^{0.063}} \quad (3.14)$$

in which,

\bar{V}_z = mean wind speed at height Z ;

L_x = length scale of turbulence in the longitudinal direction;

d = displacement length

$Z_o =$ roughness length

The second is known as Davenport's empirical expression defined as:

$$\frac{n S(n)}{v_*^2} = \frac{2}{3} \frac{n'^2}{(1+n'^2)^{4/3}} \quad (3.15)$$

where,

$$n' = \frac{n}{\bar{V}_{10}} 1200 \quad (3.16)$$

and where \bar{V}_{10} is the mean wind speed at a 10m (32.8 ft) height. It must thus be noted that this expression does not take into consideration the variation of the spectrum with respect to height.

The spectra of longitudinal velocity fluctuations have been measured at the BLWT at the Building Aerodynamics Laboratory in Concordia University at a height of one sixth of the boundary layer height has been obtained for an open terrain exposure (Stathopoulos, 1984). Figure 3.7 shows the comparison of the experimental spectrum compared to the curves obtained from Von Karman's and Davenport's equations. It can be seen that for lower wave numbers (n / \bar{V}_z) Von Karman's equation seems to coincide better with the experimental data. For the intermediate wave numbers, where the highest energy in the turbulence occurs, Davenport's equation provides a better fit. In general it can be seen that there is a good agreement in between the experimental and theoretical

values. Resulting from the analyses observed in this section, a scale of 1:400 has been suggested as ideal.

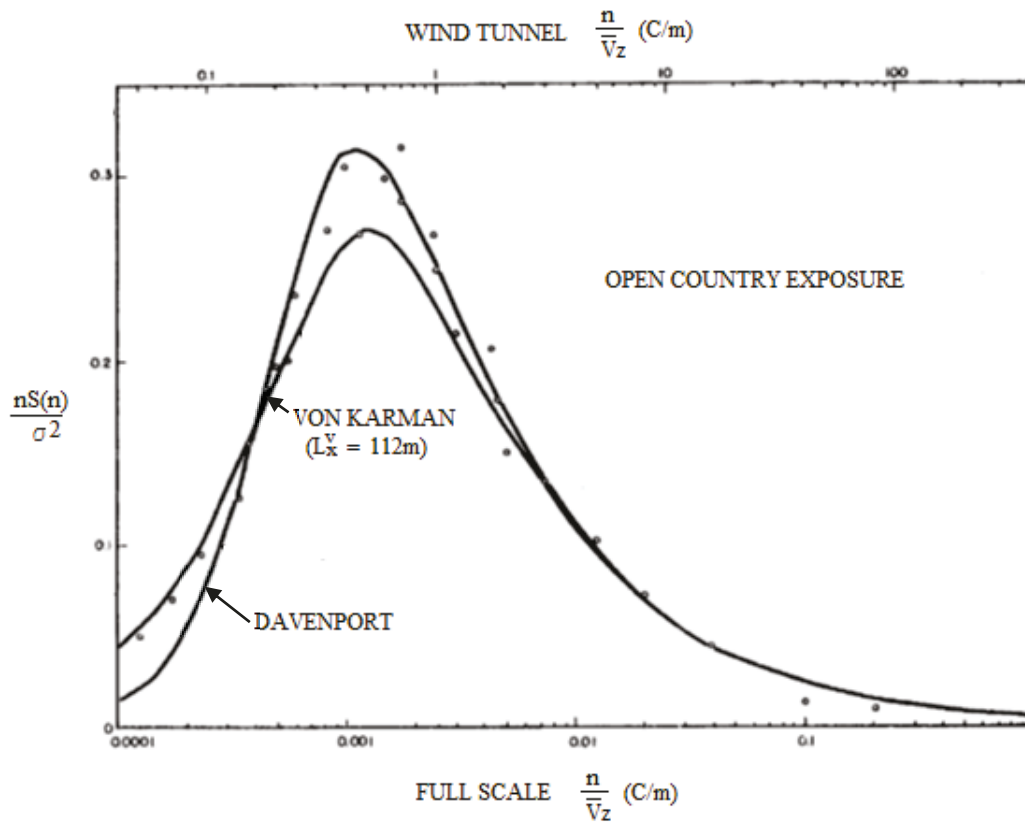


Figure 3.7 Spectra of longitudinal turbulence component at $\frac{Z}{Z_G} = \frac{1}{6}$, after Stathopoulos (1984)

3.4 PRESSURE COEFFICIENTS

The magnitude of the forces exerted on a structure exposed to wind activity depends on factors related to either the characteristics of the building or the properties of the wind. The effect that the geometry of the building has on the pressures to which it will be submitted is the principal goal of most boundary layer wind tunnel experimentation for codification purposes. The properties of the wind that have an impact on the pressures, most importantly the wind speed, can vary significantly for different geographic location, different terrain exposures and different wind directions. Pressure coefficients thus result as a convenient way to express relative pressures only as a function of the structure's geometry. In this section, the fundamental definition of a pressure coefficient is provided and the specific pressure coefficients used in this study are defined.

3.4.1 Definition of pressure coefficients

Pressure coefficients are dimensionless numbers that refer all pressures measured at the surface of the structure to the mean dynamic pressure of the upstream wind. Pressure coefficients are derived from Bernoulli's principal, which is defined as:

$$\frac{1}{2} \rho V_o^2 + p_o = \frac{1}{2} \rho V^2 + p = \text{constant} \quad (3.17)$$

where ρ is the density of the air, V_o and p_o are the velocity and the static pressure upstream from the body and V and p are the velocity and the local pressure exerted at the interface with the submerged body. Equation (3.17) can be rewritten as:

$$\frac{1}{2} \rho V_o^2 - \frac{1}{2} \rho V^2 = p - p_o = \text{constant} \quad (3.18)$$

from which the pressure coefficients are derived as:

$$\frac{1}{2} \rho (V_o^2 - V^2) = p - p_o = \text{constant} \quad (3.19)$$

$$\frac{1}{2} \rho V_o^2 \left(1 - \frac{V^2}{V_o^2}\right) = p - p_o = \text{constant} \quad (3.20)$$

$$Cp = \frac{p - p_o}{\frac{1}{2} \rho V_o^2} = \frac{p - p_o}{q} = 1 - \left(\frac{V}{V_o}\right)^2 \quad (3.21)$$

If the pressure coefficient at a specific location along the body of a structure is known, then the corresponding force can be easily obtained by multiplying the pressure coefficient by the design dynamic pressure q and the corresponding tributary area A as shown:

$$F = Cp \cdot q \cdot A \quad (3.22)$$

3.4.2 Pressure coefficients applied to this study

All data acquired by the pressure scanner is presented in dimensionless form by use of pressure coefficients in accordance to the following equation:

$$C_p = \frac{p_t - p_o}{q_{mrh}} = \frac{\Delta p}{q_{mrh}} \quad (3.23)$$

where, p_t = surface pressure at tap; p_o = static pressure; q_{mrh} = dynamic pressure at mean roof height converted from q_{pitot} by use of the power law as follows:

$$q_{mrh} = q_{pitot} \left(\frac{Z_{mrh}}{Z_g} \right)^\alpha \quad (3.24)$$

Since the attached canopy is generally a thin element exposed to wind pressures on both upper and lower surfaces it is essential to consider the pressures acting simultaneously on each plane. This is done by the use of net pressure coefficients as defined in the following equation:

$$C_{p,net} = \frac{\Delta p_{upper} - \Delta p_{lower}}{q_{mrh}} = \frac{\Delta p_{net}}{q_{mrh}} \quad (3.25)$$

where, Δp_{upper} and Δp_{lower} are measured at top and bottom components, respectively, of a pressure tap pair as illustrated in Figure 3.8. It must be noted that the negative sign represents a pressure directed away from the surface (suction) and a positive sign represents a pressure directed towards a surface. If this convention is maintained when

computing net loads in accordance with Eq. (3.25) a negative value for a $C_{p,net}$ will result in a net uplifting load, where as a positive value will result in a net downwards loading.

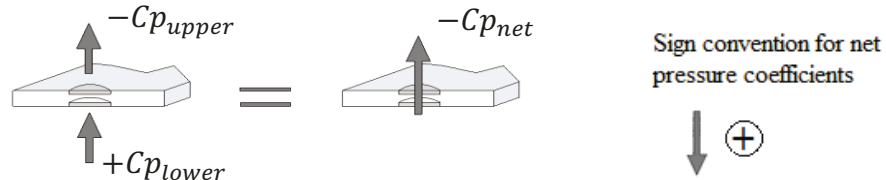


Figure 3.8 Illustration of the generation of net pressure coefficients, $C_{p,net}$

Throughout this study peak pressure coefficients may be identified as either local or area-averaged. A local peak C_p refers to the critical value experienced at a single pressure tap (or pressure tap pair in the case of local $C_{p,net}$). An area-averaged C_p refers to the peak value that the entire surface experiences determined by the average of every pressure tap (or pressure tap pair) simultaneously. Additionally, local and area-averaged pressure coefficients may be referred to as either minimum, maximum or mean. These are defined respectively as:

$$C_{p,minimum} = \frac{(\tilde{p}_t - p_a)}{q_{mrh}} \quad (3.26)$$

$$C_{p,maximum} = \frac{(\hat{p}_t - p_a)}{q_{mrh}} \quad (3.27)$$

$$C_{p,mean} = \frac{(\bar{p}_t - p_a)}{q_{mrh}} \quad (3.28)$$

where \check{p}_t , \hat{p}_t , and \bar{p}_t are the extreme upward, extreme downward, and mean pressure at a pressure tap or pressure tap pair during the entire duration of the simulated storm.

3.4.3 Pressure coefficients and velocity averaging periods

The magnitude of the design velocities depends greatly upon the time period for which it is averaged, e.g. a maximum velocity averaged over a three second duration, is expected to be considerably higher than a velocity averaged over 1 hour. The duration of the averaging period will affect the average dynamic pressure to which the pressure coefficients are normalized. Since the dynamic pressure is in the denominator (see Eq. (3.23)), longer averaging periods will result in higher magnitude pressure coefficients. It can thus be seen that pressure coefficients carry a physical meaning only when used with a design wind speed which has been averaged over the same period of the simulated storm. All results presented in this study have resulted from simulated storms of 1 hour duration. However, major building codes and standards provide pressure coefficients that conform to different averaging periods, most commonly: 3-seconds gust, 10-minutes, and 1 hour. In Chapter 6 to properly undertake code comparisons and to generate code recommendations all pressure coefficients have been converted to comply with 3-second average velocities.

If the ratio of a 3 second gust to a 1 hour wind speed ($\frac{V_{3s}}{V_{3600s}}$) is known then the conversion of a pressure coefficient measured at a 1 hour averaging period ($C_{p,3600s}$) can

be converted into a pressure coefficient corresponding to a 3 second gust ($C_{p,3s}$) as follows:

$$C_{p,3s} = \frac{\Delta p}{\frac{1}{2}\rho V_{3600s}^2 \left(\frac{V_{3s}}{V_{3600s}}\right)^2} = \frac{C_{p,3600s}}{\left(\frac{V_{3s}}{V_{3600s}}\right)^2} \quad (3.29)$$

The relationship between the velocities and the averaging period has led to numerous studies and debates, however, the Durst gust duration curve (Durst, 1960) presented in Figure 3.9 is widely regarded as a useful tool to estimate the relationship between velocities corresponding to different averaging periods $\left(\frac{V_t}{V_{3600s}}\right)$.

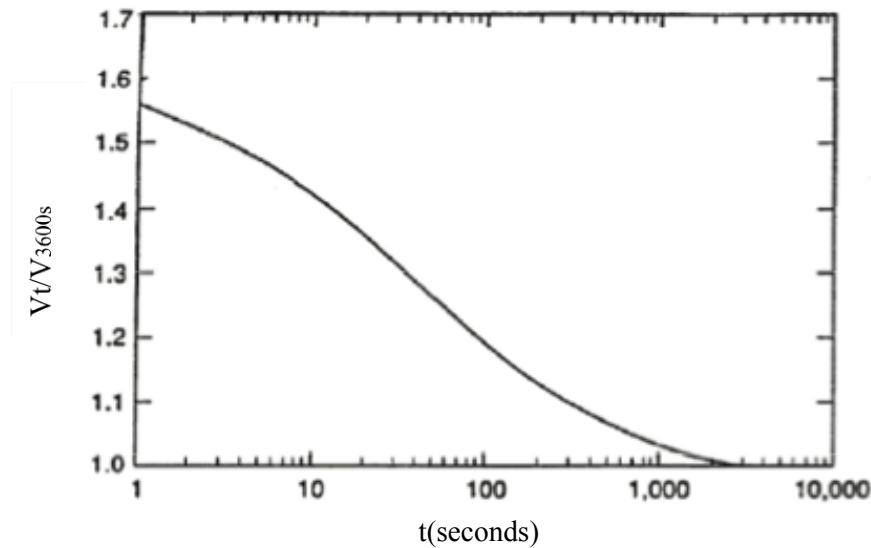


Figure 3.9 Gust duration curve, after Durst (1960)

3.5 BUILDING MODELS AND CONFIGURATIONS TESTED

The design and construction of an adequate building model is essential for any type of wind tunnel study. The selection of a scale that is physically feasible whilst conforming to the flow properties simulated at the BLWT is often a subject of much scrutiny. Additionally, in the case of a parametric study, the selection of the ranges in the relative geometries to be examined is also subjected to much judgement so as to serve geometrical configurations commonly encountered in practice. In this section, these aspects are attended to and all of the configurations to be tested are defined.

3.5.1 Selection of scale

Following the analyses of the flow properties in the BLWT at the Building Aerodynamics Laboratory of Concordia University, it has been established that a geometric scale of 1:400 is optimal for simulation experiments (Stathopoulos, 1984). However, limitations are frequently encountered and the modelling of the optimal scale is not always feasible. Experiments have been performed to assess the errors that result from varying the scale (Stathopoulos, 1983) and it has been seen that increasing the scale within an acceptable range may result in only minimal deviations of the peak and mean pressure coefficients. It has also been seen that adequately simulating the turbulence is of uppermost importance to the extreme fluctuating pressures in low rise structures (Tieleman et al. 1998).

For this study, the optimal scale of 1:400 was not a feasible option. The limitation was imposed by the thin canopy model and the importance for it to have pressure taps at both upper and lower surfaces at the same locations in the horizontal plane. This was done by sandwiching metallic tubing elements in between two thin metallic plates and welding them together. The smallest thickness that could be achieved was of 10mm ($\frac{1}{26}$ in). In a 1:400 scale this would correspond to a thickness of 40cm (15.74 in) which is unusual for most canopies encountered in practice. In a 1:100 scale, however, a 10mm ($\frac{1}{26}$ in) thickness would correspond to a 10cm (3.8 in) full-scale thickness, which conforms better to dimensions encountered in practice.

The turbulence intensity at the mean roof height for the three different parent building heights tested were found to be 17.9% (mrh = 4.5 cm), 15.5% (mrh = 8 cm), and 14.4% (mrh = 11.3 cm) thus complying with the importance of proper simulation of the turbulence intensity when dealing with low-rise buildings (Tieleman et al. 1998). Taking into consideration the technical limitations, the geometric scale of 1:100 was considered as the most suitable for the present experimentation.

3.5.2 Description of attached canopy and parent building model

The parent building was constructed out of acrylic glass with a gabled-roof of slope 4:12, base dimensions of 15 cm by 10 cm (length-width) and a ridge height of 12.30 cm to represent the 1:100 geometric scale. Figure 3.10 shows the parent building used for experimentation with its complete dimensions. The parent wall of the building model consists of five wall segments of unique widths which may be arranged in

different ways so as to provide a slot at different positions to which the canopy model can be attached. The parent building and canopy model can be seen in Fig. 3.11.

Two separate canopy models have been made out of thin sandwiched metallic plates. One of the canopy models stretches over the half length of the parent wall whereas the other stretches over the entire length (Fig 3.11 a and b respectively). Both models have the same width of 3.65 cm. Pressure taps have been placed at both upper and lower surfaces of the canopy at the same locations in the horizontal plane to form pressure tap pairs which enable the determination of net pressure coefficients. Pressure tap locations for both canopy models are shown in Figure 3.12. The half-length canopy model has a

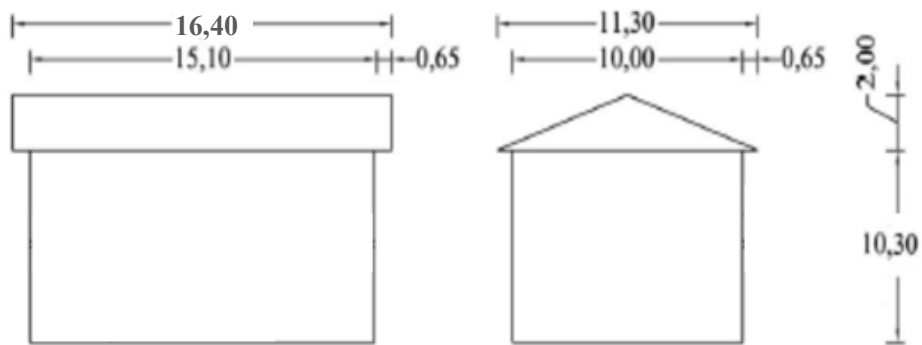
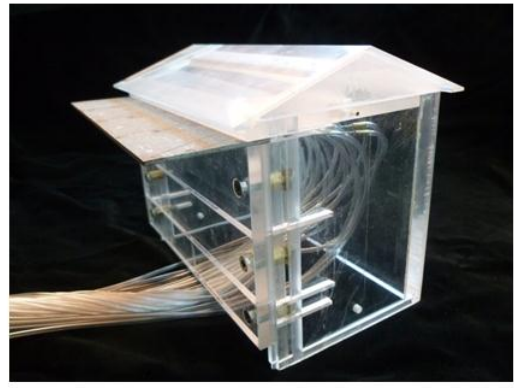


Figure 3.10 Building models tested (dimensions in cm)

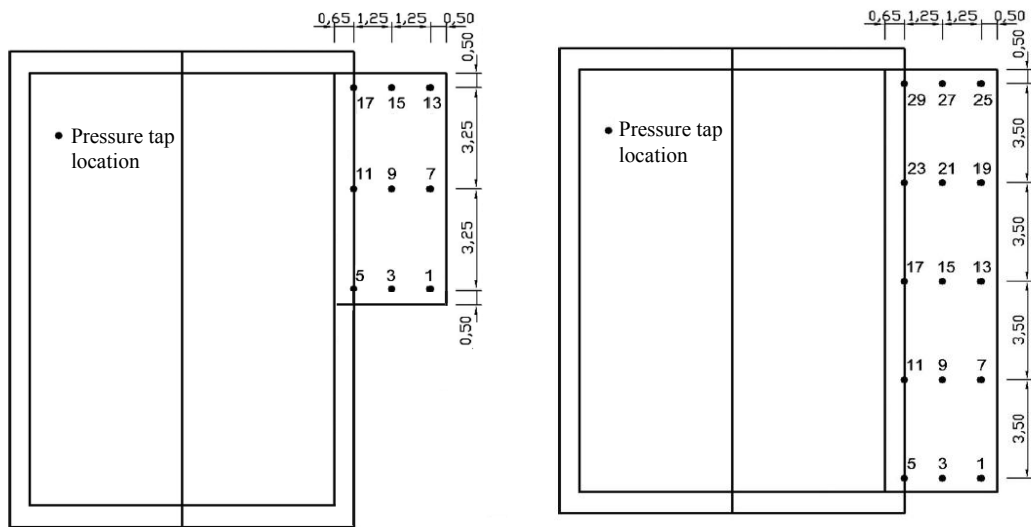


(a)



(b)

Figure 3.11 Building model with different canopies in place



*even numbered channels are located underneath the channels shown

Figure 3.12 Top view of building and canopy model showing pressure tap locations

total of 18 pressure taps (9 pressure tap pairs) and the full-length canopy model has a total of 30 pressure taps (15 pressure tap pairs).

The transformable model allows for many different geometrical relationships between the canopy and the parent building. Every unique parent building-to-canopy geometric relationship will be referred to as a configuration during the course of this study. The modifiable dimensions and their respective ranges are illustrated in Figure 3.13. By shifting the slot at which the canopy is attached along the Y axis, the height of the canopy (h_c) can be varied. The eave height of the building (h) can also be varied by fixing the model to an adjustable base. The length of the canopy along the X axis (l_c) can be modified by employing either the full-length or the half-length canopy model as defined before. The half-length canopy may also be shifted along the X axis to account for different edge distances (ed). In addition, the width of the canopy may be varied along the Z direction by either pushing or pulling the canopy model inside the slot of the parent building.

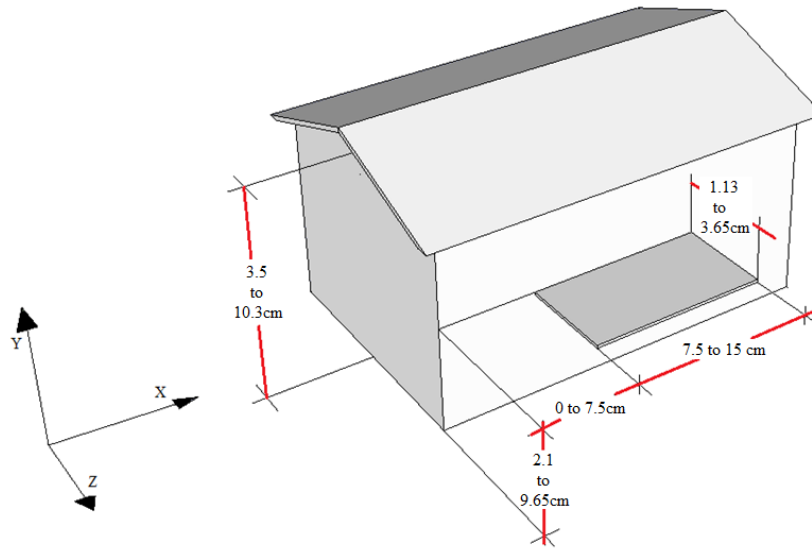


Figure 3.13 Ranges of the canopy and parent building model dimensions

3.5.3 Definition of Parameters and Configurations Tested

The adjustable model allows for a great number of configurations to be tested. In the case of a parametric study, the testing of numerous configurations is important in order to have a higher confidence in the trends observed. However, the amount of time dedicated to the experimentation and analysis of data results as a limiting factor regarding the number of configurations that can be tested. A total of 63 configurations has been esteemed to be an efficient compromise between time and dependability for this parametric study. Table 3.2 provides all of the dimensions corresponding to each individual configuration. It may be seen that each configuration is unique in at least one of the following four geometrical ratios:

-ratio of the canopy height to the eave height $\{ \frac{hc}{h} \}$

-ratio of the canopy height to the canopy width $\{ \frac{hc}{wc} \}$

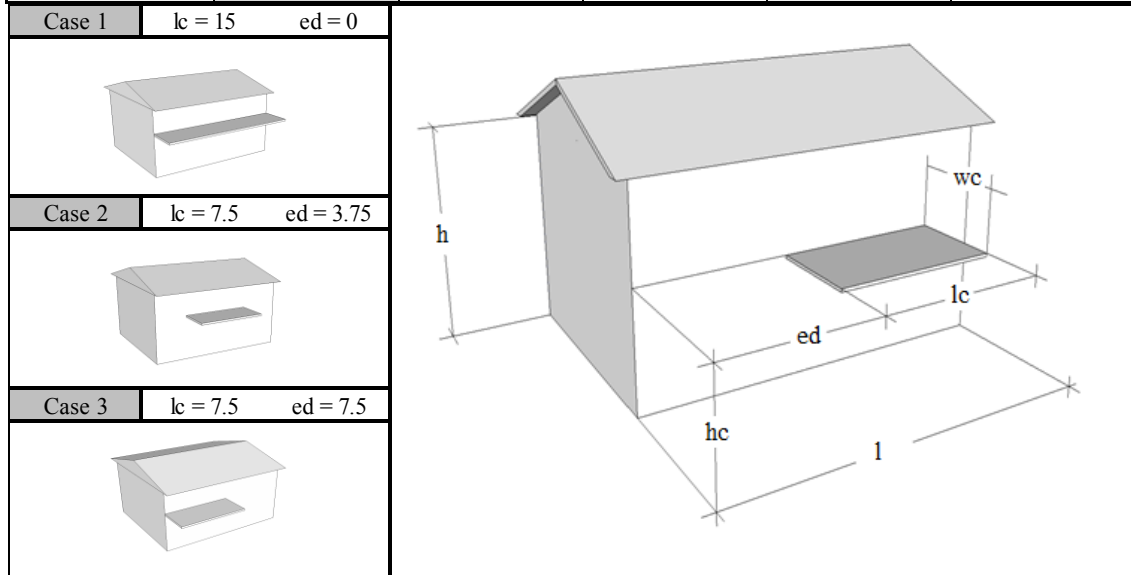
-ratio of the length of the canopy to the length of the parent wall $\{ \frac{lc}{l} \}$

-ratio of the edge distance to the canopy length $\{ \frac{ed}{lc} \}$

These ratios serve as the principal parameters for the observations of this study. Their effect on the wind loading patterns exerted on the attached canopy are presented in detail on Chapters 4 and 5.

Table 3.1 Configurations tested and definition of nomenclature used

Configuration	h	hc	wc	hc/h	hc/wc	
1	3.5	2.85	3.65	0.81	0.78	
2			2.38		1.20	
3			1.13		2.52	
4	7	6.35	3.65	0.91	1.74	
5			2.38		2.67	
6			1.13		5.62	
7	3.5	3.65	3.65	0.50	0.96	
8			2.38		1.47	
9			1.13		3.10	
10	10.3	9.65	3.65	0.94	2.64	
11			2.38		4.05	
12			1.13		8.54	
13		7	3.65	3.65	0.68	1.92
14				2.38		2.94
15				1.13		6.19
16		3.5	3.65	3.65	0.34	0.96
17				2.38		1.47
18				1.13		3.10
19	2.1	3.65	3.65	0.20	0.58	
20			2.38		0.88	
21			1.13		1.86	



CHAPTER 4

PRESSURE COEFFICIENTS ON UPPER AND LOWER SURFACES SEPARATELY

4.1 GENERAL

Canopies are often constructed as a beam and joist system to which the sheathing elements are fastened. Sheathing elements are commonly attached to the upper side of the joists (refer to Appendix A for construction plans). However, it is not uncommon to add an additional layer of sheathing underneath the joists as can be seen in Figure 4.1. When both sides of a sheathing element are unexposed to wind loads the pressures acting independently on upper and lower surfaces are essential for the design of the fastening system with the joists. Furthermore, cladding elements such as roof tiles and shingles commonly fixed to the sheathing are always exposed to wind loads in only one surface. Figure 4.2 shows a sketch illustrating the principal components of an attached canopy with sheathing elements on both upper and lower surfaces. The analyses and observations made on this section serve as the basis for their recommended design provisions. Although the failure of these components will rarely result in the complete failure of the canopy, lose sheathing and component and cladding elements may act as projectiles resulting in more significant damage to neighbouring buildings or to the parent building itself.



Figure 4.1 Canopies with sheathing attached to the lower surface of the beam and joist system

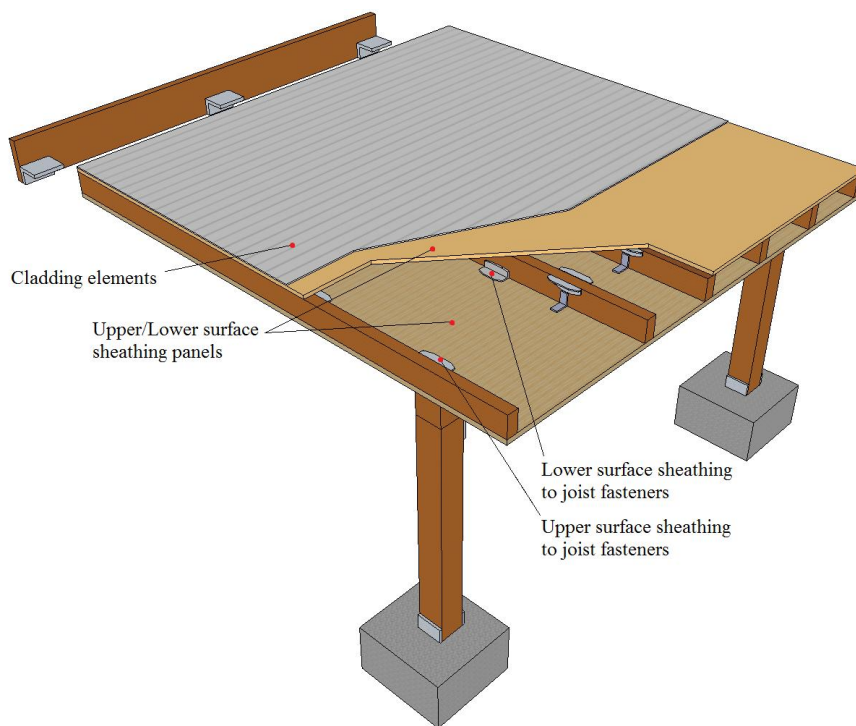


Figure 4.2 Attached canopy (not to scale) with sheathing at both upper and lower surfaces highlighting components affected by upper and lower surface pressure coefficients

4.2 EFFECT OF WIND DIRECTION ON SURFACE PRESSURES

Pressure coefficients on attached canopies may vary significantly with wind direction. A total of 28 azimuths have been examined for each of the 63 configurations. These are illustrated in Figure 4.3 where it can be noted that a 0° wind direction refers to the direction perpendicular to the containing wall and a 90° (270°) wind direction refers to the direction parallel to the containing wall.

Figures 4.4 and 4.5 display the maximum and minimum C_p values as a function of wind direction on upper and lower surfaces of the canopy. It may be observed that the peak pressure coefficients vary significantly for different wind directions. It may also be seen that the peaks do not necessarily occur at the same wind direction for upper and lower surfaces. For this reason, every peak C_p value presented in this chapter refers to its corresponding critical wind direction unless otherwise stated.

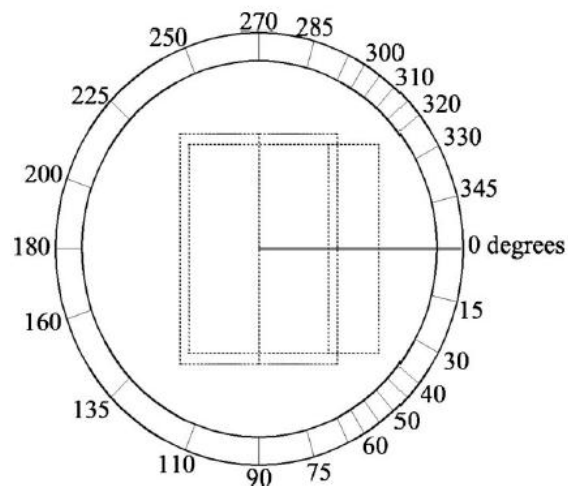


Figure 4.3 Wind directions tested for each of the 63 configurations, after Zisis (2010)

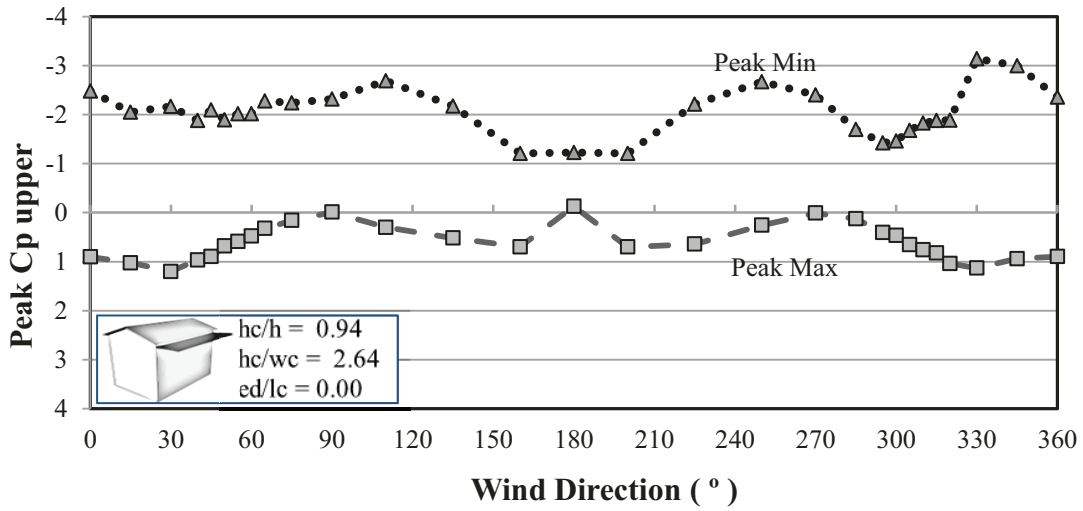


Figure 4.4 Effect of wind direction on peak minimum, and peak maximum C_p on the upper surface of a canopy extending over the full length of the parent wall

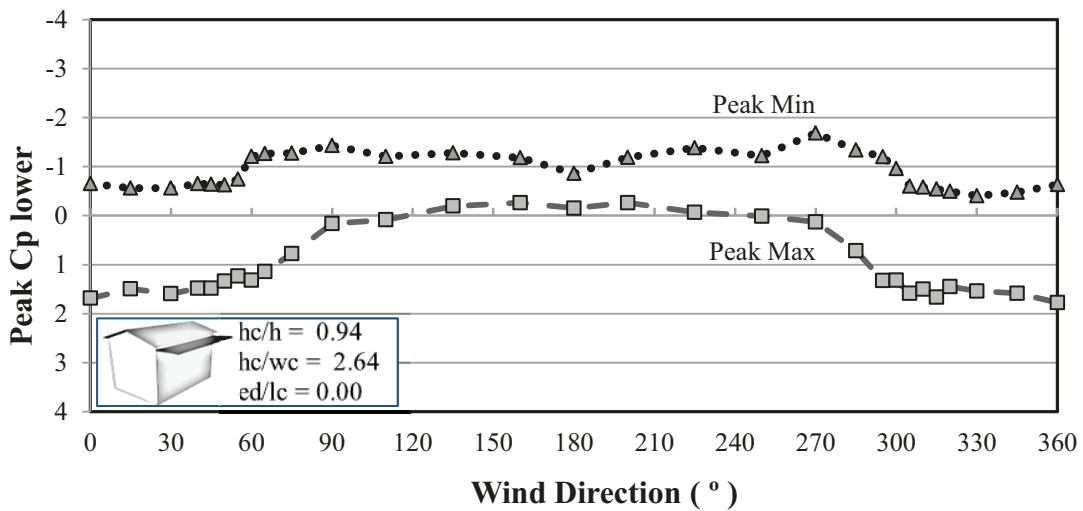


Figure 4.5 Effect of wind direction on peak minimum, and peak maximum C_p on the lower surface of a canopy extending over the full length of the parent wall

4.3 PRESSURES ON UPPER AND LOWER SURFACES

In this section the impact that each geometrical ratio has on the pressures exerted upon the canopy is examined. This is done by varying an isolated parameter while maintaining the others constant. Four dependant variables are investigated for each case: the local minimum and maximum C_p (Loc. Min. ; Loc. Max.) which refer to the critical values experienced at a single pressure tap, and the area-averaged minimum and maximum C_p (Area-avg. Min. ; Area-avg. Max.), which refer to the peak value that the entire surface experiences determined by the critical simultaneous averages at every pressure tap.

4.3.1 Effect of hc/h , hc/wc and ed/lc on the upper surface of the canopy

Peak local and area-averaged $C_{p,upper}$ values as a function of the $\frac{hc}{h}$ ratio (see Table 3.2 for definition of parameters) are presented in Figure 4.6. It can be seen that an increase in the $\frac{hc}{h}$ ratio results in an increase of the local min $C_{p,upper}$. For higher $\frac{hc}{h}$ ratios the magnitude of the local min $C_{p,upper}$ can be up to 1.8 times larger than that of lower ratios. It has also been noted that the $\frac{hc}{h}$ ratio has very little effect on the area-averaged min $C_{p,upper}$ which generally has a value near -1.0. In the case of the local and area-averaged max $C_{p,upper}$ very little change is found for lower $\frac{hc}{h}$ ratios. For $\frac{hc}{h} > 0.68$ an inversely proportional relationship has been found to occur between the max $C_{p,upper}$

and the $\frac{hc}{h}$ ratio. Additionally, it can be seen that the magnitude of the local max $C_{p,upper}$ for higher $\frac{hc}{h}$ ratios can be nearly 2 times smaller than that of a lower ratio.

Peak local and area-averaged $C_{p,upper}$ values as a function of the $\frac{hc}{wc}$ ratio are presented in Figure 4.7. It can be seen that very little change in the local and area-averaged min $C_{p,upper}$ results when the $\frac{hc}{wc}$ ratio is varied. The same can be said about the local and area-averaged max $C_{p,upper}$. In general, Figure 4.7 suggests that the magnitudes of local and area-averaged pressures on the upper surface of the attached canopy are nearly independent of the $\frac{hc}{wc}$ ratio.

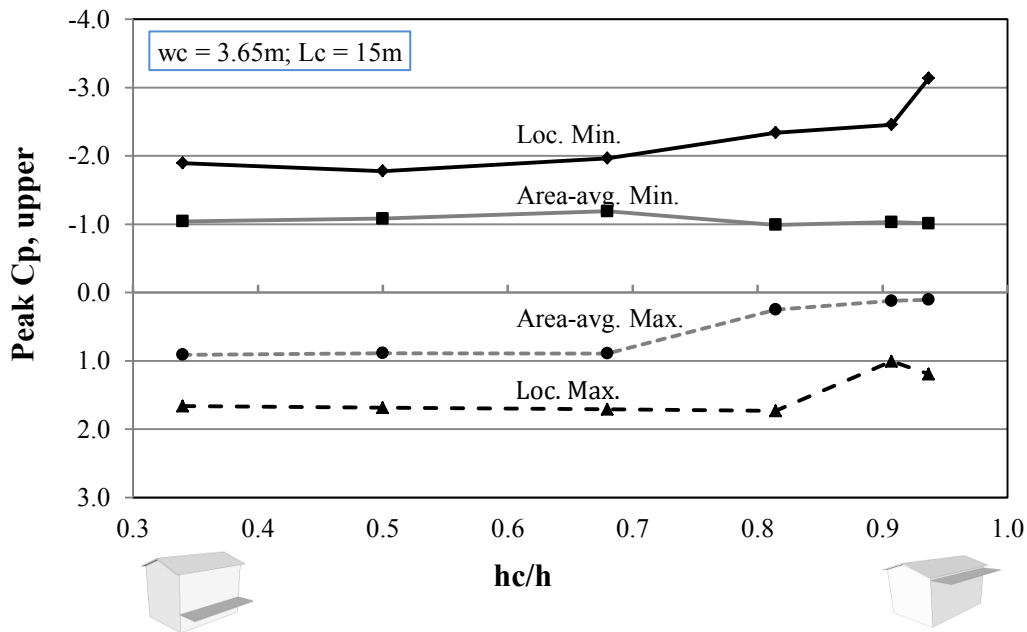


Figure 4.6 Effect of hc/h on peak local, and area-averaged $C_{p,upper}$

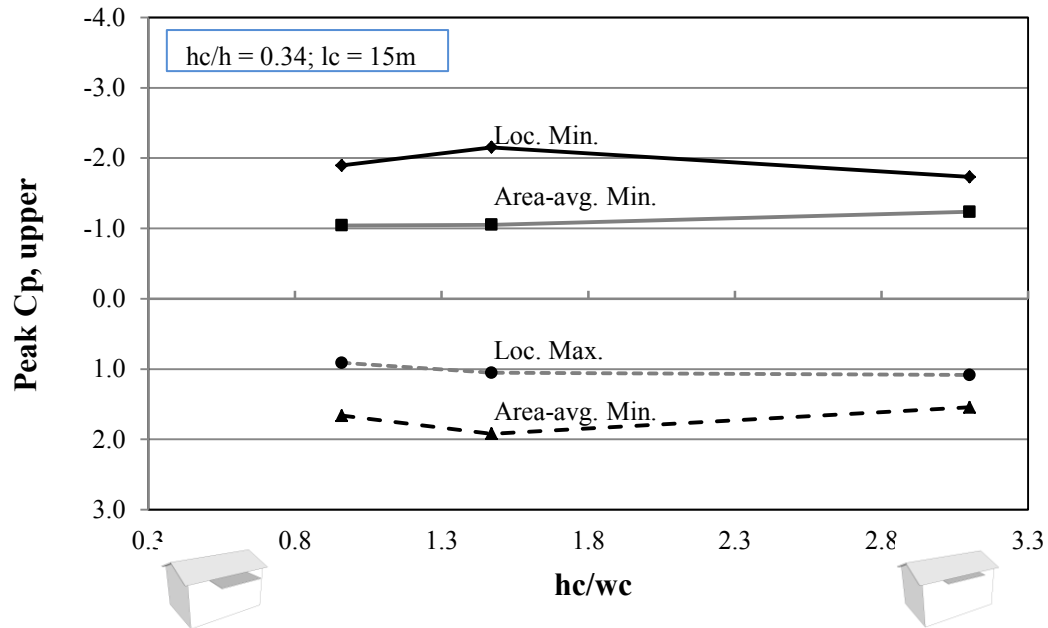


Figure 4.7 Effect of hc/wc on peak local, and area-averaged Cp_{upper}

Figure 4.8 shows the effect that the $\frac{lc}{l}$ ratio and the largest edge distance (ed) have on the local and area-averaged upper surface pressure coefficient. For the case of net pressure coefficients, the $\frac{lc}{l}$ ratio has a marked impact on the local min Cp_{upper} . It can be seen that for a canopy extending over the full length of the parent wall ($\frac{lc}{l} = 1$; $\frac{ed}{lc} = 0$) the magnitude of the highest local suction may be 1.5 times higher than that for canopies extending over half the length ($\frac{lc}{l} = 0.5$). On the contrary, very little difference is observed between a canopy placed at the corner of the parent wall and one placed at the center. It may also be noted that area averaged min Cp_{upper} as well as local and area averaged max Cp_{upper} display little or no sensitivity to the $\frac{lc}{l}$ and the $\frac{ed}{lc}$ ratios.

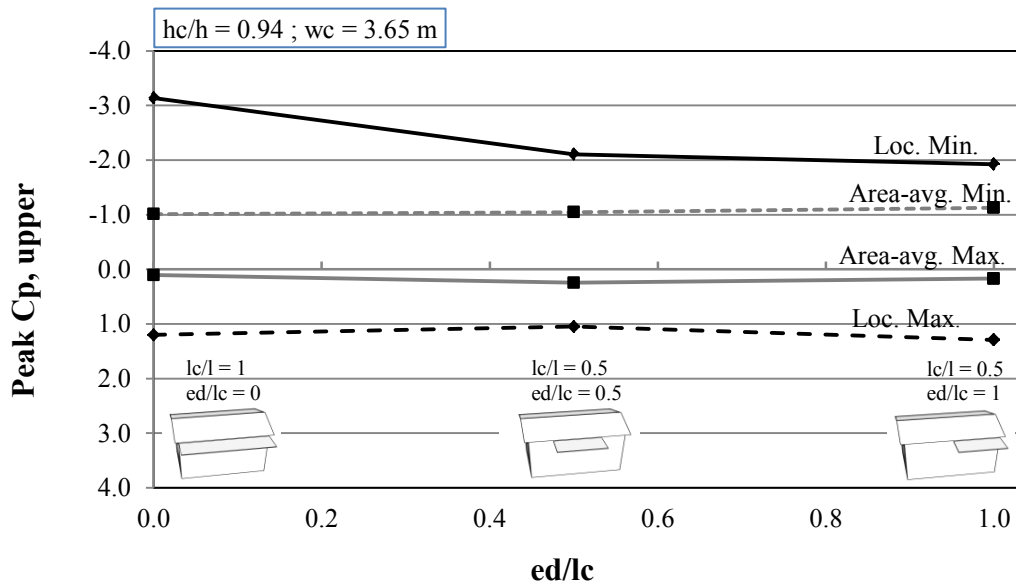


Figure 4.8 Effect of length and edge distance on peak local and area-averaged $C_{p,upper}$

4.3.2 Effect of hc/h , hc/wc and ed/lc on the lower surface of the canopy

Peak local and area-averaged $C_{p,lower}$ values as a function of the $\frac{hc}{h}$ ratio are presented in Figure 4.9. It can be seen that both local and area-averaged min $C_{p,lower}$ display very little sensitivity to the $\frac{hc}{h}$ ratio. The highest local min $C_{p,lower}$ amongst the configurations shown has a value of -1.75 whereas the lowest value was -1.43. The Area-averaged min $C_{p,lower}$ generally has a value of around -1.0 regardless of the $\frac{hc}{h}$ ratio. This is consistent with what was seen for the area-averaged suction on the upper surface of the canopy. Similarly, it can be seen that the area-averaged max $C_{p,lower}$ displays little sensitivity to changes in the $\frac{hc}{h}$ ratio. Additionally, these variations are small and do not

occur in a well-defined trend. The local max $Cp_{,lower}$ also displays little sensitivity to the $\frac{hc}{h}$ ratio, however, the magnitudes increase slightly as the ratio is increased. It can be concluded from Figure 4.9 that the magnitudes of local and area-averaged pressures on the lower surface of the attached canopy are nearly unaffected by the variation of the $\frac{hc}{hc}$ ratio.

Peak local and area-averaged $Cp_{,lower}$ as a function of the $\frac{hc}{wc}$ ratio are shown in Figure 4.10. It can be seen that both local and area-averaged min $Cp_{,lower}$ display a slight direct proportionality with the $\frac{hc}{wc}$ ratio. However, little sensitivity is seen since the largest local min $Cp_{,lower}$ has a value that is only 1.10 times larger than the smallest. In the case of the local and area-averaged max $Cp_{,lower}$ the same slight direct proportionality with the $\frac{hc}{wc}$ ratio can be observed. The largest local max $Cp_{,lower}$ is only 1.15 times larger than the smallest shown. It can be concluded that the local and area-averaged pressures on the lower surface of the attached canopy are nearly independent of the $\frac{hc}{wc}$ ratio.

Figure 4.11 shows local and area-averaged lower surface pressure coefficients as a function of the $\frac{ed}{lc}$ ratio. It can be seen that both local and area averaged minimum and maximum $Cp_{,lower}$ appear to be unaffected by the $\frac{lc}{l}$ ratio and the largest edge distance (ed).

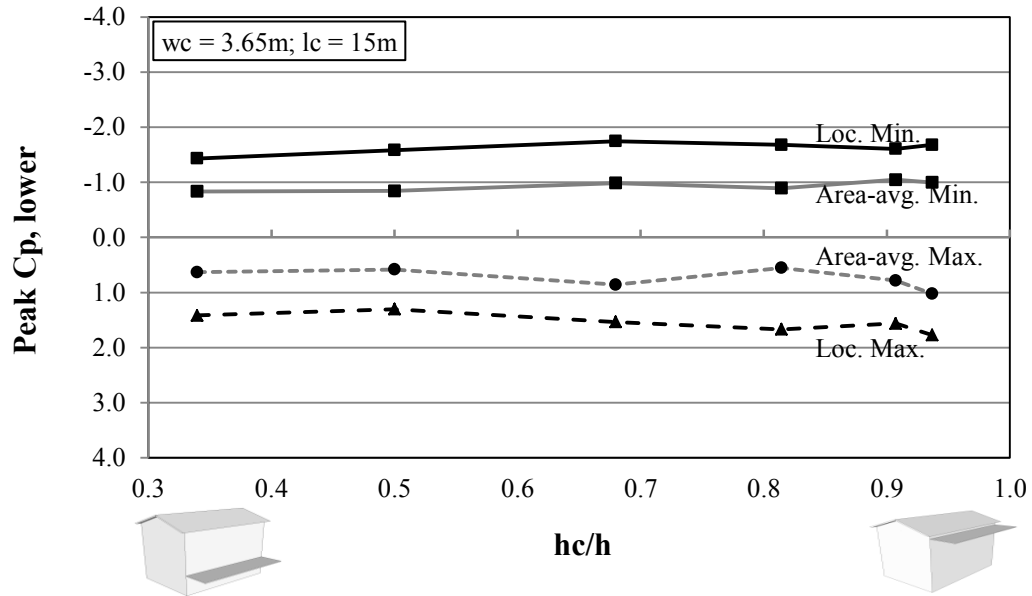


Figure 4.9 Effect of hc/h on peak local, and area-averaged $C_{p,lower}$

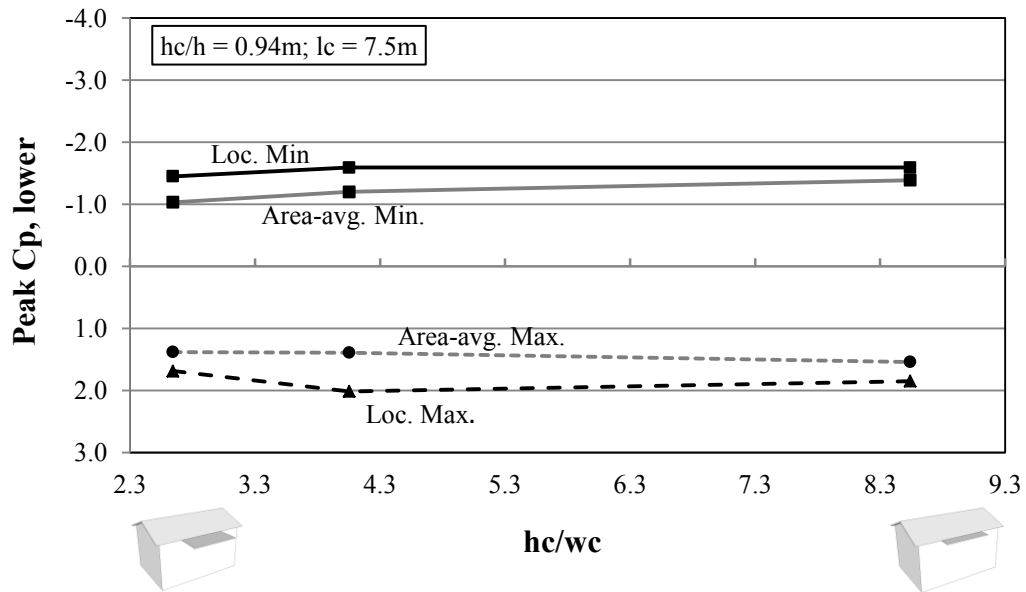


Figure 4.10 Effect of hc/wc on peak local, and area-averaged $C_{p,lower}$

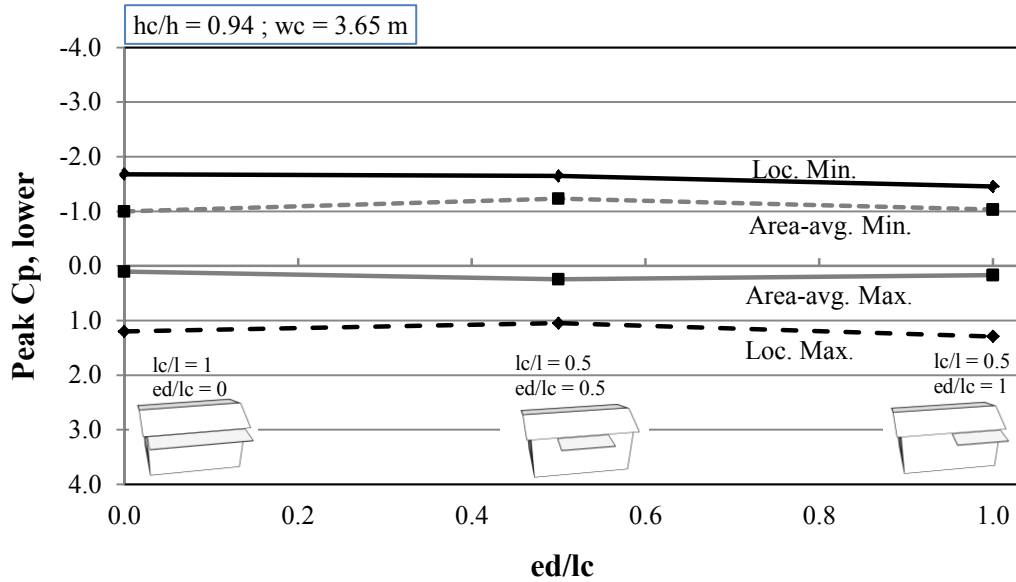


Figure 4.11 Effect of length and edge distance on peak local and area-averaged $C_{p,lower}$

4.4 LOCAL PRESSURE COEFFICIENTS ON REGIONS OF UPPER AND LOWER SURFACES

Local C_p values have been found to differ considerably at different locations within the attached canopy. It has been seen that higher uplifting forces occur at the leading edge and corner regions, where separation of flow occurs, as opposed to the interior regions, where lower suctions and higher pressures are to be expected due to the proximity to the stagnation points in the parent wall. This is an important aspect to be considered for the design of component and cladding elements, such as fasteners and roofing shingles or tiles.

The surface of the attached canopy has been divided into three regions: corner, edge and interior. The schematic in Figure 4.12 defines the limits of each region. A local peak C_p associated to a region refers to the highest magnitude C_p found in any single pressure tap inside that region.

Peak local pressure coefficients acting at the different regions of the upper surface of the canopy are given on Figure 4.13 as a function of the $\frac{hc}{h}$ ratio. It can be seen that for $\frac{hc}{h} \leq 0.68$ there is very little difference between the highest $\min C_{p,upper}$ occurring at the different regions. In contrast, for $\frac{hc}{h}$ ratios larger than 0.68 the difference is significant. The highest suction at the corner region is 1.2 times larger than the highest suction at the edge region and nearly 2 times larger than that of the interior region. In the case of the $\max C_{p,upper}$ there is very little difference between the peaks occurring in the interior and edge regions regardless of the $\frac{hc}{h}$ ratio. In the corner regions, however, a marked reduction is observed.

Peak local pressure coefficients acting at the different regions of the lower surface of the canopy are given on Figure 4.14 as a function of the $\frac{hc}{h}$ ratio. The peak $\min C_{p,lower}$ appear to occur with similar magnitudes in any of the three regions and no clear trend can be identified. In the case of the $\max C_{p,lower}$ there is very little difference between the magnitudes of the peaks occurring at the edge and interior region, and once again these are generally higher than the peaks occurring at the corners.

Tabulated results for peak pressure coefficients at the different regions of the canopy are provided in Appendix B1 for every configuration tested in this study.

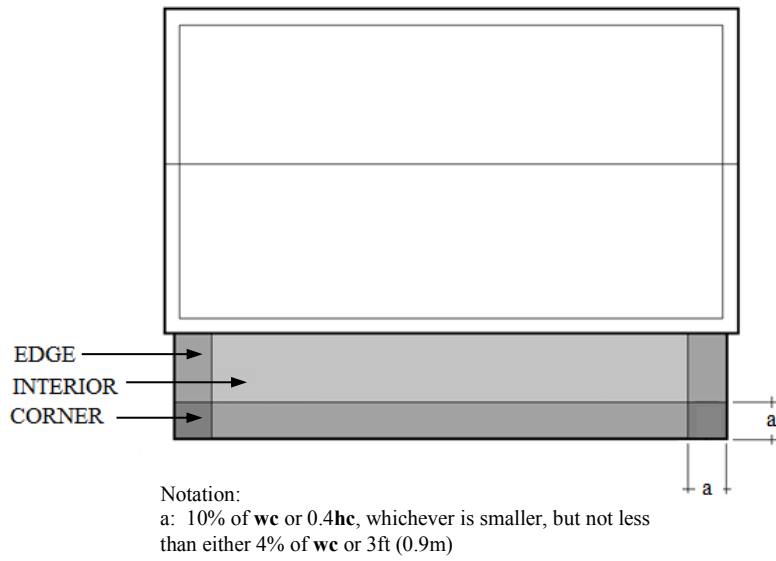


Figure 4.12 Division of regions on the attached canopy (adapted from ASCE 7-10 for flat low-pitch roofs)

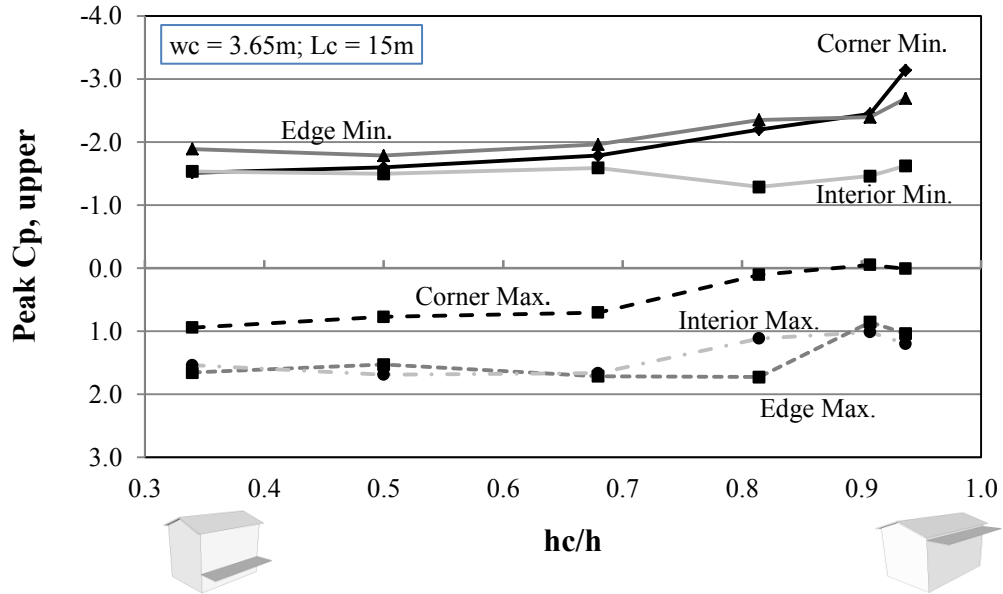


Figure 4.13 Peak local $C_{p, upper}$ at different regions of the canopy as a function of hc/h

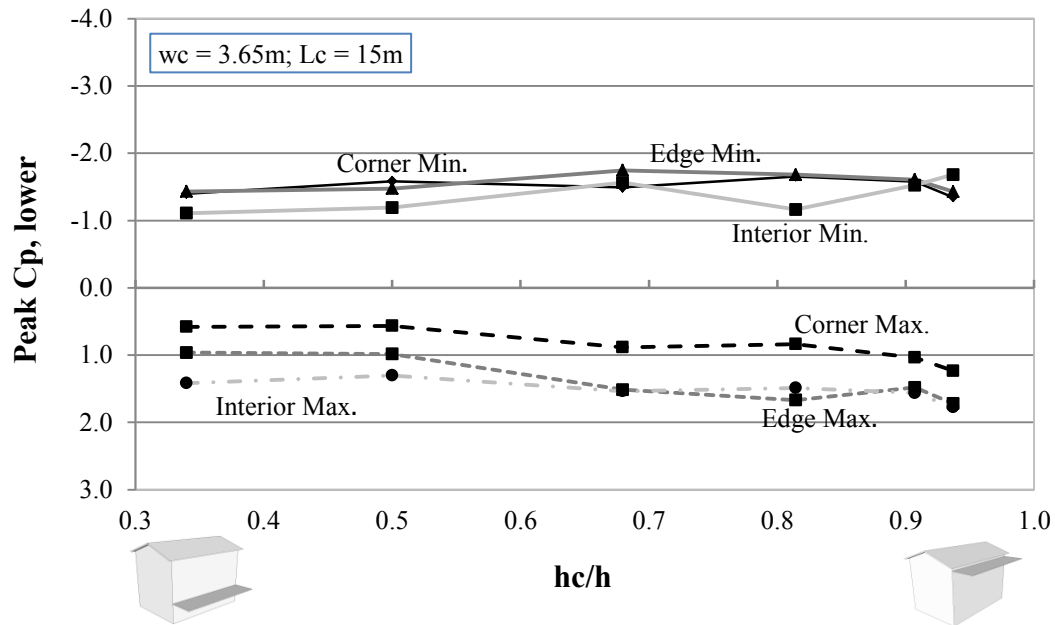


Figure 4.14 Peak local Cp_{lower} at different regions of the canopy as a function of hc/h

4.5 ENVELOPES OF PPRESSURE COEFFICIENTS ON UPPER AND LOWER SURFACES

The area-averaging effect has been assessed for the pressures acting on both upper and lower surfaces of the canopy separately by averaging the peak pressures experienced at increasing numbers of adjacent pressure tabs and assigning them to their corresponding tributary area. Figure 4.15 shows the peak suction acting on the upper surface (min Cp_{upper}) as a function of their corresponding tributary area for each of the 63 configurations tested. Each graph contains the 21 area-averaging curves obtained for the corresponding Case (see Table 3.2). Envelope lines for each of the three cases have been

superimposed into the corresponding graphs. It can be noted that the envelope line for the curves of Case 1 is significantly higher than for the other two cases.

The same approach was followed for the suctions acting on the lower surface of the canopy. Figure 4.16 shows the peak min $Cp_{,lower}$ as a function of their corresponding tributary area for every configuration tested. It can be noted once again that the envelope line for the curves of Case 1 is significantly higher than that of Cases 2 and 3.

The monotonically decreasing relationship between the tributary area and the magnitudes of the peak pressure coefficients is observed for every configuration tested. In addition, the significant difference in the magnitudes of the envelope for Case 1 with the envelopes of Cases 2 and 3, suggests that the peak min $Cp_{,upper}$ and $Cp_{,lower}$ are sensitive to the the $\frac{lc}{l}$ ratio which is consistent with what was seen in Figure 4.8.

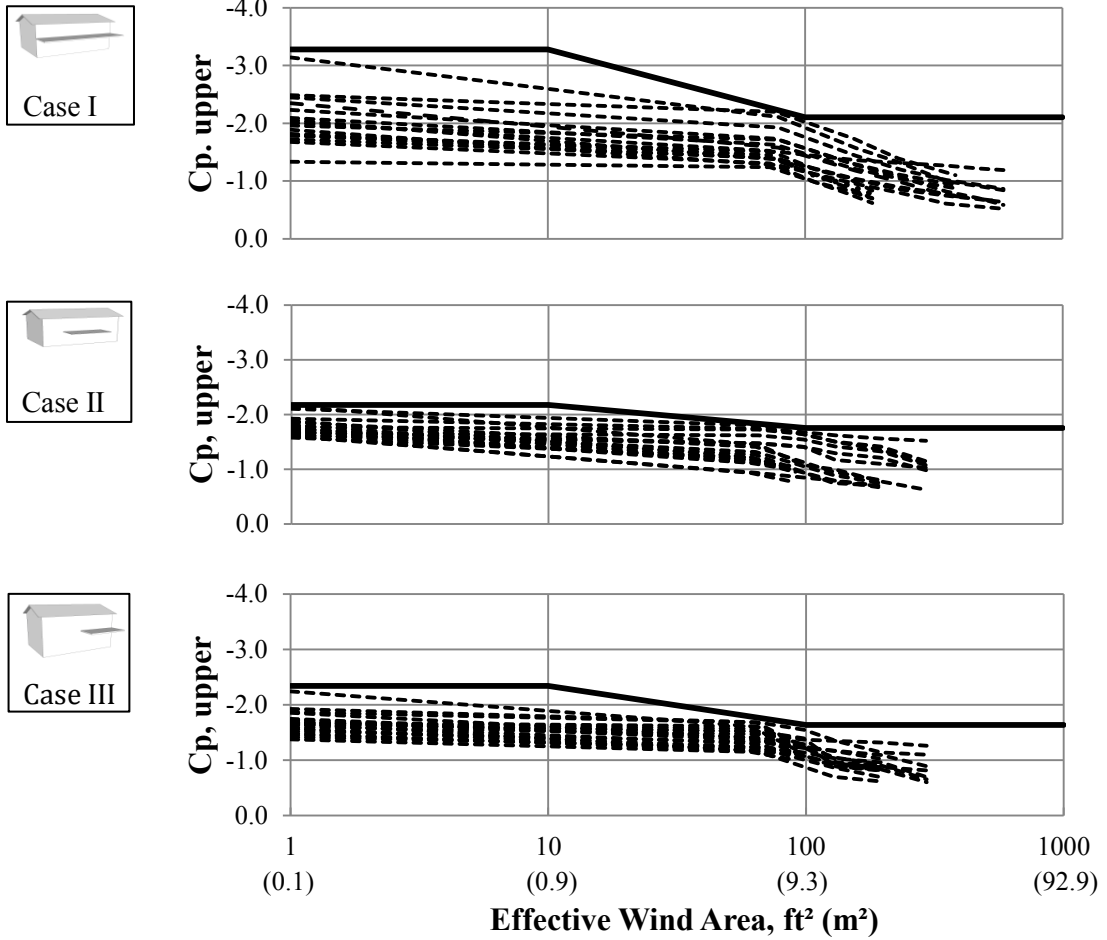


Figure 4.15 Area-averaging effect and corresponding envelopes for the upper surface of the canopy on all configurations tested

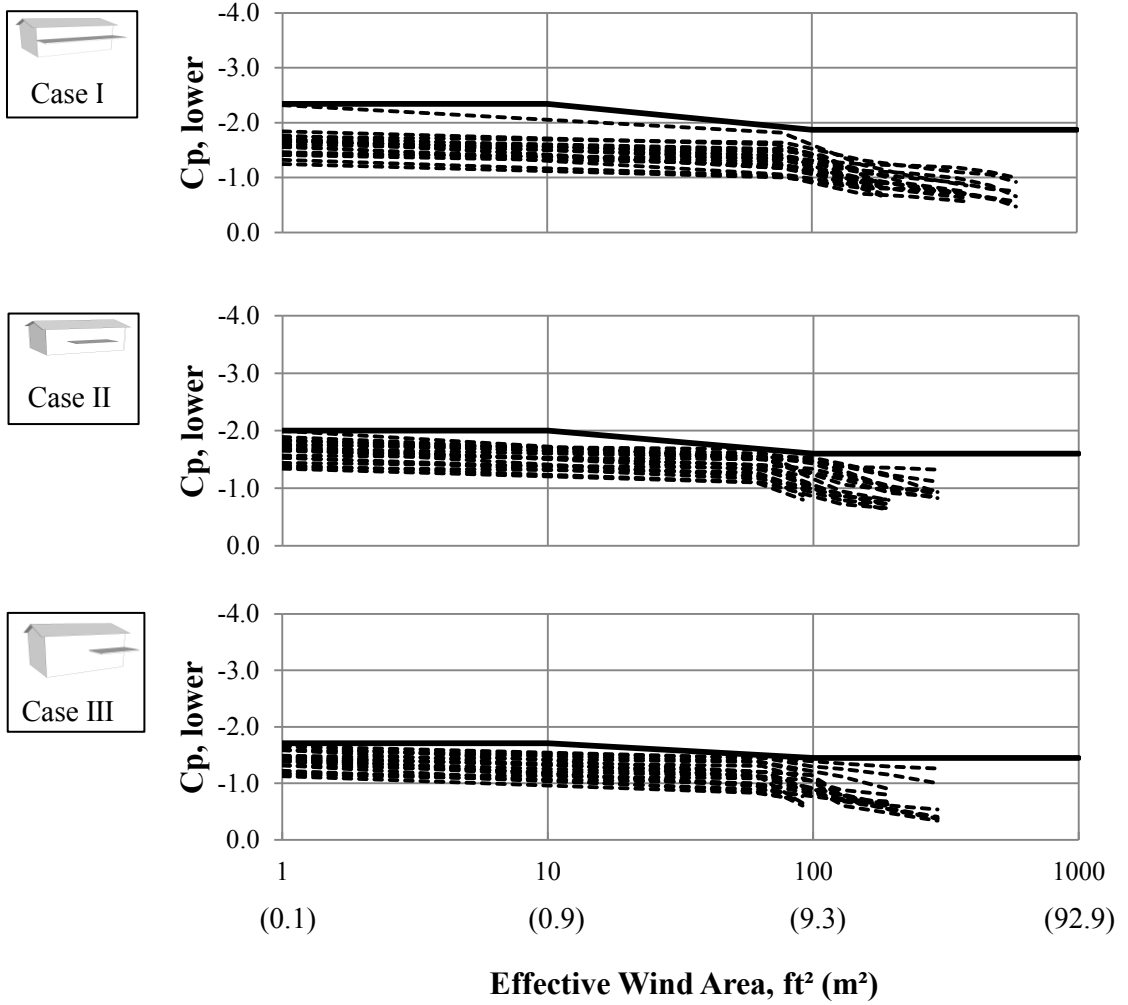


Figure 4.16 Area-averaging effect and corresponding envelopes for the lower surface of the canopy on all configurations tested

The most critical envelopes for the min Cp_{upper} and min Cp_{lower} as a function of the tributary area are presented together in Figure 4.17. These envelopes have both been obtained for Case 1, which represents a canopy extending over the entire length of the parent wall ($\frac{lc}{l} = 1$). Local suction forces at the lower surface of the canopy are considerably lower than those at the upper surface, whereas a smaller difference can be seen as the effective area is increased.

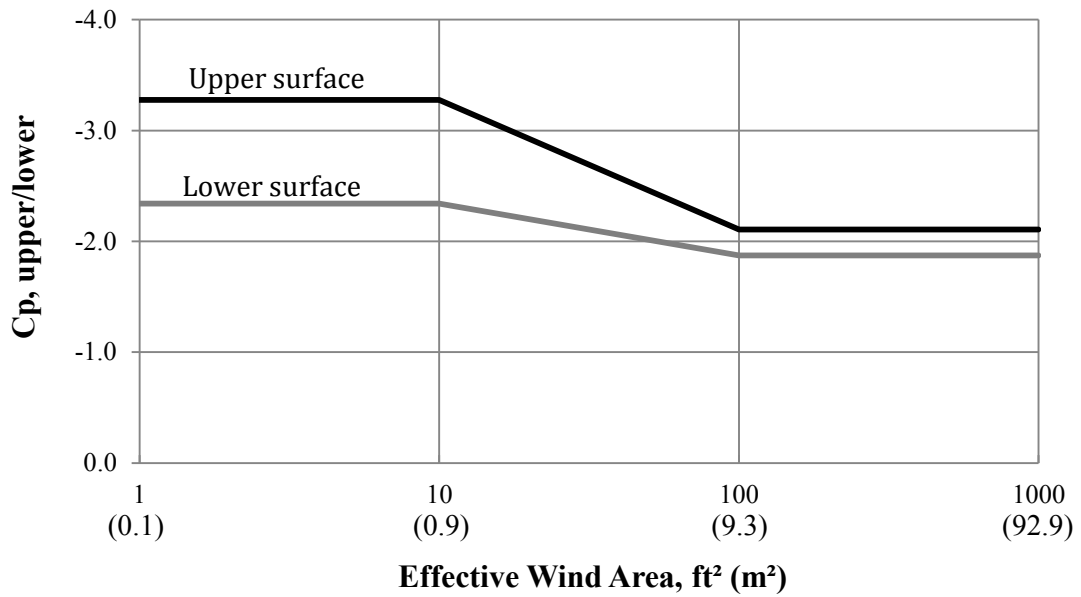


Figure 4.17 Envelopes for pressure coefficients as a function of effective areas at upper and lower surfaces of all 63 configurations combined

CHAPTER 5

NET PRESSURE COEFFICIENTS ON ATTACHED CANOPIES

5.1 GENERAL

Attached canopies are exposed to wind loads on both upper and lower surfaces simultaneously. Pressures applied to the sheathing elements are transferred to the main structural components of the canopy, namely the joists, header beam and the columns. This section focuses on the peak local and area-averaged net loads experienced by the canopy for different geometrical configurations. Figure 5.1 shows a sketch illustrating the principal components of a conventional canopy attached to a low-rise structure. The analyses and observations made on this section serve as the basis for the design of the labeled components. Detailed construction plans of conventional wooden canopies attached to low rise structures are provided in Appendix A.

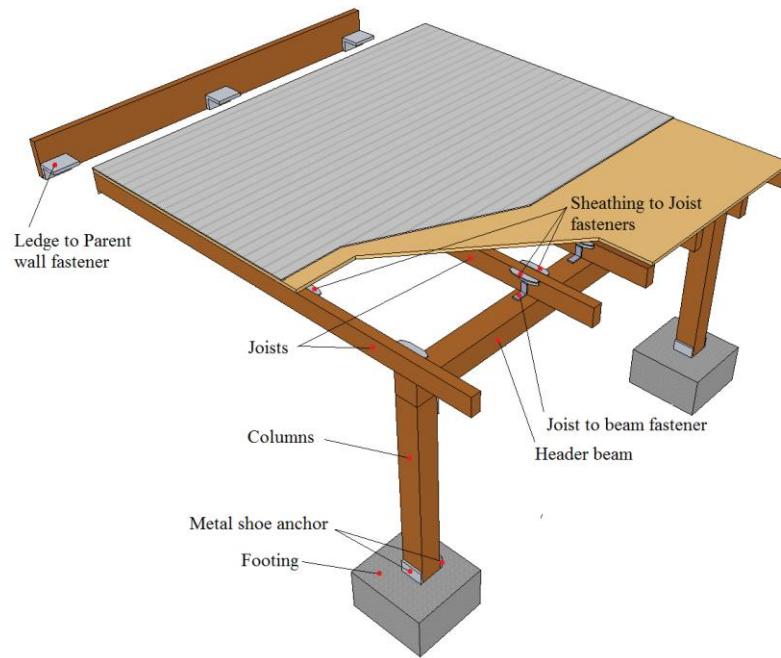


Figure 5.1 Drawing of a conventional canopy attached to a low rise building (not to scale) indicating the components affected by net loads

5.2 EFFECT OF WIND DIRECTION ON CRITICAL NET PRESSURE COEFFICIENTS

It has been seen that pressure coefficients on attached canopies may vary significantly with wind direction. A total of 28 azimuths have been examined for each of the 63 configurations (see Figure 4.3). It can be noted that a 0° wind direction refers to the direction perpendicular to the containing wall and a 90° (270°) wind direction refers to the direction parallel to the containing wall.

Figures 5.2 and 5.3 display the maximum, minimum and mean $C_{p,net}$ values as a function of wind direction for two different configurations (refer to Appendix B2 for

other configurations). For a canopy extending over the entire length of the parent wall as shown in Figure 5.2 it can be seen that the highest magnitudes for peak minimum $Cp_{,net}$ values occur at the 330° (30°) wind direction. The highest peak maximum $Cp_{,net}$ occurs at the 225° (135°) wind direction. In addition, the lowest magnitudes for both maximum and minimum $Cp_{,net}$ values were found to occur when the canopy is placed at the leeward wall (180°). It must be noted that peak $Cp_{,net}$ values display a great sensitivity to wind direction. In the configuration examined, the peak minimum $Cp_{,net}$ obtained at 330° (30°) degrees is more than five times that encountered at 180°.

In the case presented in Figure 5.3 for a canopy extending half the length of the parent wall and placed eccentrically along the length of the parent wall, a very different behavior is observed. The highest magnitude peak minimum $Cp_{,net}$ values are found to occur for wind directions running parallel to the building ridge 90° (270°) and the highest peak maximum $Cp_{,net}$ values occur at wind directions nearly perpendicular to the ridge 15° (345°). As in the previous case, the lowest magnitudes for both maximum and minimum $Cp_{,net}$ values were found to occur when the canopy is placed at the leeward wall.

It can thus be concluded that wind direction has a significant impact on the peak $Cp_{,net}$. Figure 5.4 shows the critical wind directions for all of the 63 configurations separately for Cases I, II, and III. It can be seen that different wind directions result as critical for different configurations. For this reason, every peak $Cp_{,net}$ value presented in this chapter refers to its corresponding critical wind direction unless otherwise stated.

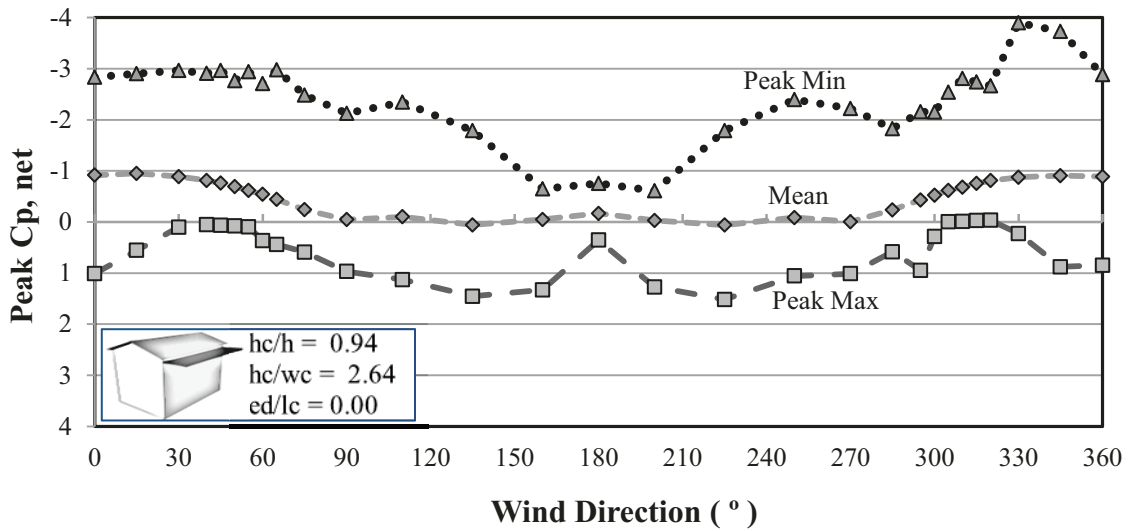


Figure 5.2 Effect of wind direction on peak minimum, peak maximum and mean $C_{p,net}$ for a canopy extending over the full length of the parent wall

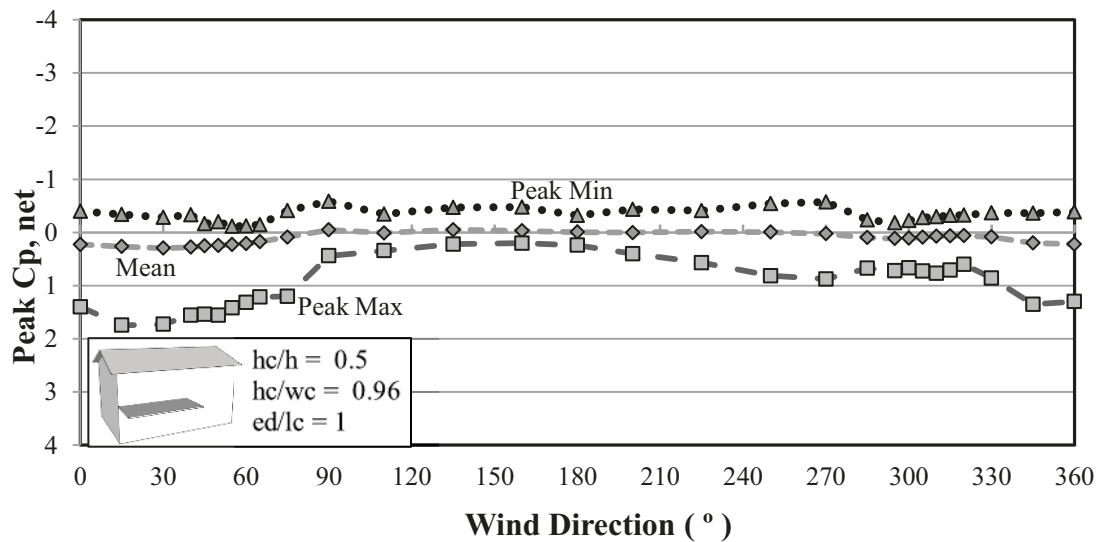
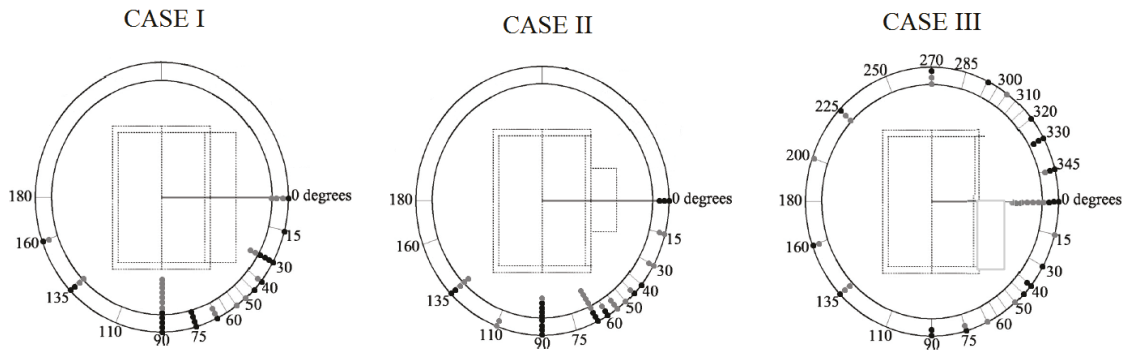


Figure 5.3 Effect of wind direction on peak minimum, peak maximum and mean $C_{p,net}$ for an eccentrically placed canopy extending over half of the length of the parent wall



- Wind direction at occurrence of C_p , Peak (min)
- Wind direction at occurrence of C_p , Peak (max)

Figure 5.4 Wind directions at the occurrence of minimum and maximum peak C_p , net

5.3 VISUALIZATION OF FLOW AROUND THE CANOPY

Flow visualization experiments have been performed for a canopy attached at both the mid height, and near the eave height of the parent wall. Still shots for zero degree wind direction are provided in Figures 5.5 and 5.6 for these configurations. For a canopy attached at the mid height, stagnation of flow occurs at the parent wall both above and below the canopy. Stagnation of flow above the canopy will result in a downward flow running along the surface of the parent wall which will ultimately inflict a downward force on the upper surface of the canopy. Stagnation of flow in the parent wall underneath the canopy will in turn generate flow directed towards the lower surface of the canopy resulting in an upward force. These two counteracting forces at upper and lower surfaces are expected to result in a decreased net uplifting pressure coefficient (min $C_{p,net}$).

In the case of a canopy attached closer to the eave height, flow stagnates more significantly at the parent wall underneath the canopy (see Figure 5.6) resulting in a dominating upwards flow which generates a force directed towards the lower surface of the canopy. In contrast, high levels of flow separation occur at the upper surface of the canopy resulting in dominating suction. The combination of high suction acting on the upper surface and high pressures on the lower surface is expected to result in an increased uplifting force, i.e. a higher net uplifting pressure coefficient.

It can thus be expected that the higher the location of the canopy along the parent wall, i.e. the higher the $\frac{hc}{h}$ ratio, the higher the net uplifting pressures will be. Conversely, it may also be expected that higher net downward forces occur for lower $\frac{hc}{h}$ ratios.

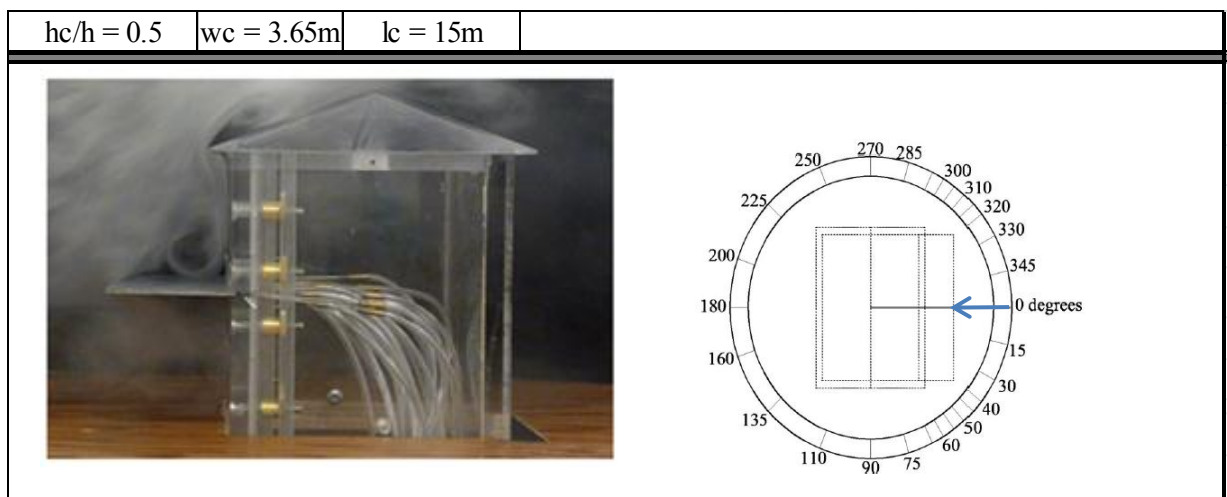


Figure 5.5 Flow visualization for a canopy attached at the mid height of the parent wall and a zero degree azimuth

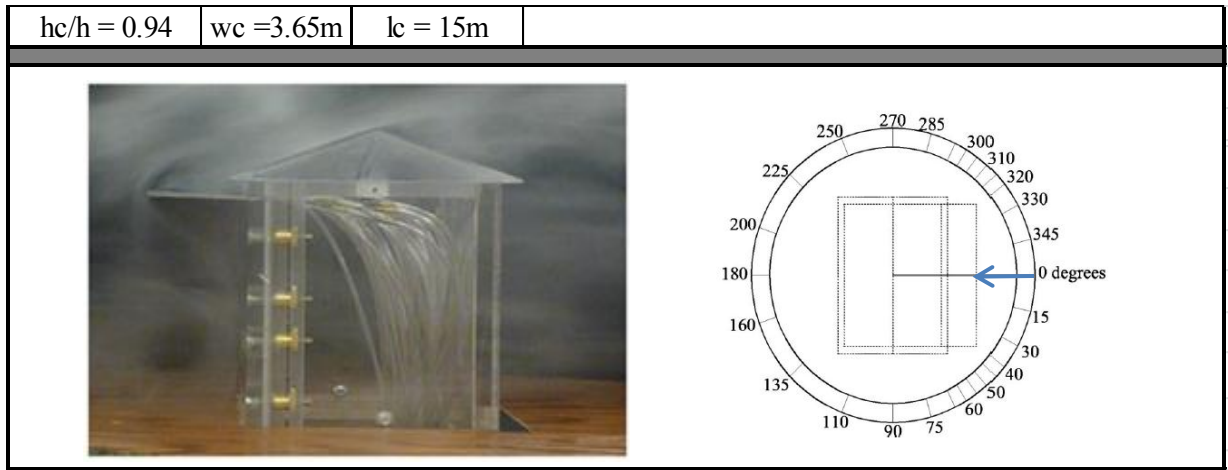


Figure 5.6 Flow visualization for a canopy attached close to the eave height of the parent wall and a zero degree azimuth

5.4 NET PRESSURES AND CORRELATION COEFFICIENTS

Instrumentation of the canopy model with pressure taps at both upper and lower surfaces allows for the monitoring of pressure coefficients at either surface separately (Cp_{upper} ; Cp_{lower}) or their simultaneous effect at the same position of the canopy (Cp_{net}). This provides the possibility of a clearer understanding of the wind loading patterns that the attached canopy is exposed to. Pressure and correlation coefficient contour plots for a canopy attached to both the mid height, and eave height of the parent wall are given in Figures 5.7 and 5.8, respectively, again for a zero degree wind direction. Figure 5.7 shows that for a wind direction perpendicular to the parent wall the upper surface of the canopy experiences downward loading of higher magnitudes than the suction. In the bottom surface pressures are significantly higher than suction as well. It must be noted however that despite having a peak max Cp_{lower} of more than 1.20, the

peak min $Cp_{,net}$ was found to be -0.20. This phenomenon of counteracting forces can be further observed by the correlation coefficient contour plot (see Figure 5.7) exhibiting a high positive value between upper and lower surfaces of the canopy. It can be seen that the combined effect of pressures acting on upper and lower surfaces of canopies placed far from the eave (lower $\frac{hc}{h}$ ratios) will result in significant reductions to the loads experienced in either side, thus resulting in a reduced min $Cp_{,net}$.

In contrast, it can be seen from Figure 5.8 that for a canopy placed closer to the eave height dominant suction occurs on the upper surface in combination with dominant pressures on the lower surface. The high suction in the upper surface, particularly along the corners and leading edges, are attributed to the phenomenon of flow separation (refer

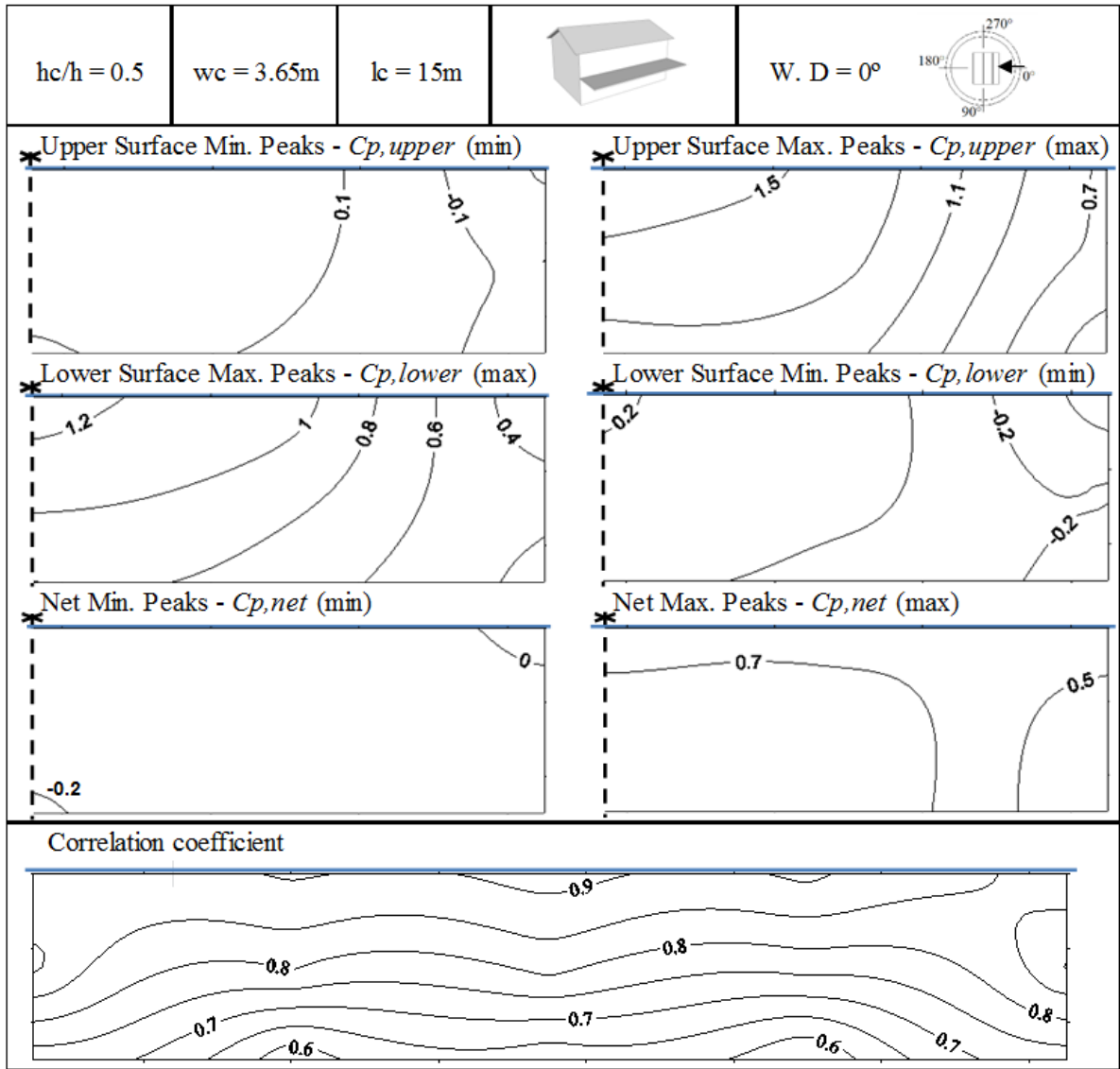


Figure 5.7 Pressure and correlation coefficient contour plots for a canopy attached at the mid height of the parent wall and a zero degree azimuth

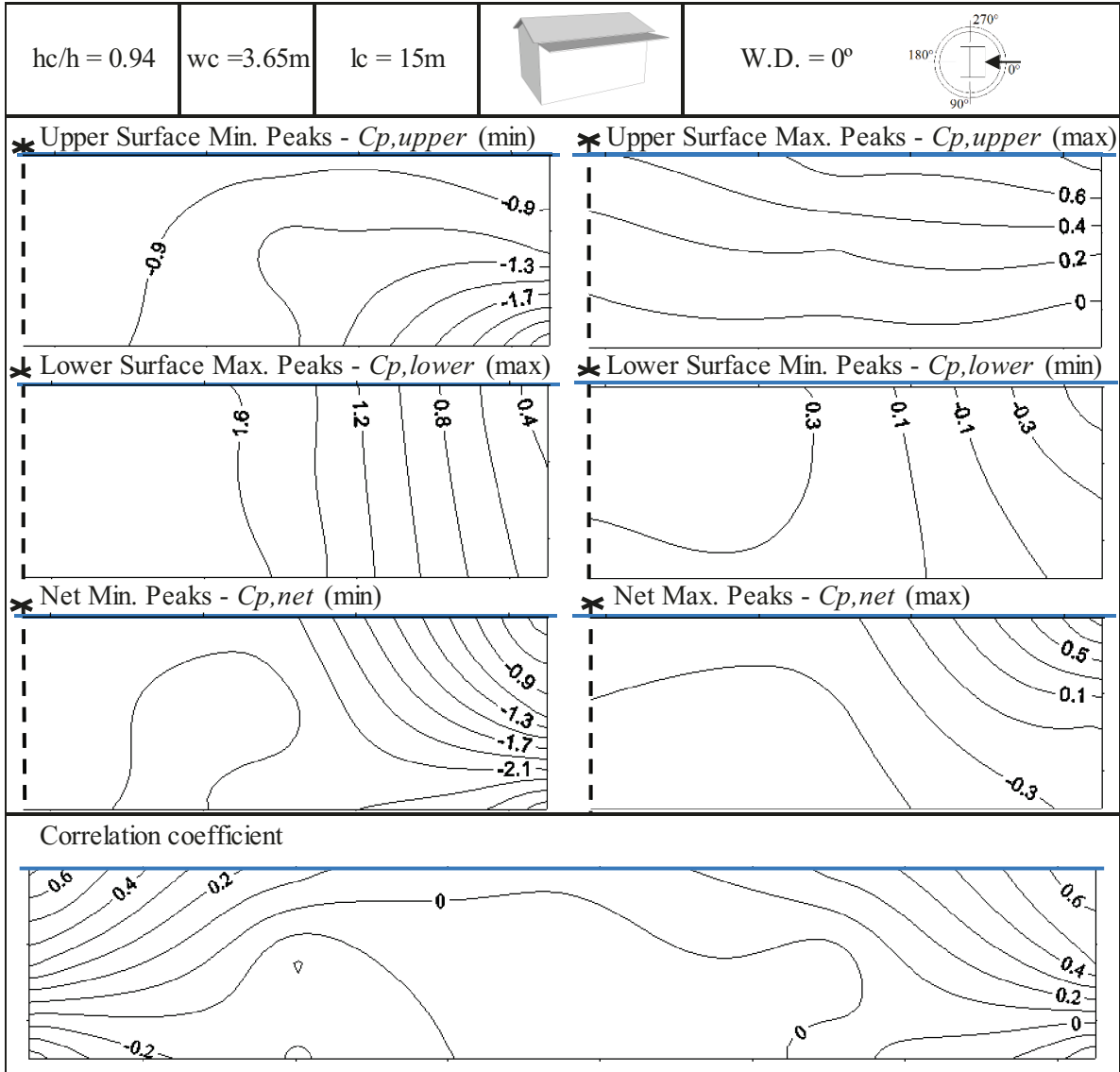


Figure 5.8 Pressure and correlation coefficient contour plots for a canopy attached close to the eave height of the parent wall and a zero degree azimuth

to Figure 5.6 for flow visualization photograph). The dominant high pressures on the lower surface of the canopy result from the upward flow generated by the stagnation of flow underneath the surface of the canopy. In this case a peak min $Cp_{,upper}$ of -2.30, in combination with a peak max $Cp_{,lower}$ of 0.60, results in a peak min $Cp_{,net}$ of -2.70. The correlation coefficients for this configuration range from weak to zero implying that the high suction occurring at the upper surface of the canopy do not occur in a well-defined pattern with the positive pressures in the lower surface of the canopy. This can be reflected by the fact that the min $Cp_{,net}$ value is increased, but only by a small amount over the individual contribution of the min $Cp_{,upper}$ and max $Cp_{,lower}$ to the net uplifting forces on the canopy. Despite their weak correlation, the combined effect of the high suction and high pressure contributions at upper and lower surfaces respectively, result in an increase min $Cp_{,net}$ for higher $\frac{hc}{h}$ ratios.

It has been seen, however, that peak $Cp_{,net}$ values do not necessarily occur at wind directions perpendicular to the length of the canopy. Pressure and correlation coefficient contour plots for a canopy attached at the mid height of the parent wall are given in Figure 5.9 for the critical wind direction. When compared to the contours for a zero degree wind direction for the same configuration (refer to Fig. 5.7) it can be seen that the peak min $Cp_{,upper}$ is significantly increased at the leftmost corner and the peak max $Cp_{,lower}$ is decreased. Furthermore, the correlation coefficient at the same corner has been decreased. As a result, the peak min $Cp_{,net}$ has been increased by more than 4 times the magnitude of that found for the zero degree wind direction.

Pressure and correlation coefficient contour plots for a canopy attached near the eave height of the parent wall are given in Figure 5.10 for the critical wind direction.

When compared to the contours for a zero degree wind direction for the same configuration (refer to Fig. 5.8) it can be seen that the min Cp_{upper} and max Cp_{lower} are significantly increased at the rightmost corner. It may be also seen that the correlation coefficient is slightly increased. As a result the min Cp_{net} is increased by nearly 1.5 times the magnitude of that found for the zero degree wind direction. It is to be noted that the peak min $Cp_{net} = -3.89$ recorded was the largest observed for any configuration examined. Additional contour plots for Cases II and III are provided in Appendix B3.

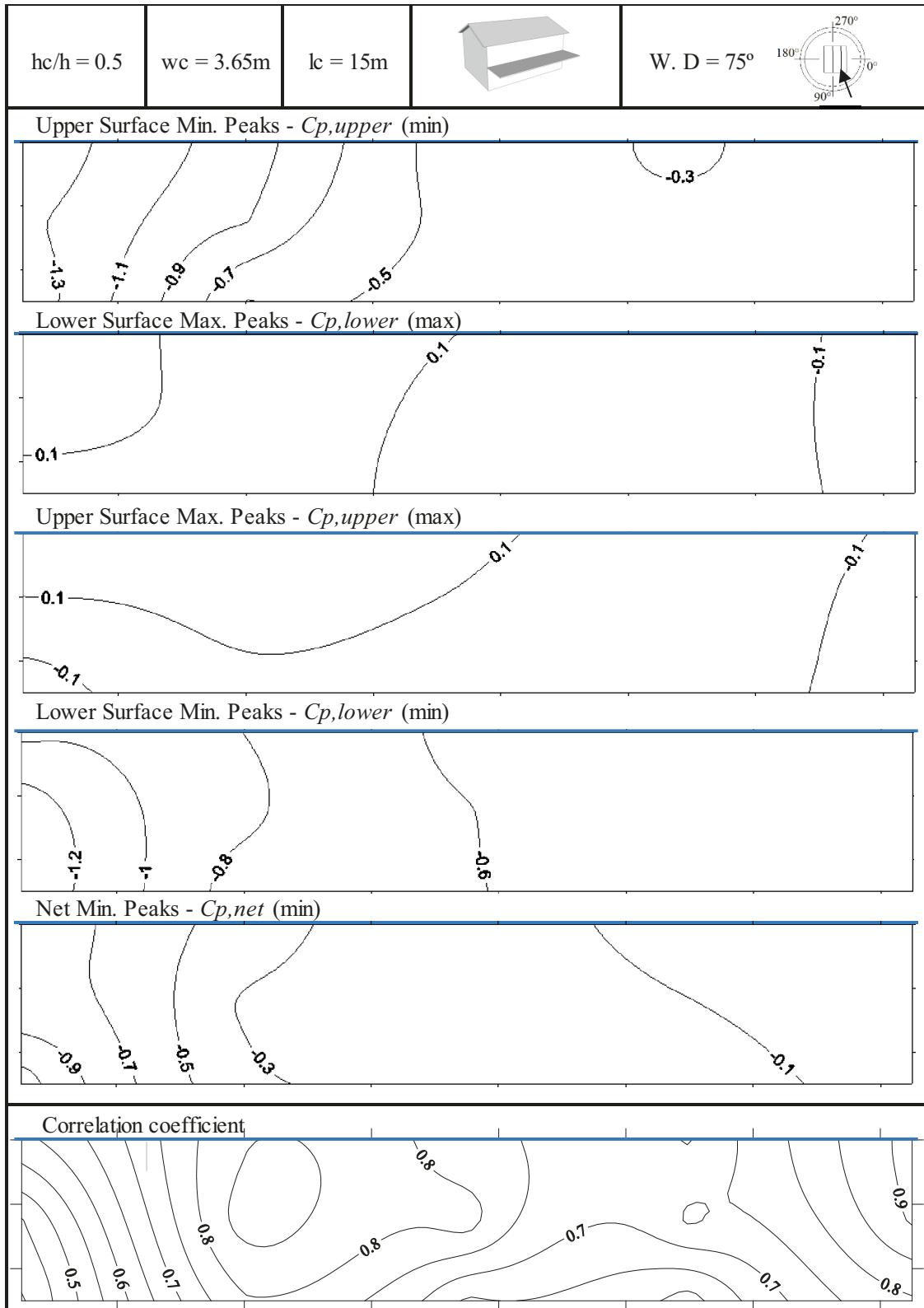


Figure 5.9 Pressure and correlation coefficient contour plots for a canopy attached at the mid height of the parent wall and the critical wind direction (75°)

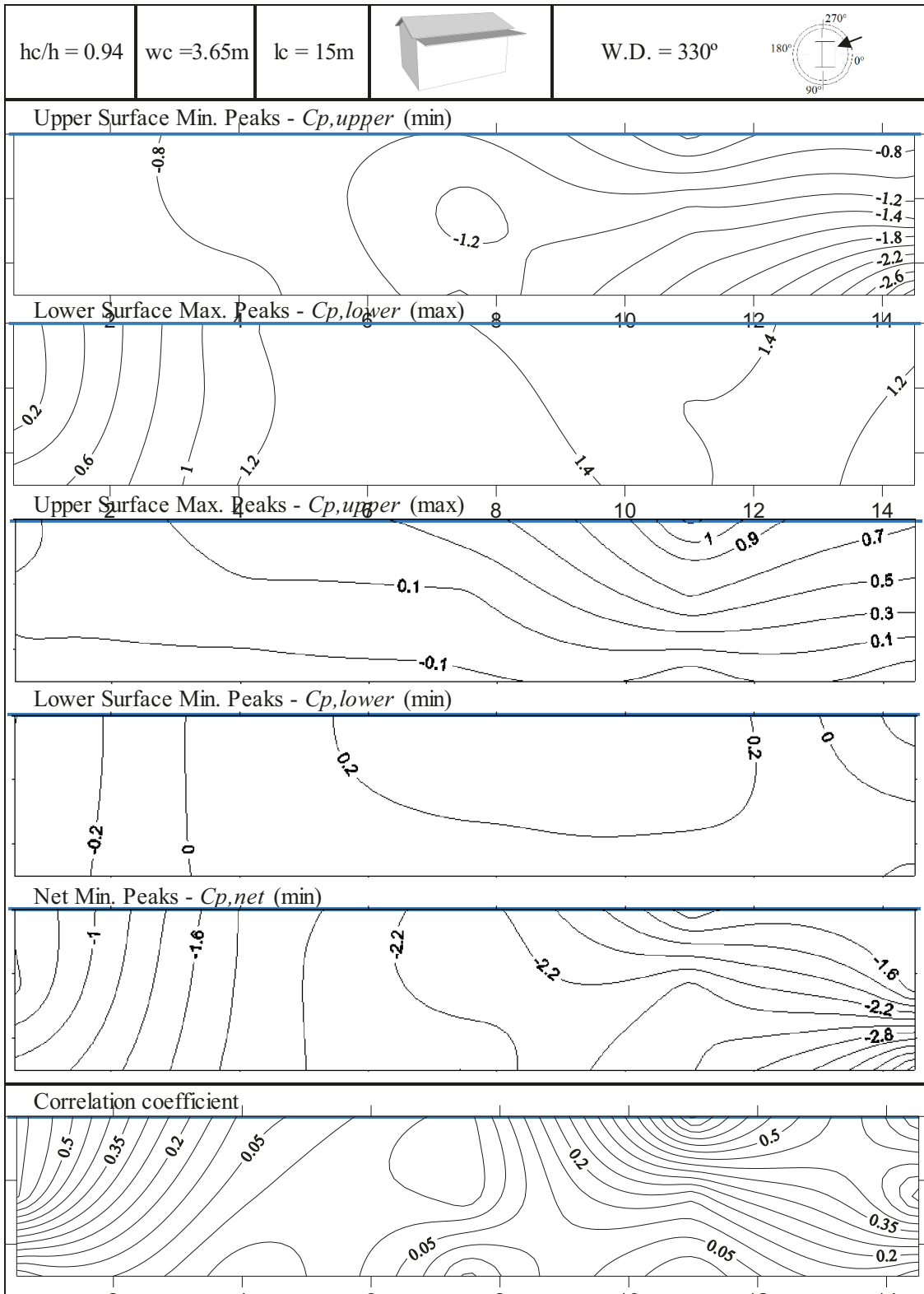


Figure 5.10 Pressure and correlation coefficient contour plots for a canopy attached close to the eave height of the parent wall and the critical wind direction

5.5 EFFECT OF PARAMETERS ON NET PRESSURE COEFFICIENTS

In this section the impact that each parameter has on the loads exerted upon the canopy is examined. This is done by varying an isolated parameter while maintaining the others constant. Four dependant variables are investigated for each case: the local minimum and maximum $Cp_{,net}$ (Loc. Min. ; Loc. Max.) which refer to the critical values experienced at a single pressure tap pair, and the area-averaged minimum and maximum $Cp_{,net}$ (Area-avg. Min. ; Area-avg. Max.) which refer to the peak value that the entire surface experiences determined by the critical simultaneous averages at every pressure tap pair.

5.5.1 Effect of $\frac{hc}{h}$

Local and area-averaged $Cp_{,net}$ values as a function of the $\frac{hc}{h}$ ratio are presented in Figure 5.11. It can be seen that a higher location of the canopy along the parent wall will generally result in higher net uplifting pressures (min $Cp_{,net}$) on the canopy. It may also be noted that for $\frac{hc}{h}$ ratios smaller than 0.5, peak min $Cp_{,net}$ values display little sensitivity to a slight increase in the canopy height. For intermediate heights ($0.5 < \frac{hc}{h} < 0.9$) a higher sensitivity is seen as the slope for the local peak min $Cp_{,net}$ is increased. Finally, for $\frac{hc}{h}$ values greater than or equal to 0.9 a more notable increase occurs. The change from a low to a high $\frac{hc}{h}$ ratio can result in an increase of more than 3 times the magnitude of the peak local min $Cp_{,net}$. It can thus be concluded that net uplifting

pressures are highly sensitive to the $\frac{hc}{h}$ ratio. This is consistent with what was expected based on the analyses of the flow visualization photographs and what was found in the pressure coefficient contour plots.

The net downward pressure coefficients ($\max C_{p,net}$), on the other hand, portray a smaller sensibility to the $\frac{hc}{h}$ ratio. Figure 5.11 shows that the area-averaged $\max C_{p,net}$ decreases slightly as the $\frac{hc}{h}$ ratio is increased. In the case of the maximum local $C_{p,net}$ values, no trend appears to be well defined. However, the highest maximum local $C_{p,net}$ encountered is only 1.3 times larger than the smallest. It can thus be seen that net downwards pressures are considerably less sensitive to the $\frac{hc}{h}$ ratio than the net uplifting pressures.

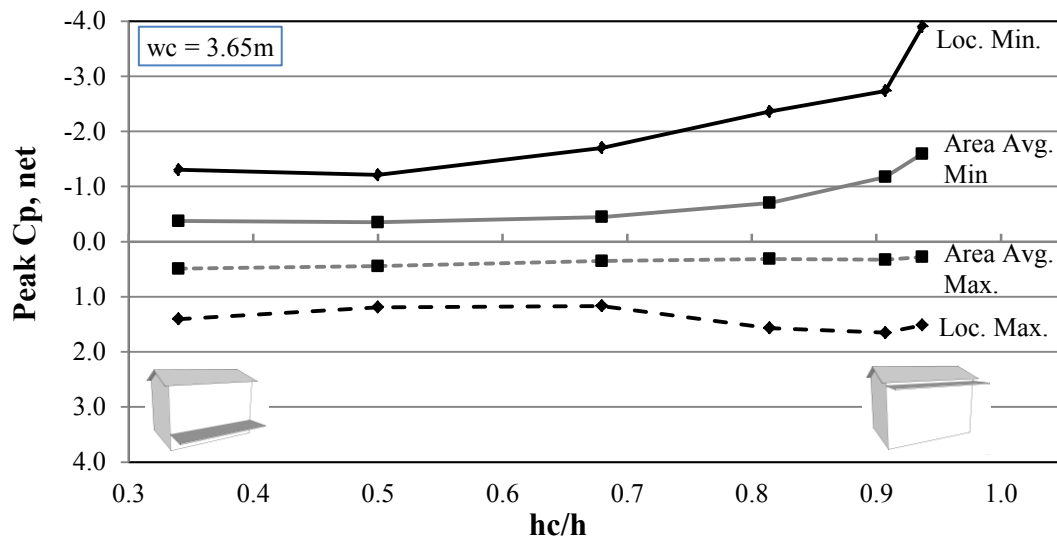


Figure 5.11 Effect of hc/h on local, and area-averaged $C_{p,net}$ for $w_c = 3.65\text{m}$

5.5.2 Effect of $\frac{hc}{wc}$

Local and area-averaged $Cp_{,net}$ values as a function of the $\frac{hc}{wc}$ ratio are presented in Figure 5.12 for an $\frac{hc}{h}$ ratio of 0.94, since this showed to be more critical in Figure 5.11. When the width of the canopy (wc) is decreased while maintaining its $\frac{hc}{h}$ ratio constant, the net uplifting forces will initially increase, which can be explained by the reduction of surface area for the reattachment of flow to take place. However, when the width is further reduced the vortices generated in the gap between the canopy and the roof overhang have a greater influence on the net uplifting forces. This results in a marked reduction of both local and area-averaged min $Cp_{,net}$ values. In addition, it must be noted that the highest local min $Cp_{,net}$ encountered is only 1.3 times larger than the lowest.

Net downward pressure coefficients, on the other hand, portray an inversely proportional relationship to the $\frac{hc}{wc}$ ratio, probably due to the effect of stagnation occurring at the portion of the parent wall located underneath the canopy. The portion of the total canopy area exposed to the strongest upwards flow becomes more significant when wc is decreased. As a result, the net downward loading is decreased. The highest local max $Cp_{,net}$ encountered is 2.5 times larger than the lowest.

Given that the proximity to the roof overhang, as well as the dominance of upward flow are considered to be determinant factors in the effect of $\frac{hc}{wc}$ ratio on a building with a high $\frac{hc}{h}$ ratio, the interest to examine the effect of $\frac{hc}{wc}$ on a lower $\frac{hc}{h}$

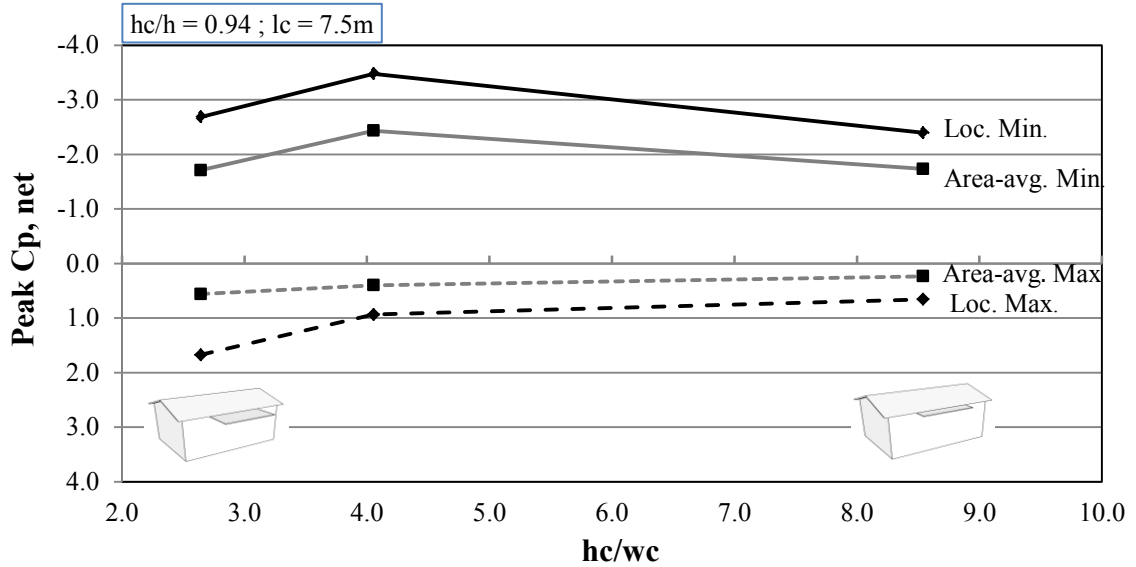


Figure 5.12 Effect of $\frac{hc}{wc}$ on local and area-averaged $Cp_{,net}$ for $\frac{hc}{h} = 0.94$

ratio arises. Figure 5.13 shows the local and area-averaged $Cp_{,net}$ values as a function of $\frac{hc}{wc}$ for an $\frac{hc}{h}$ ratio of 0.34. Clearly at this lower $\frac{hc}{h}$ ratio the effect of $\frac{hc}{wc}$ on the net uplifting forces appears to be negligible for both local and area-averaged peak $Cp_{,net}$ values.

In the case of the net downward pressures, increasing $\frac{hc}{wc}$ results in a marked increase of the max $Cp_{,net}$ values. This trend is contrary to that found for the case of high $\frac{hc}{h}$ ratio, but for lower $\frac{hc}{h}$ ratios, the downward flow along the parent wall is dominant over the upward flow. As a result, the portion of the total canopy area exposed to the strongest downward flow becomes more significant when wc decreases. It can be concluded that the effect of $\frac{hc}{wc}$ is different for low or high $\frac{hc}{h}$ ratios.

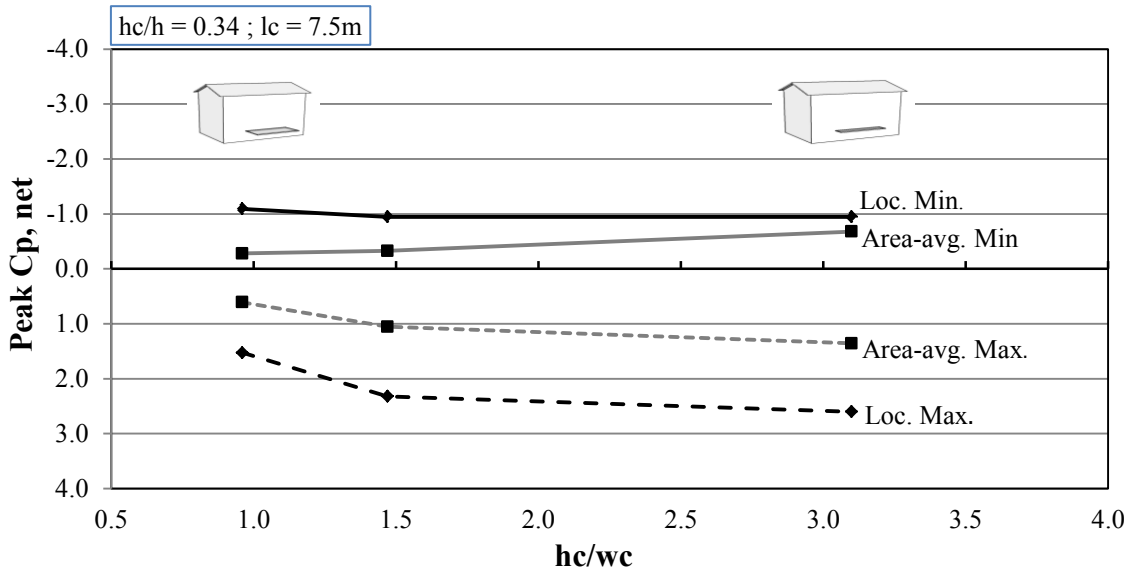


Figure 5.13 Effect of $\frac{hc}{wc}$ ratio on local and area-averaged $Cp_{,net}$ for $\frac{hc}{h} = 0.34$

5.5.3 Effect of canopy length (lc) and location (ed)

The last geometric parameters examine the effect of the length of the canopy (lc) and the largest edge-to-edge distance (ed) on net pressure coefficients. Local and area-averaged $Cp_{,net}$ values as function of the $\frac{ed}{lc}$ ratio are presented in Figure 5.14 for a constant $\frac{hc}{h}$ and a constant wc equal to 3.65m. An increase in the $\frac{ed}{lc}$ ratio generally corresponds to a decrease in the magnitude of the local min $Cp_{,net}$, whereas the area-averaged min $Cp_{,net}$ portrays little sensitivity. It is also to be noted that the case of the full-length canopy ($\frac{lc}{l} = 1$) has a significantly higher local min $Cp_{,net}$ in comparison to the other two mid-length canopy ($\frac{lc}{l} = 0.5$) cases. It can be concluded that the $\frac{lc}{l}$ ratio is

significant for the net uplifting pressures, whereas the edge distance seems to be of secondary importance.

In the case of the net downward pressure coefficients there appears to be no significant difference between the full-length canopy model and the mid-length models. The same can be said about the distance from the edge, which shows only a slight increase when going from a canopy placed at the center ($\frac{ed}{lc} = 0.75$) to a canopy placed at the corner ($\frac{ed}{lc} = 1$) of the parent wall.

Therefore, it can be said that local uplifting forces are sensitive to changes in the $\frac{lc}{l}$ ratio, and less sensitive to the largest edge-to-edge distance (ed). Local downwards loading forces, on the other hand, are more sensitive to the $\frac{ed}{lc}$ ratio and display little sensitivity to the $\frac{lc}{l}$ ratio.

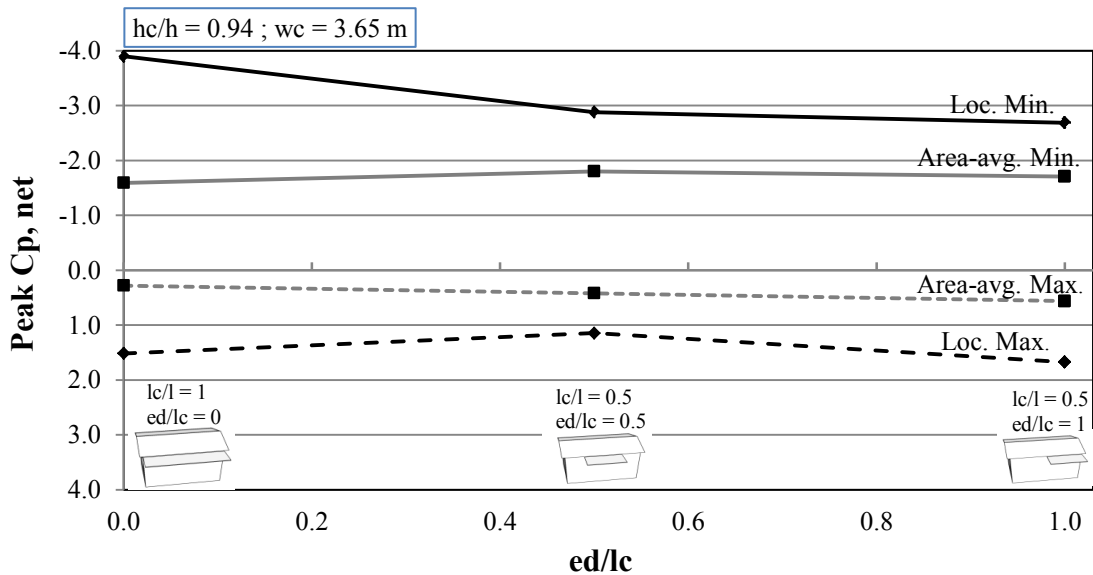


Figure 5.14 Effect of length and edge distances on local and area-averaged $Cp_{,nets}$

5.6 NET LOCAL PRESSURE COEFFICIENTS DIVIDED BY REGIONS

Local $C_{p,net}$ values have also been found to differ considerably at different regions within the attached canopy (see Figure 4.12 for the delimitation of regions). Figure 5.15 shows 3-d and 2-d contour plots of the local $C_{p,net}$ values measured at the attached canopy for a wind direction perpendicular to the ridge (0°). The differences in the magnitudes of local $C_{p,net}$ at different regions of the attached canopy can be observed. It can be seen that for the configuration shown the highest local suction (at the corner) is around 3 times the magnitude of the lowest suction (at the interior).

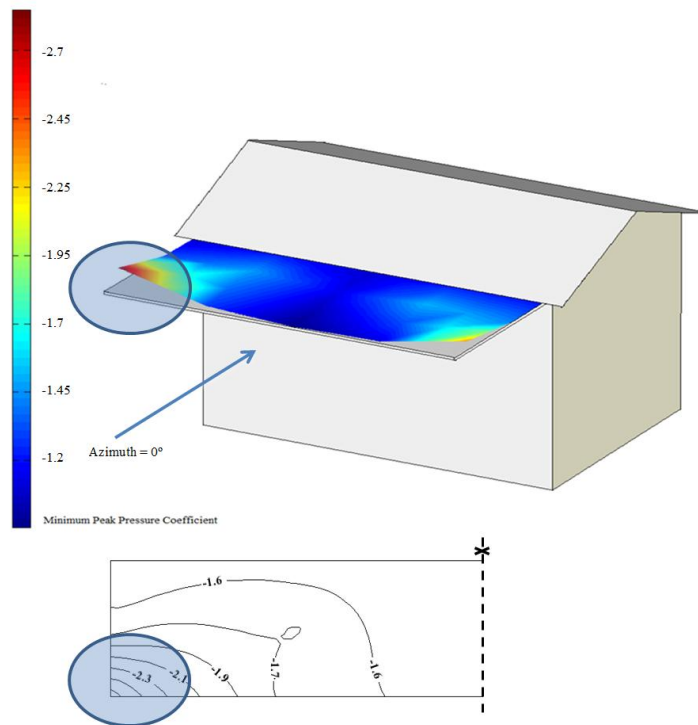


Figure 5.15 Two and three dimensional representations of the distribution of the net pressure coefficients on attached canopy

Figure 5.16 shows the local peak C_p values at the different regions of the upper surface as a function of the $\frac{hc}{h}$ ratio. It can be seen that the uplifting forces for $\frac{hc}{h}$ ratios lower than 0.50 occur at higher magnitudes around the edge regions. For higher $\frac{hc}{h}$ ratios on the other hand, a marked difference can be seen in between the corner peak uplift and that found at the interior region. The peak local uplift at the corner region for an $\frac{hc}{h}$ of 0.94 was found to have about 1.5 times the magnitude of that found in the interior.

For the case of positive downward loading, a slight difference can be seen between the corner and the interior region. The greatest difference between the corner and interior peak can be seen at an $\frac{hc}{h}$ of 0.84 where the local maximum peak at the

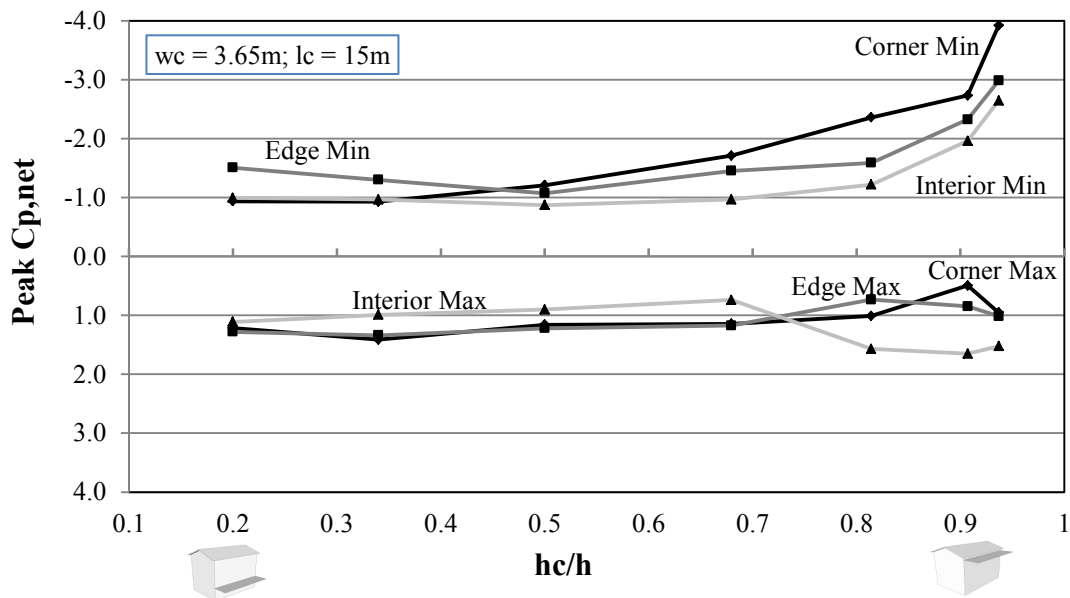


Figure 5.16 Peak local $C_{p,nets}$ as a function of $\frac{hc}{h}$ at the different regions of the canopy

interior was more than 3 times the magnitude of that found in the corner. It may also be noted that little difference is seen between the edge and corner region.

It can be thus concluded that the location for which the peak pressure coefficient is estimated in the canopy is considerably affected by the $\frac{hc}{h}$ ratio. Higher uplifting forces will occur around the corner regions for high $\frac{hc}{h}$ ratios and around the edges for lower ratios. Downward forces on the other hand, generally occur with higher magnitudes at the interior regions for high $\frac{hc}{h}$ ratios.

5.7 COMPARISONS WITH EXPERIMENTAL RESULTS OF PREVIOUS STUDIES

As previously stated, several wind standards and codes of practice, containing provisions for the design of attached canopies, show significant inconsistencies. Publications regarding the wind tunnel experimentation and analysis that led to the development of the AS/NZS and the DIN design guidelines have been made available. These comprehensive studies (Jancauskas and Holmes 1985; Hölscher et al. 2007) facilitate the comparisons between the findings of the present study and their experimental values.

Comparisons between the experimental results that led to the AS/NZS provisions published by Jancauskas and Holmes and those of the present study are presented in the three plots of Figure 5.17. The geometrical ratios tested by Jancauskas and Holmes are

not necessarily the same as those tested as part of this study. For ease of comparison, they have been grouped into the three different graphs for the defined ranges of $\frac{hc}{h}$ ratios and analyzed as a function of the $\frac{hc}{wc}$ ratio. It can be seen that the results of the present study generally portray a good agreement with the previous results. However, it must also be noted that the range of the present study extends over higher values of $\frac{hc}{wc}$ ratios for which previous data was not available.

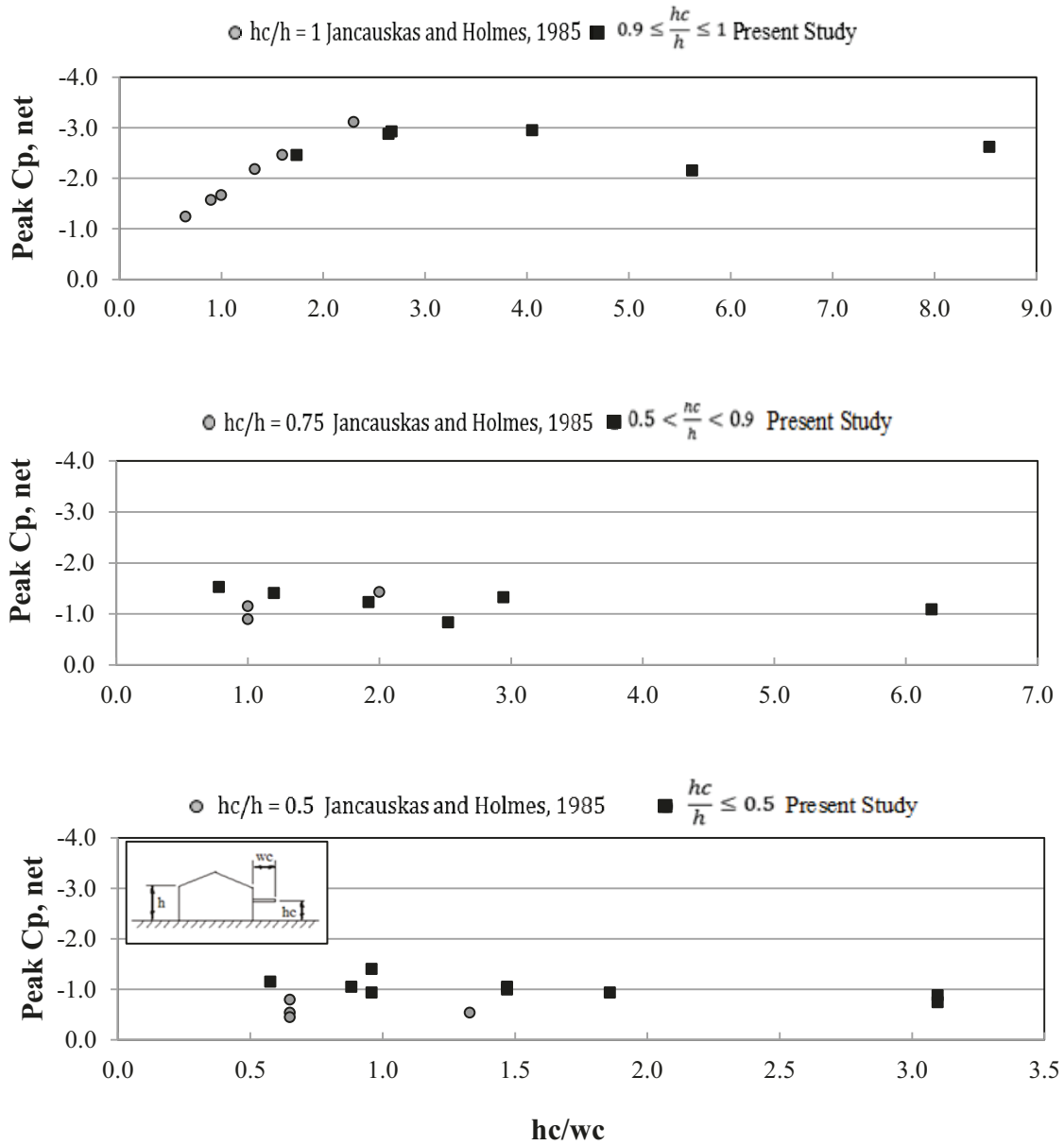


Figure 5.17 Comparison between results of the present study and Jancauskas and Holmes, 1985

The experimental results and analysis that led to the design guidelines provided in the DIN have been made available (Hölscher et al. 2007) and are compared with those of the present study in Figure 5.18. The latter are considerably higher, however, this can be partially attributed to the fact that the previous experiments were performed for suburban terrain exposure whereas the present study was performed for an open country exposure.

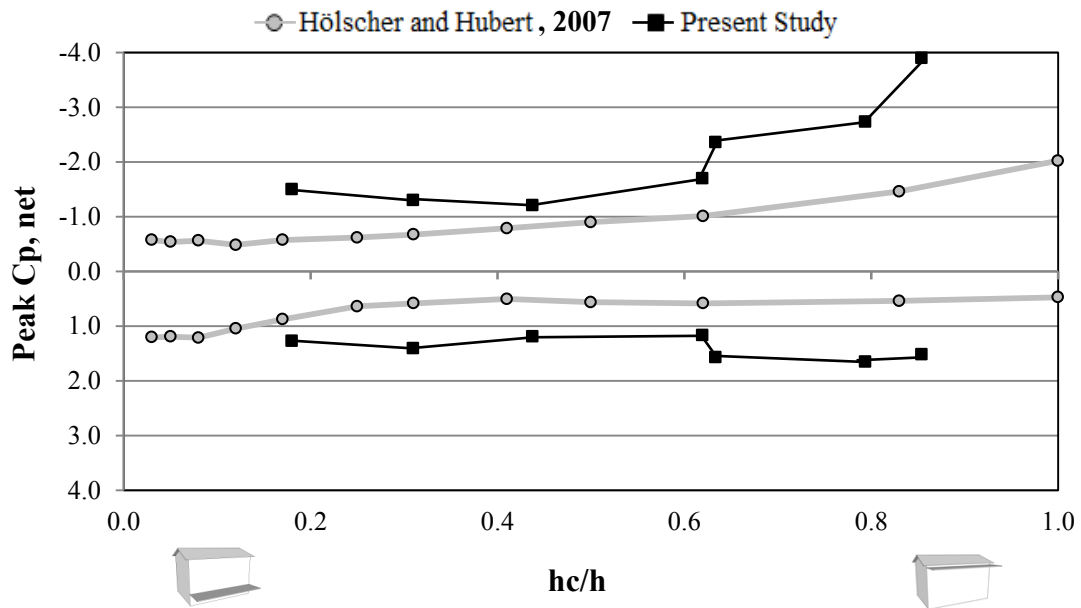


Figure 5.18 Comparison between results of the present study and Hölscher et al. 2007

5.8 ENVELOPES OF NET PRESSURE COEFFICIENTS

In order for this parametric study to be suitable for the different dimensions that may be encountered in practice it is of great significance to examine the peak pressures experienced by different effective areas. The area-averaging effect on min and max $C_{p,net}$ peaks has been derived by considering single or multiple sets of pressure taps and assigning them to their corresponding effective surface area. The three plots shown in Figure 5.19 contain all of the experimental curves obtained in terms of peak net pressure coefficients as a function of the increasing effective area (refer to Appendix B1 for tabulated net pressure coefficients of all configurations). Each plot contains 21 curves corresponding to the respective case as defined in Table 3.2. The expected monotonically decreasing relationship between the effective area and the magnitudes of the peak pressure coefficients is observed.

Based on the previous observations regarding the effect of the $\frac{hc}{h}$ ratio on peak $C_{p,net}$, all of the curves shown in Figure 5.19 have been grouped into one of the following three categories:

- $0.9 \leq \frac{hc}{h} \leq 1$
- $0.5 < \frac{hc}{h} < 0.9$
- $\frac{hc}{h} \leq 0.5$

Consequently, the envelope lines for each of the corresponding categories have been superimposed onto each plot. It can be noted that the envelope with the highest net uplifting peak is found for Case I ($\frac{ed}{lc} = 0$), whereas the highest net downwards loading peak occurs for Case III ($\frac{ed}{lc} = 1$). In the case of net downward loading it can be seen that the experimental curves for different $\frac{hc}{h}$ ranges appear to be intertwined. This reaffirms the observation that net downward loads are less sensitive to the $\frac{hc}{h}$ ratio. For this reason a single maximum envelope is provided for all $\frac{hc}{h}$ ratios.

The critical maximum and minimum envelope lines amongst the three Cases for each range of $\frac{hc}{h}$ ratio have been plotted together into Figure 5.20. This figure condenses all experimental data as a function of the effective area considering only the $\frac{hc}{h}$ ratio since it has been found to have the greatest influence on peak pressure coefficients.

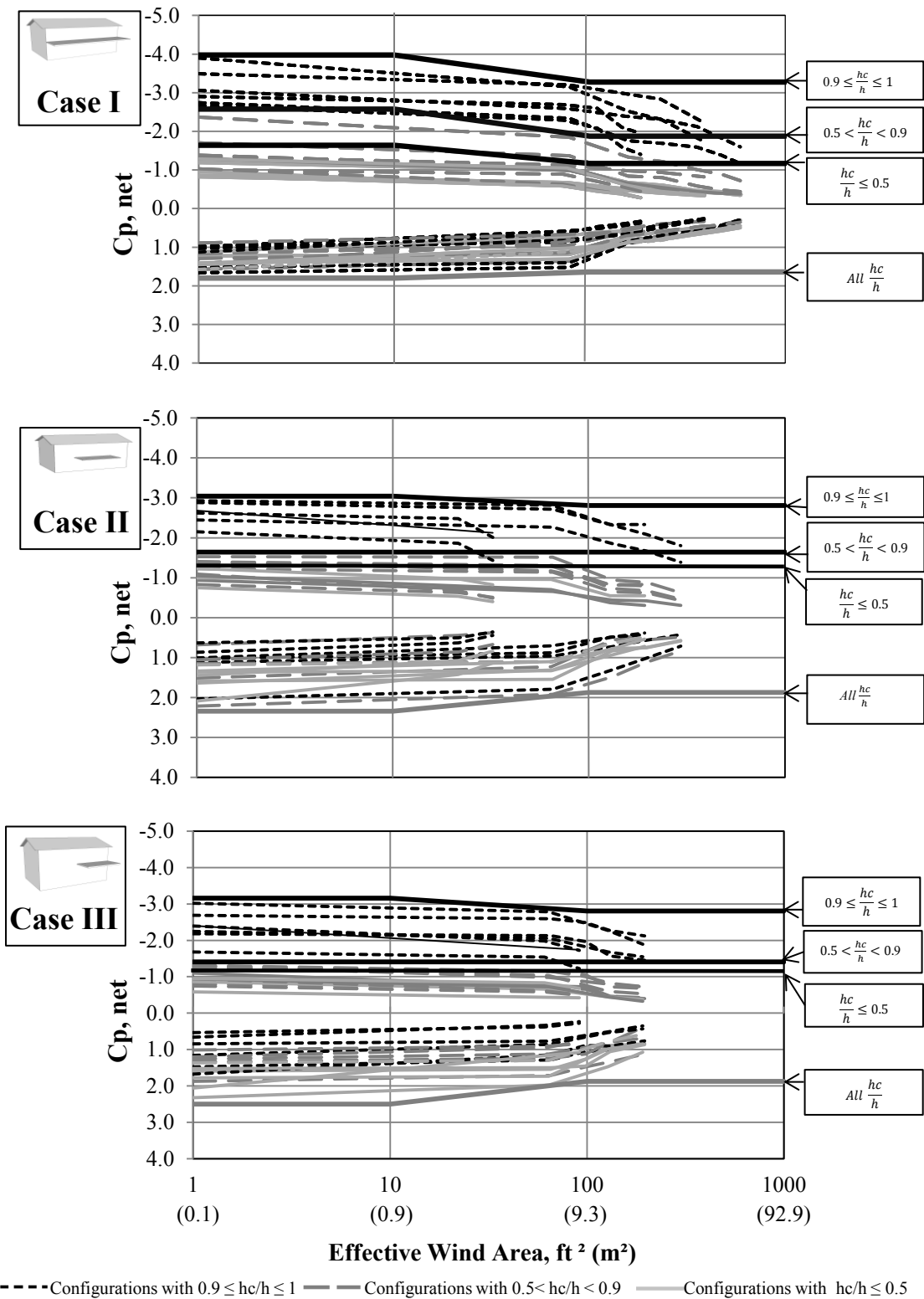


Figure 5.19 Area averaging effect and envelopes for the corresponding ranges of Cases I, II and III separately

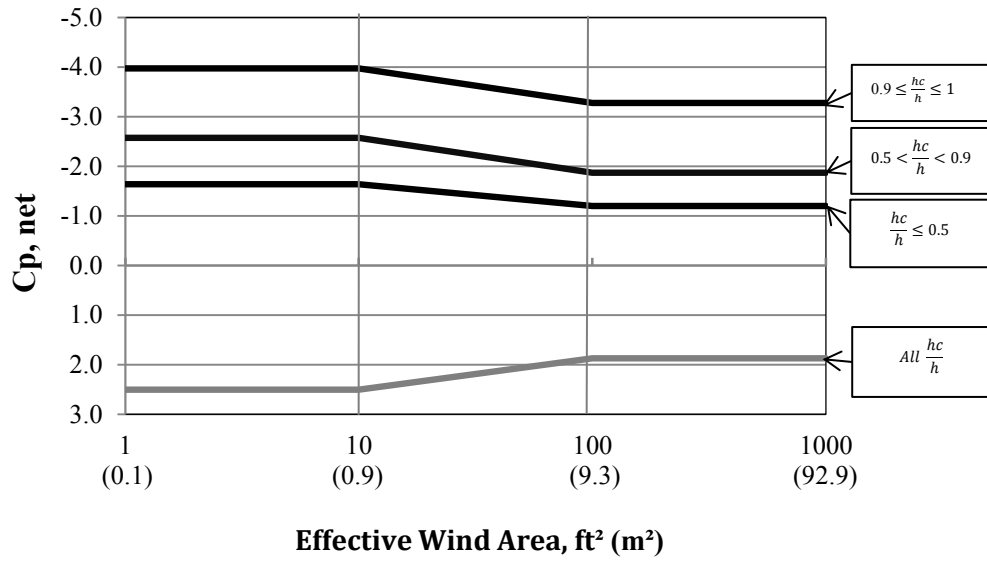


Figure 5.20 Area averaging effect and corresponding envelopes for all 63 configurations combined

CHAPTER 6

TOWARDS CODIFICATION

6.1 GENERAL

This section provides the recommendations for the wind loading design of attached canopies. The proposed pressure coefficients here presented are the result of the analyses and observations made in Chapters 4 and 5.

Comparisons between the present recommendations and the AS/NZS and the DIN design guidelines for net pressure coefficients are provided. These guidelines are the result of the previously discussed studies of Jancauskas and Holmes (1985) and Hölscher et al. (2007). Additional comparisons with the ASCE 7 provisions for roof overhangs and roofs of partially enclosed buildings are provided to assess the differences that practitioners may encounter when designing the wind loads accordingly.

It is to be noted that all pressure coefficients presented from here on have been converted to conform to a 3-sec gust averaging period for codification purposes. The conversions were approximated by use of the Durst curve for gust duration (Durst 1960).

6.2 RECOMMENDED DESIGN GUIDELINES FOR ATTACHED CANOPIES

6.2.1 Design guidelines for suctions on upper and lower surfaces

Recommended provisions for the design of suctions on upper and lower surfaces of attached canopies are provided in Figure 6.1. These design guidelines lines have been generated from the envelopes of all experimental data obtained for upper and lower surfaces separately (see Figures 4.15, 4.16, and 4.17). A directionality factor of 0.8 has been applied to all envelopes to account for the unlikelihood that the critical wind speed occurs at the critical wind direction for a specific building configuration. These recommended min GCp_{upper} and GCp_{lower} design values are given as a function of the effective area of the canopy considered.

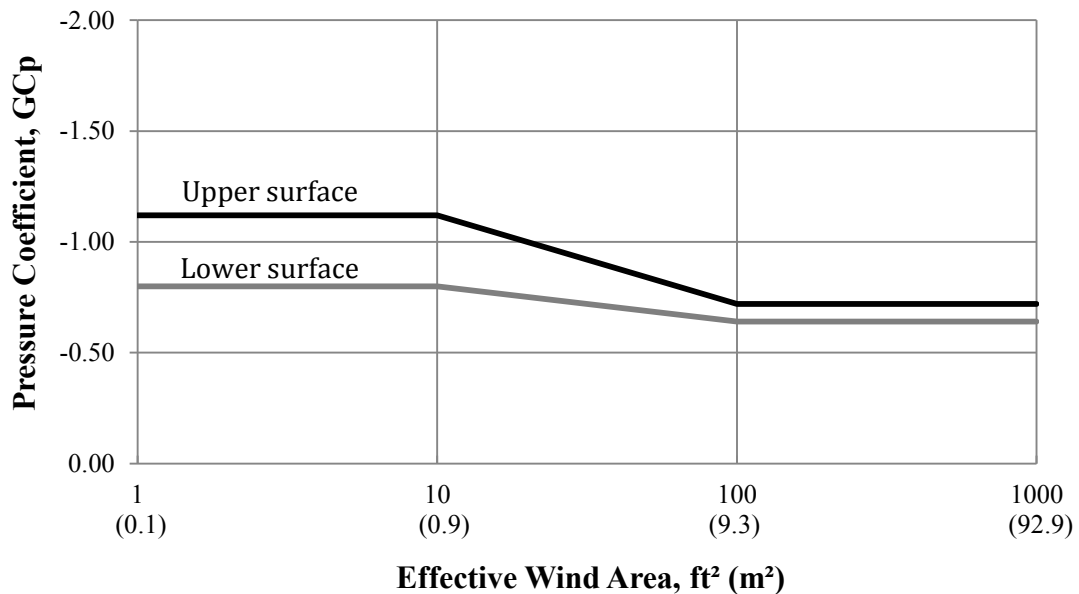


Figure 6.1 Proposed design values for min Cp_{upper} and Cp_{lower} on attached canopies

In addition, recommended $\min GC_{p,upper}$ and $GC_{p,lower}$ design values may be multiplied by the reduction factors US_{Rf} and LS_{Rf} (see Table 6.1). These reduction factors have been generated from the observations made on Chapter 4 to account for the effect of the $\frac{lc}{l}$ ratio which was seen to have a considerable impact on the suctions on upper and lower surfaces. The recommended $\min GC_{p,upper}$ and $GC_{p,lower}$ can thus be obtained by the following equations:

$$GC_{p,upper} = US_{Rf} \cdot GC_p \quad (6.1)$$

$$GC_{p,lower} = LS_{Rf} \cdot GC_p \quad (6.2)$$

in which the GC_p is obtained from the corresponding curve (upper or lower) on Figure 6.1 as a function of the effective area.

Table 6.1 Geometrical reduction factors for $\min GC_{p,upper}$ and $GC_{p,lower}$

	LS_{Rf}	US_{Rf}
$\frac{lc}{l} = 1$	1	1
$\frac{lc}{l} = 0.5$	0.7	0.85

*For intermediate lc/l ratios use linear interpolation

6.2.2 Design guidelines for net loads

Recommended provisions for the design of attached canopies are provided in Figure 6.2. These design guidelines lines have been generated from the envelopes of all experimental data obtained from the current study (see Figures 5.19, and 5.20). A directionality factor of 0.8 has been applied to all envelopes to account for the unlikelihood that the critical wind speed occurs at the critical wind direction for a specific building configuration. These recommended $GCp_{,net}$ design values are given as a function of the $\frac{hc}{h}$ ratio and the effective area of the canopy considered.

These curves can be used on their own as a simple yet conservative design guideline for the net pressure coefficients ($GCp_{,net}$) on attached canopies. It must be noted however that these simplified provisions only take into consideration the $\frac{hc}{h}$ ratio whereas it has been seen that the other parameters examined may also have a significant effect on the local net pressure coefficients. It is for this reason that reduction factors dependant on the geometrical $\frac{hc}{wc}$ and $\frac{lc}{l}$ ratios are introduced in Table 6.2. The values presented in this table are the result of intricate examination of every single configuration tested. The recommended local $GCp_{,net}$ can thus be obtained by the following equation:

$$\text{Minimum } GCp_{,net \text{ local}} = U_{Rf} * GCp_{,net} \quad (6.3)$$

$$\text{Maximum } GCp_{,net \text{ local}} = D_{Rf} * GCp_{,net} \quad (6.4)$$

where $GCp_{,net}$ is obtained as a function of $\frac{hc}{h}$ from Figure 6.2, and the uplifting and downward loading reduction factors (U_{Rf} and D_{Rf}) are given as a function of $\frac{hc}{wc}$, and $\frac{lc}{l}$ on Table 6.2.

The addition of the reduction factor increases the complexity of the design procedure, however, a more economical design covering a much wider range of geometric configurations is provided. An assessment of the recommended design guidelines considering the reduction factor in comparison to the experimental results is provided in Appendix C1.

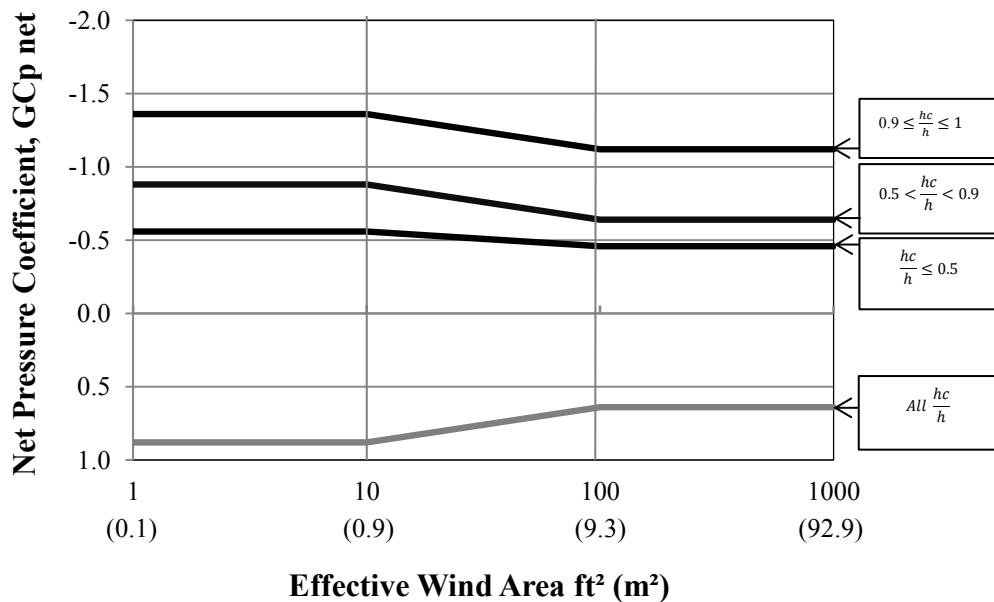


Figure 6.2 Proposed design values for $GCp_{,net}$ on attached canopies

Table 6.2 Geometrical reduction factor for the local GCp_{net} obtained from Figure 6.1

		Uplifting Reduction Factor = U_{Rf}		Downwards Reduction Factor = D_{Rf}	
		$\frac{lc}{l} = 1$	$\frac{lc}{l} = 0.5$	$\frac{lc}{l} = 1$	$\frac{lc}{l} = 0.5$
$\frac{hc}{h} \leq 1$	$0.9 \leq \frac{hc}{h} \leq 1$				
	$\frac{hc}{WC} \leq 3$	1	0.75	0.65	0.75
	$\frac{hc}{WC} \leq 6$	0.75	0.75	0.45	0.35
$0.5 < \frac{hc}{h} < 0.9$	$\frac{hc}{WC} \leq 1$	1	0.65	0.65	0.85
	$\frac{hc}{WC} \leq 4$	0.45	0.45	0.40	0.50
$\frac{hc}{h} \leq 0.5$	$\frac{hc}{WC} \leq 1$	1	0.90	0.70	0.75
	$\frac{hc}{WC} \leq 2.5$	0.60	0.60	0.70	1.00

*Use linear interpolation for intermediate values

6.3 COMPARISONS WITH CURRENT DESIGN PROVISIONS

Several wind standards and building codes of practice provide design guidelines for wind loading on attached canopies as was discussed in Chapter 2. In this section the provisions of the AZ/NZS and the DIN are compared to the recommendations of the present study, since the studies that led to their proposed values have been made available. Furthermore, the recommendations of the present study are compared to the ASCE provisions overhangs, and roofs of partially enclosed structures.

6.3.1 AZ/NZS 1170.2:2002

Comparisons between the values proposed by the AS/NZS and the recommended envelopes of the present study for the Cp_{net} as a function of the effective area are presented in Figure 6.3. In general a good agreement has been observed. It must be noted that for $\frac{hc}{h} = 1$ the AS/NZS recommends higher values than those recommended in the present study for the range of $0.9 \leq \frac{hc}{h} \leq 1$. For $\frac{hc}{h} = 0.75$ in the AS/NZS a good agreement is seen with the range of $0.5 < \frac{hc}{h} < 0.9$ from the present recommendations. For $\frac{hc}{h} = 0.5$ the min GCp_{net} recommended by the AS/NZS are considerably lower than the present recommendations. In the case of the max GCp_{net} it can be seen that the three different values corresponding to the AS/NZS recommendations for $\frac{hc}{h}$ ratios of 1, 0.75, and 0.5, respectively, are all within the values of the present recommendations.

Comparisons between the AZ/NZS provisions and the experimental findings of the present study have been included in Appendix C2.

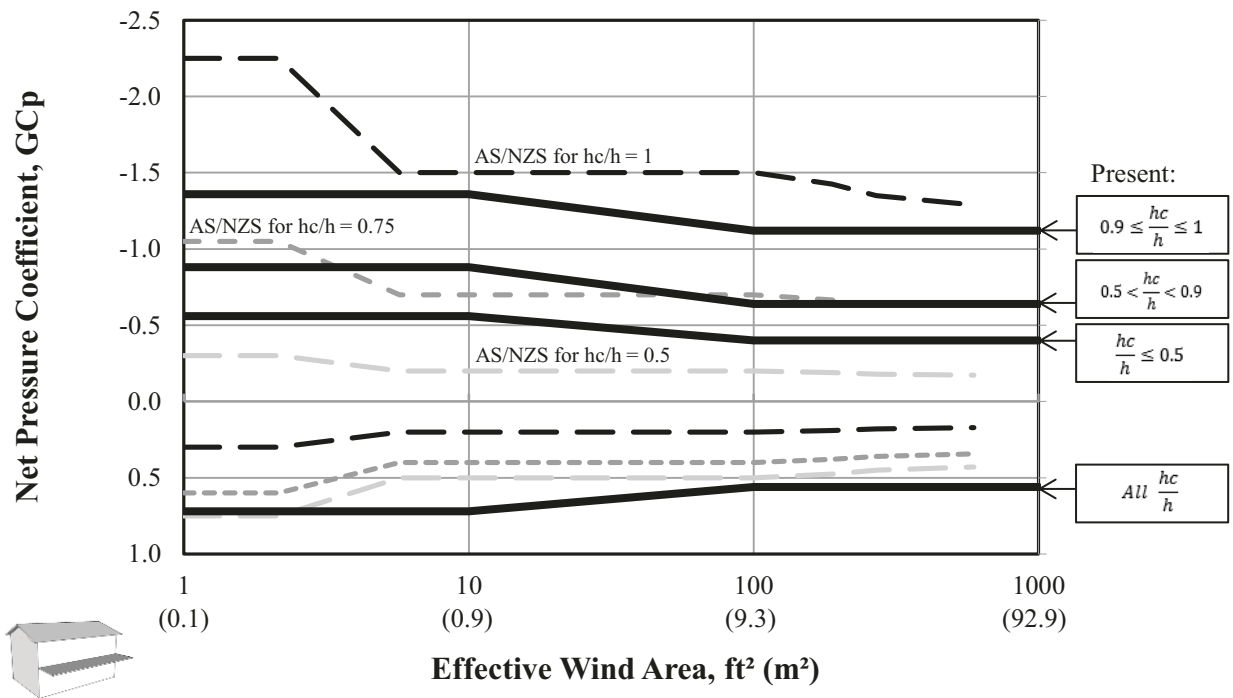


Figure 6.3 Comparisons between the recommended envelopes of the present study and AS/NZS provisions

6.3.2 DIN EN 1991-1-4/NA:2010-12

Comparisons between the design provisions on the DIN and those of the present study are provided in Figure 6.4 as a function of $\frac{hc}{h}$ for three configurations. It can be seen that the recommended values for local min $GCp_{,net}$ generally display a good agreement in which the recommendations of the present study are slightly higher than the recommendations of the DIN. In the case of the local max $GCp_{,net}$ it can be seen that both the DIN and the present study recommend the same values regardless of the $\frac{hc}{h}$ ratio for this range. It may also be noted that the recommendations of the present study for the highest downwards loading is considerably higher than that recommended by the DIN.

Comparisons between the DIN provisions and the experimental findings of the present study have been included in Appendix C3.

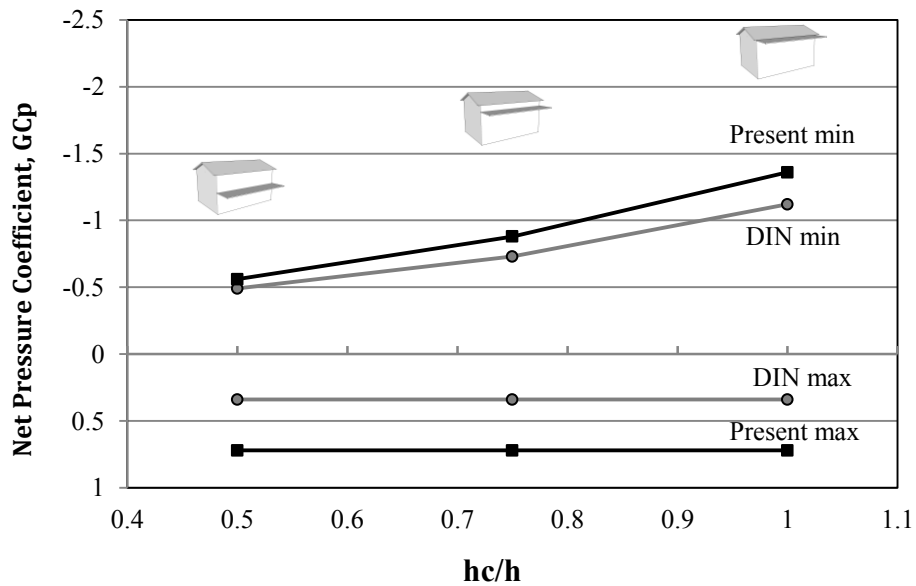


Figure 6.4 Comparison between the recommended local net pressure coefficients of the present study and the DIN provisions for three different hc/h ratios

6.3.3 ASCE 7-10 overhangs and partially enclosed structure

Due to the lack of provisions in the major North American codes and standards, practitioners often consider the attached canopies as either extensions of the roof overhangs or as the roofs of partially enclosed structures. Upon making such assumptions, canopies are often designed in accordance to the corresponding provisions in the ASCE 7-10. However, it is to be expected that this will result in significant differences with the experimental values obtained for attached canopies as was seen in Chapter 2.

Comparisons between the $GCp_{,net}$ values provided by the ASCE 7 provisions for roof overhangs and the recommendations of the present study are shown in Figure 6.5. It can be seen that treating a canopy as if it were an extended roof overhang may result in a design that is conservative by a maximum of 9 times, or non-conservative by a value of over 1.5 times the experimental values obtained at the corner regions. These marked differences are attributed to high levels of suction on the upper surface of the corner regions of the overhang in combination with high pressures on the lower surface resulting from stagnation on the windward wall. Additionally, the effect of the roof slope has also been seen to have an effect on the pressures around the corner regions.

Comparisons between the $GCp_{,net}$ values provided by the ASCE 7 provisions for flat roofs of partially enclosed buildings and the recommendations of the present study are shown in Figure 6.6. It can be seen that for $\frac{hc}{h} = 0.5$ values proposed for net uplifting loads on flat roofs of partially enclosed buildings are 3 times higher than those proposed

in the present study for a canopy. This is to be expected, since the roof of a partially enclosed building has no parent wall extending over it, thus no downwards flow is present at the upper surface. For $\frac{hc}{h} = 1$, on the other hand, it can be seen that the proposed values are very similar to each other. This is also to be expected, since neither of the two cases result in any considerable obstruction of flow at the upper surface of the canopy. In the case of downward forces, recommended values for canopies are consistently higher. This is can be explained once again by the effect of the downwards flow resulting from stagnation at the parent wall above the canopy.

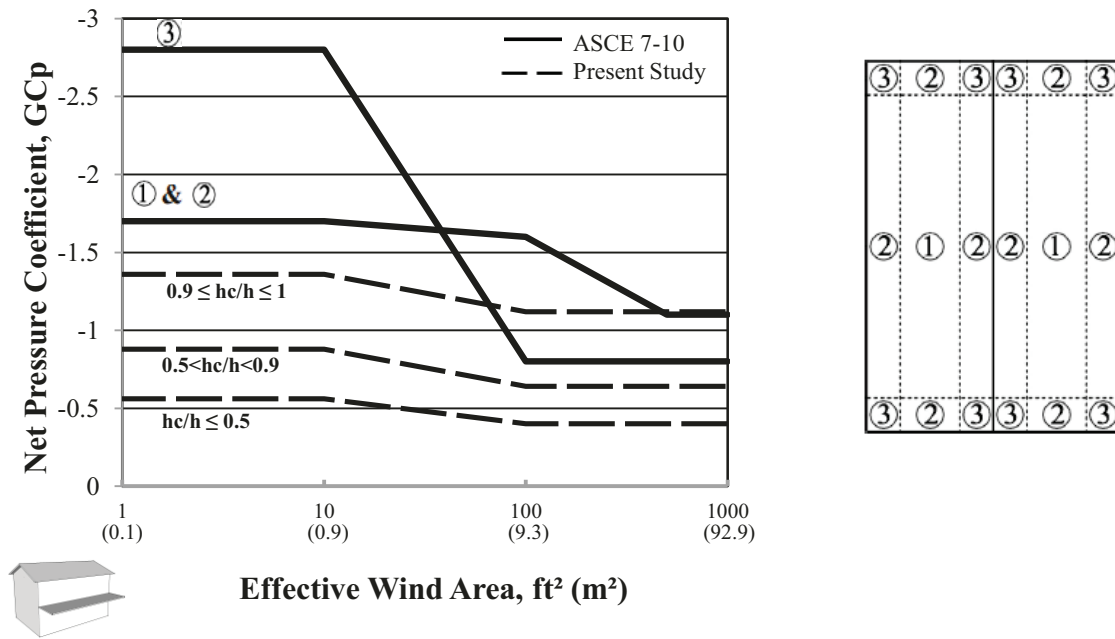


Figure 6.5 Comparisons between the recommended design values for a full length canopy and ASCE 7-10 provisions for overhangs on gable roof of slope smaller than 7° (Figure 30.4-2A)

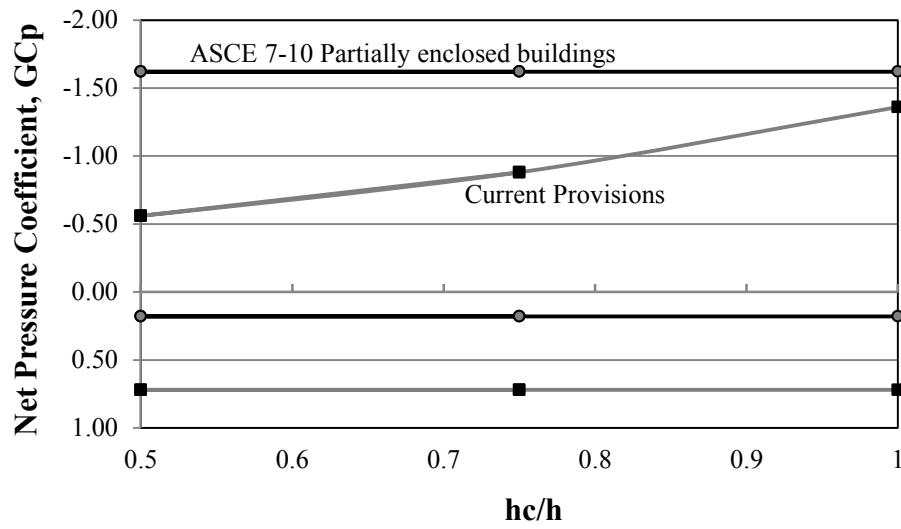


Figure 6.6 Comparisons between the recommended design values for three different hc/h ratios and ASCE 7-10 provisions for the roof of a partially enclosed building (Figure 28.4-1)

CHAPTER 7

CONCLUSIONS AND RECOMMENDATIONS FOR FUTURE STUDIES

7.1 SUMMARY

Wind tunnel experimentation has been performed on a total of 63 different configurations to serve as the basis for a parametric study of the wind loading effect on attached canopies. The effect of wind direction on net pressure coefficients has been examined and it has been shown that the critical peaks may occur for different wind directions depending on the configuration. Local and area-averaged net pressure coefficients (Cp_{net}) as well as pressure coefficients acting on upper and lower surfaces separately (Cp_{upper} and Cp_{lower}) have been analyzed as a function of four basic geometrical ratios to examine the trends and relationships that they exhibit with each other. Pressure and correlation coefficient contour plots have also been presented so as to provide a better understanding of the flow patterns occurring around the canopy.

Recommended design guidelines for GCp_{upper} , GCp_{lower} and GCp_{net} on attached canopies have been provided resulting from extensive data analyses and interpretation.

Comparisons between the recommendations and experimental findings of the present study and those associated with the AZ/NZS 1170.2:2002 and the DIN EN 1991-1-4/NA:2010-12 have been provided.

7.2 CONCLUSIONS

The conclusions generated from this study can be summarized as follows:

- Critical wind directions were found to vary significantly from configuration to configuration, however, the highest uplifting local loads generally occur between the range of 30° and 90° .
- The ratio of the height of the canopy to the eave height of the building (hc/h) was found to be the most influential parameter on the peak net pressure coefficients.
- The ratio of the length of the canopy to the length of the parent wall (lc/l) and the ratio of the height to the width of the canopy (hc/wc) were found to be of secondary importance and the location of the canopy with respect to the edge of the parent wall was found to have a marginal importance.
- Local net uplifting pressure coefficients are higher around the corner regions for high hc/h ratios, whereas little difference between regions is seen for low hc/h ratios.
- Local net downwards pressure coefficients are generally higher around the interior region.
- The lc/l ratio is the most influential in the design of suction at upper and lower surfaces.

-Suctions are generally higher on the upper surface of the canopy than on the lower surface.

-Suctions on the upper and lower surfaces of the canopy are generally higher on the edge and corner regions for high h_c/h ratios, whereas little difference between the regions is seen for low h_c/h .

-Both differences and similarities have been found between the available design guidelines of other codes and standards and those generated from the present study. These differences could be expected since a greater range of configurations has been tested in the present study.

-Designing attached canopies by adapting provisions available in major North American building codes for geometrically similar building components will lead in most cases to highly inadequate design wind loads.

7.3 LIMITATIONS AND RECOMMENDATIONS FOR FUTURE STUDIES

Amongst the parameters tested, the h_c/h , l_c/l , and h_c/w_c ratios were seen to have the most significant impact on pressure coefficients on attached canopies. A wide range of h_c/h and h_c/w_c ratios have been tested, however, the same can not be said about the l_c/l ratio. Perhaps this parameter requires additional experimentation.

Additionally, a significant difference has been found to occur between the recommendations of the present study and the provisions of the ASCE for overhangs on roofs with small slopes. This difference has been attributed amongst other geometrical differences to the slope of the overhang in comparison to the present experimental setup

for attached canopies with a 0° slope. Wind tunnel testing on attached canopies with different roof slopes could potentially widen the range of this study.

The present study is limited to canopies attached to low-rise structures. The lowest ratio of canopy height to parent wall height tested was of 0.2. However, it is not uncommon to find canopies attached to high-rise structures where considerably different results are to be expected due to the large area of parent wall above the canopy height. Further experimentation with smaller h_c/h ratios could be of great interest for codification purposes. In addition, wind loads on podia attached to high-rise buildings also represent an area for future expansion.

REFERENCES

- ASCE. (2010). Minimum design loads for building and other structures. *ASCE/SEI 7-10*, Reston, Va.
- British Standard Institute. (1997). Loading for buildings—Part 2: Code of practice for wind loads. *BS 6399-2*, London.
- CEN. (2004). Eurocode 1: Actions on structures—General actions—Part 1.4: Wind actions. *Pr EN 1991-1-4*, Brussels.
- Counihan, J. (1975) Adiabatic Atmospheric Boundary Layers: A Review and Analysis of Data from the Period 1880-1972. *Atmos. Environ.*, 871-905
- Davenport, A.G., Stathopoulos, T., Surry, D. (1985) Reliability of wind loading specifications for low Buildings. Procedures, International Conference on Structural Safety and Reliability, ICOSSAR 85, Kobe, Japan.
- Davenport, A. G. (2002). Past, present and future of wind engineering. *Journal of Wind Engineering and Industrial Aerodynamics*, 90(12-15), 1371-1380.
- DIN. (2010). Einwirkungen auf Tragwerke - teil 4: Windlasten. *DIN EN 1991-1-4:2010-12*, Berlin.

Durst, C.S. (1960). Wind speeds over short periods of time. *Meteorological Magazine*, 89, 181-186.

Goyal, R., Ahuja, A.K., and Prasad. J. (2007) Wind loads on buildings with attached canopies, *Asian Journal of Civil Engineering*, Vol. 8 No. 3, 239-246

Holmes, J. D. (2001). *Wind loading of structures*. Spon Press, New York.

International Code Council. (2012a). *International building code (IBC)*, Fall Church, Va.

International Code Council. (2012b). *International residential code (IRC)*, Fall Church, Va.

IS. (1987). *Indian Standard code of practice for design loads-(Part 3-wind loads) for buildings and structures, IS: 875 (Part-3)-1987*, New Delhi.

Jancauskas, L., and Holmes, J. (1985). Wind loads on attached canopies." *Procedures*, National Conference on Wind Engineering, Texas Tech Univ., Lubbock, Tex.

Jensen, M. (1958). The model-law for phenomena in natural wind. *Ingenioren - International Edition*, 2(4), 121-128.

Jensen, M., & Franck, N. (1965). Model-scale tests in turbulent wind. Part II. Danish Technical Press.

National Research Council of Canada. (2010). National Building Code of Canada (NBCC), Ottawa, ON.

ÖNORM. (1993). Belastungsannahmen im Bauwesen – Statische Windeinwirkungen ÖNORM B 4014-1:1993 05 01, Vienna.

Paluch, M.J., Loredou-souza, A.M. and Blessmann, J. (2003). Wind loads on attached canopies and their effects on the pressure distribution over arch roof industrial building, Journal of Wind Engineering and Industrial Aerodynamics, 91, 975-994.

Shiotani, M. (1971), Structure of Gusts in High Winds, parts 1-4, The Physical Sciences laboratory, Nikon University, Furabachi, Chiba, Japan

Scanivalve Corporation, ZOC 33/64Px – Electronic Pressure Scanning Module, Instruction and Service Manual

Scanivalve Corporation, DSMLINK V2.90, Installation and Operation Manual

Scanivalve Corporation, DSM 3000 – Digital Service Module, Instruction and Service Manual

SIA (2003), Einwirkungen auf Tragwerke, Schweizerischer ingenieur- und Architektenverein. SIA 261:2003, Zurich

Simiu, E., and Scanlan, R. (1996). Wind Effects on Structures: Fundamentals and Applications to design, 3rd Ed., Wiley & Sons, New York.

Standards Australia International Ltd.–Standards New Zealand. (2002). Australian/New Zealand standards, structural design actions—Part 2, wind actions. *AS/NZS 1170.2*.

Stathopoulos, T. & Surry, D. (1983). Scale effects in wind tunnel testing of low buildings. *Journal of Wind Engineering and Industrial Aerodynamics*, 13(1-3), 313-326.

Stathopoulos, T. (1984). Design and fabrication of a wind tunnel for building aerodynamics. *Journal of Wind Engineering and Industrial Aerodynamics*, 16(2-3), 361-376.

Stathopoulos T., (1985) Wind Loads on Low-Rise Buildings: A Review of the State of the Art. *Engineering Structures*, Volume 6, No. 2, pp. 119-135

Tieleman, H. W., Hajj, M. R., & Reinhold, T. A. (1998). Wind tunnel simulation requirements to assess wind loads on low-rise buildings. *Journal of Wind Engineering and Industrial Aerodynamics*, 74-76, 675-685.

Tieleman, H. W., Reinhold, T. A., & Marshall, R. D. (1978). On the wind-tunnel simulation of the atmospheric surface layer for the study of wind loads on low-rise buildings. *Journal of Wind Engineering and Industrial Aerodynamics*, 3(1), 21-38.

Uematsu, Y., Iizumi, E., and Stathopoulos, T. (2007). Wind force coefficients for designing free-standing canopy roofs. *Journal of Wind Engineering and Industrial Aerodynamics*, 95_9–11_, 1486–1510.

Uematsu, Y., Stathopoulos, T., and Iizumi, E. (2008a). Wind loads on free-standing canopy roofs: Part 1. Local wind pressures. *Journal of Wind Engineering and Industrial Aerodynamics*, 96_6–7_, 1015–1028.

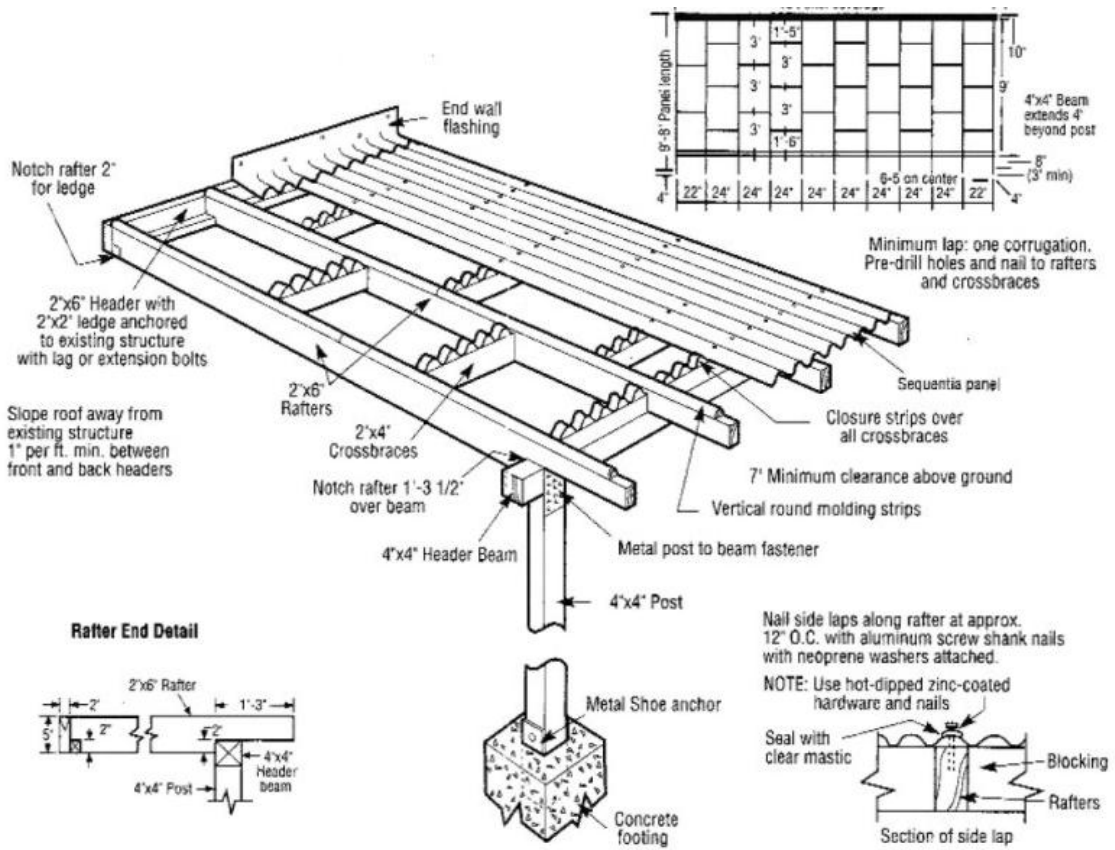
Uematsu, Y., Stathopoulos, T., and Iizumi, E. (2008b). Wind loads on free-standing canopy roofs: Part 2. Overall wind forces. *Journal of Wind Engineering and Industrial Aerodynamics*, 96_6–7_, 1029–1042.

Zisis, I. and Stathopoulos, T. (2010). Wind-induced pressures on patio covers. *ASCE Journal of Structural Engineering*, Volume 136, No. 9, pp. 1172-1181.

Zisis, I., Stathopoulos, T., and Candelario, J. D.. (2011). Codification of wind loads on a patio cover based on a parametric wind tunnel study. 13th International Conference in Wind Engineering, Amsterdam, Netherlands.

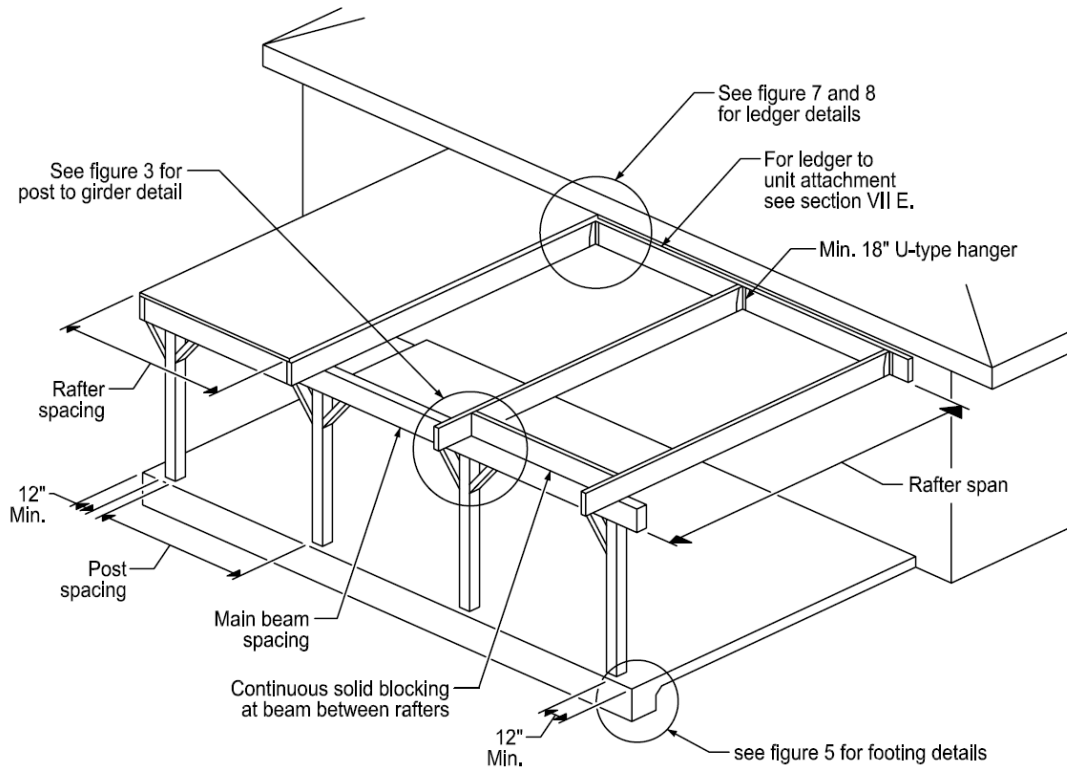
APPENDIX A

Appendix A1 Isometric and construction details for a typical wooden attached canopy. Source - <http://www.umbugug.com/2012/05/>

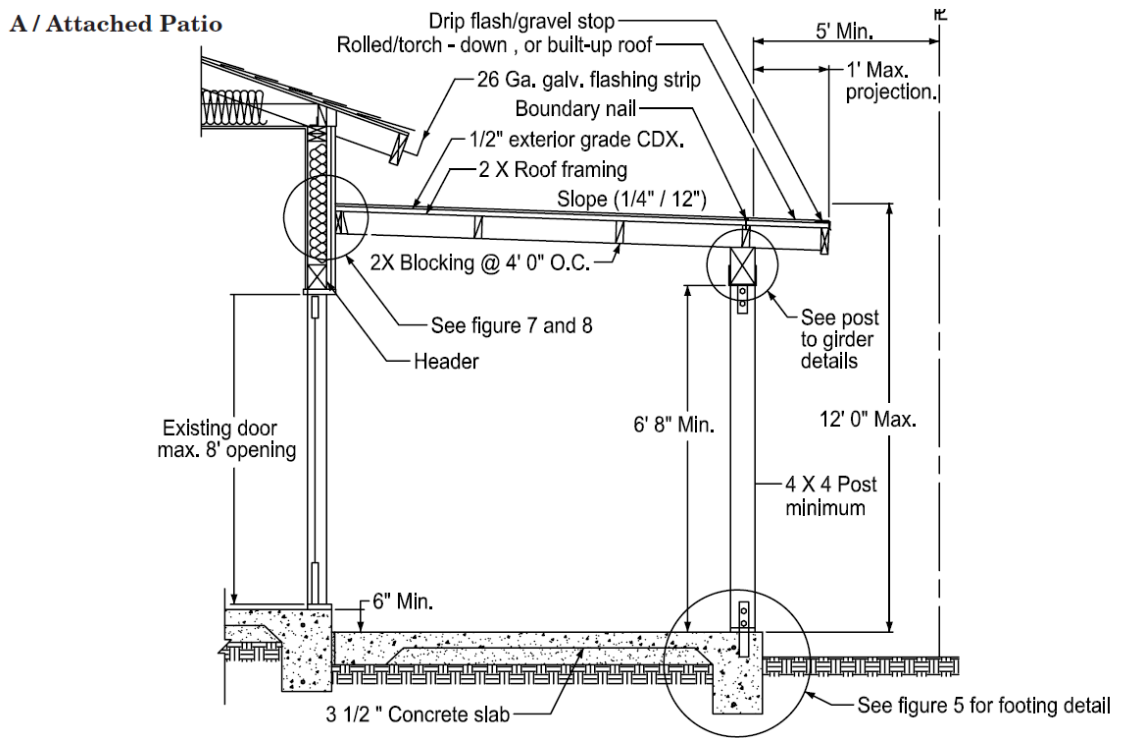


Appendix A2 Isometric view for a typical wooden attached canopy.
Source - <http://www.sandiego.gov/development-services/industry/pdf>

Figure 2 / Typical Patio



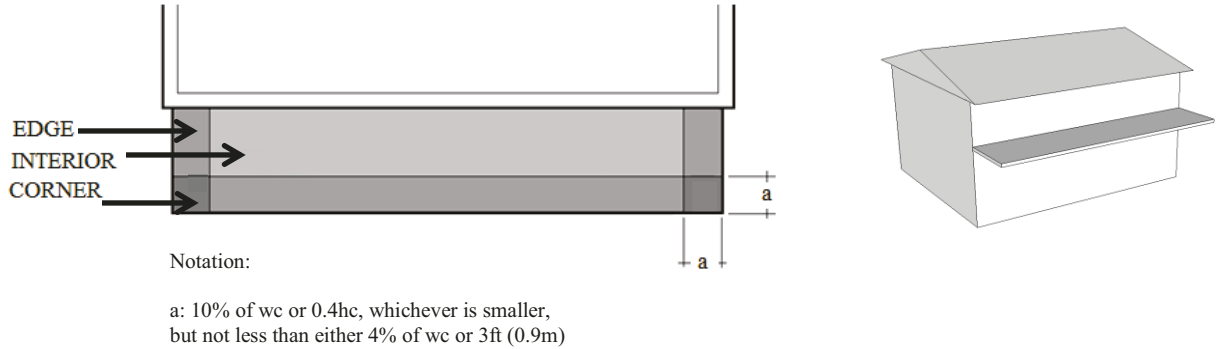
Appendix A3 Construction details for a wooden canopy attached to a low rise building.
 Source – <http://www.sandiego.gov/development-services/industry/pdf>



APPENDIX B

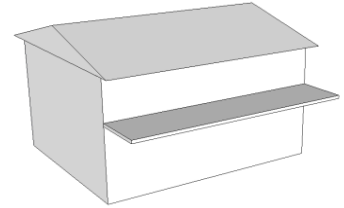
Appendix B1 Tabulated results for local, and area averaged pressure coefficients for all of the configurations studied (see table 3.2), pressure coefficients are referenced to the dynamic velocity pressure based on the hourly mean speed at the mean roof height.

CASE I - Upper surface pressure coefficients by region



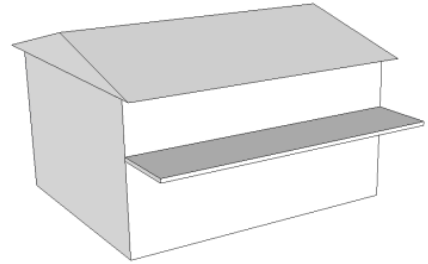
Config.	Peak local pressure coefficient at different regions						Area-Averaged	
	CORNER		EDGE		INTERIOR		ENTIRE SURFACE	
	Min.	Max.	Min.	Max.	Min.	Max.	Min.	Max.
1	-2.20	0.11	-2.35	1.73	-1.29	1.11	-0.99	0.25
2	-1.60	0.02	-1.79	1.32	-1.38	0.90	-1.20	0.23
3	-1.33	0.35	-1.26	0.80			-1.00	0.42
4	-2.45	-0.05	-2.39	0.86	-1.46	1.01	-1.03	0.12
5	-2.23	0.37	-1.96	1.15	-1.77	0.74	-1.14	0.19
6	-1.56	0.19	-1.72	0.72			-1.25	0.33
7	-1.60	0.77	-1.79	1.53	-1.50	1.69	-1.08	0.89
8	-1.46	1.16	-1.91	1.70	-1.69	1.91	-1.15	1.04
9	-1.58	1.51	-1.68	1.87			-1.09	1.21
10	-3.14	0.01	-2.69	1.04	-1.62	1.20	-1.01	0.10
11	-2.49	0.31	-2.17	1.02	-1.82	0.52	-1.18	0.03
12	-2.01	0.08	-1.95	0.43			-1.33	0.09
13	-1.79	0.70	-1.96	1.71	-1.59	1.67	-1.19	0.89
14	-1.81	1.16	-2.09	1.45	-1.95	1.66	-1.30	0.91
15	-1.82	1.47	-1.69	1.72			-1.18	1.09
16	-1.51	0.94	-1.89	1.66	-1.53	1.54	-1.04	0.91
17	-1.64	1.30	-2.16	1.54	-1.78	1.93	-1.05	1.05
18	-1.57	1.53	-1.74	1.55			-1.24	1.08
19	-1.48	0.97	-2.06	1.47	-1.51	1.61	-0.96	0.86
20	-1.52	0.61	-1.64	1.54	-1.75	1.82	-1.11	0.93
21	-1.42	0.77	-1.65	1.41			-1.05	0.80

CASE I - Lower surface pressure coefficients by region



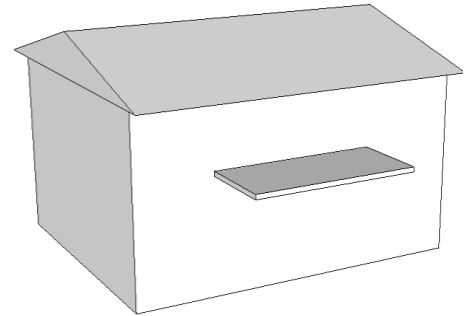
Config.	Peak local pressure coefficient at different regions						Area-Averaged	
	CORNER		EDGE		INTERIOR		ENTIRE SURFACE	
	Min.	Max.	Min.	Max.	Min.	Max.	Min.	Max.
1	-1.66	0.84	-1.68	1.67	-1.16	1.49	-0.89	0.55
2	-1.65	0.71	-2.31	1.27	-1.03	1.49	-0.92	0.54
3	-1.41	0.60	-0.95	0.76			-0.79	0.23
4	-1.58	1.04	-1.61	1.48	-1.52	1.56	-1.04	0.78
5	-1.64	1.49	-1.70	2.11	-1.61	2.14	-1.09	1.30
6	-1.84	1.46	-1.76	1.76			-1.12	0.87
7	-1.58	0.56	-1.47	0.98	-1.19	1.30	-0.84	0.58
8	-1.54	0.86	-1.55	1.26	-1.25	1.35	-0.98	0.71
9	-1.66	1.21	-1.47	1.36			-1.03	0.77
10	-1.35	1.23	-1.43	1.72	-1.68	1.77	-1.00	1.02
11	-1.56	1.58	-1.70	1.83	-1.61	1.83	-1.16	1.21
12	-1.77	1.58	-1.72	1.92			-1.24	0.97
13	-1.49	0.88	-1.75	1.51	-1.56	1.54	-0.98	0.86
14	-1.70	0.97	-1.67	1.44	-1.41	1.50	-1.12	0.80
15	-1.62	1.14	-1.65	1.41			-1.10	0.89
16	-1.40	0.58	-1.43	0.96	-1.11	1.42	-0.83	0.63
17	-1.43	0.75	-2.33	1.10	-1.09	1.34	-0.95	0.67
18	-2.05	0.57	-1.45	1.11			-1.21	0.66
19	-1.05	0.46	-1.24	0.75	-0.85	1.19	-0.84	0.49
20	-1.32	0.64	-1.23	0.79	-0.99	1.21	-0.92	0.38
21	-1.46	0.68	-1.20	0.88			-0.97	0.31

CASE I-Net Pressure coefficients



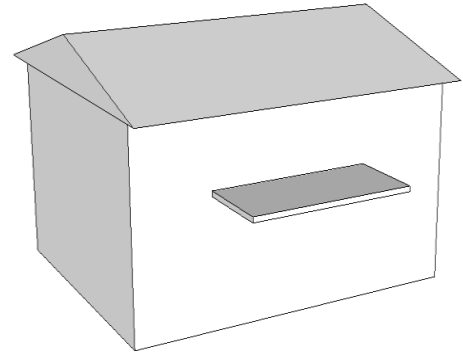
Configuration	Peak Net Pressure coefficient			
	Local		Area-avg.	
	Min.	Max.	Min.	Max.
1	-2.36	1.57	-0.7	0.32
2	-1.36	1.15	-0.59	0.21
3	-1.01	1.43	-0.42	0.47
4	-2.73	1.65	-1.17	0.33
5	-3.06	0.98	-1.73	0.26
6	-2.67	0.98	-1.4	0.37
7	-1.21	1.19	-0.35	0.44
8	-0.84	1.45	-0.35	0.47
9	-0.96	1.1	-0.28	0.51
10	-3.9	1.52	-1.59	0.28
11	-3.5	1.03	-2.22	0.28
12	-2.9	1.12	-1.94	0.33
13	-1.7	1.17	-0.44	0.35
14	-1.37	1.3	-0.37	0.44
15	-1.04	0.89	-0.3	0.47
16	-1.3	1.41	-0.37	0.49
17	-1.29	1.57	-0.35	0.61
18	-0.85	1.44	-0.28	0.82
19	-1.5	1.27	-0.33	0.63
20	-1.03	1.52	-0.28	0.77
21	-0.73	1.73	-0.26	0.98

CASE II-Upper surface pressure coefficients by region



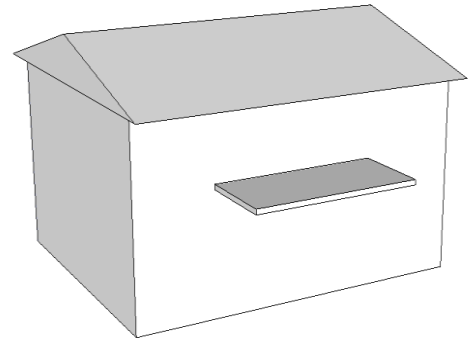
Config.	Peak local pressure coefficient at different regions						Area-Averaged	
	CORNER		EDGE		INTERIOR		ENTIRE SURFACE	
	Min.	Max.	Min.	Max.	Min.	Max.	Min.	Max.
1	-1.66	0.43	-1.57	1.40	-1.38	0.95	-1.29	0.60
2	-1.64	0.72	-1.49	1.44	-1.40	0.87	-1.10	0.24
3	-1.65	1.36	-1.69	1.15			-1.59	1.06
4	-2.15	0.52	-1.84	1.14	-1.39	1.03	-1.30	0.42
5	-1.74	0.71	-1.69	1.00	-1.42	0.73	-1.07	0.21
6	-1.81	1.15	-1.61	0.92			-1.50	0.87
7	-1.81	1.39	-1.92	1.79	-1.56	1.52	-1.53	1.35
8	-1.75	1.60	-1.64	1.76	-1.40	1.75	-1.14	1.53
9	-1.71	1.85	-1.60	1.69			-1.51	1.61
10	-2.11	0.31	-2.05	1.05	-1.35	0.50	-1.05	0.24
11	-1.77	0.52	-1.77	0.82	-1.46	0.46	-1.04	0.21
12	-1.61	0.63	-1.60	0.56			-1.39	0.34
13	-1.68	1.19	-1.57	1.52	-1.21	1.42	-1.15	1.26
14	-1.76	1.65	-1.86	1.71	-1.47	1.80	-1.48	1.59
15	-1.74	1.76	-1.45	1.70			-1.47	1.58
16	-1.43	1.38	-1.62	1.72	-1.36	1.55	-1.14	1.20
17	-1.60	1.43	-1.33	1.52	-1.23	1.67	-1.15	1.22
18	-1.58	1.59	-1.31	1.70			-1.26	1.51
19	-1.57	1.35	-1.73	1.77	-1.77	1.71	-1.27	1.31
20	-1.69	1.83	-1.71	1.88	-1.44	1.77	-1.29	1.48
21	-1.88	1.74	-1.41	1.63			-1.28	1.46

CASE II-Lower surface pressure coefficients by region



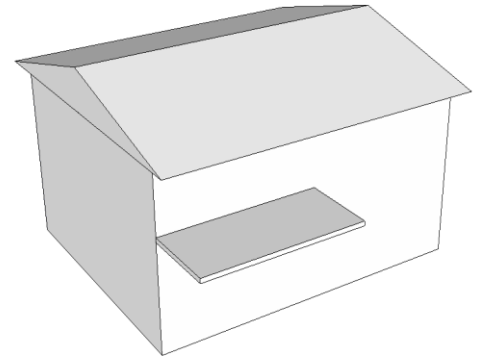
Config.	Peak local pressure coefficient at different regions						Area-Averaged	
	CORNER		EDGE		INTERIOR		ENTIRE SURFACE	
	Min.	Max.	Min.	Max.	Min.	Max.	Min.	Max.
1	-1.57	0.83	-1.41	1.40	-1.27	1.16	-1.25	0.89
2	-1.40	1.05	-1.32	1.41	-1.17	1.16	-1.08	0.77
3	-1.36	1.39	-1.21	1.19			-1.17	1.06
4	-1.99	1.35	-1.97	1.78	-1.46	1.52	-1.32	1.32
5	-1.69	1.65	-1.57	1.84	-1.17	1.66	-1.08	1.18
6	-1.67	1.83	-1.41	1.73			-1.34	1.60
7	-1.89	0.96	-1.80	1.26	-1.24	1.21	-1.26	1.00
8	-1.67	1.16	-1.48	1.28	-1.12	1.29	-0.93	1.18
9	-1.44	1.21	-1.31	1.24			-1.19	1.17
10	-1.59	1.52	-1.65	1.75	-1.50	1.76	-1.23	1.53
11	-1.74	1.69	-1.53	1.75	-1.17	1.75	-1.20	1.54
12	-1.53	1.75	-1.45	1.74			-1.39	1.63
13	-1.84	1.10	-1.39	1.34	-1.24	1.28	-1.12	1.13
14	-1.84	1.44	-1.62	1.53	-1.19	1.53	-1.21	1.41
15	-1.75	1.58	-1.38	1.49			-1.34	1.42
16	-1.77	1.01	-1.41	1.26	-1.07	1.21	-1.04	1.01
17	-1.44	1.04	-1.28	1.12	-1.02	1.18	-1.06	1.06
18	-1.34	1.12	-1.12	1.16			-1.08	1.10
19	-1.80	0.85	-1.82	0.99	-1.08	0.96	-1.08	0.84
20	-1.54	0.87	-1.20	1.13	-1.06	1.16	-1.08	0.92
21	-1.25	0.99	-1.14	0.93			-1.11	0.91

CASE II-Net Pressure coefficients



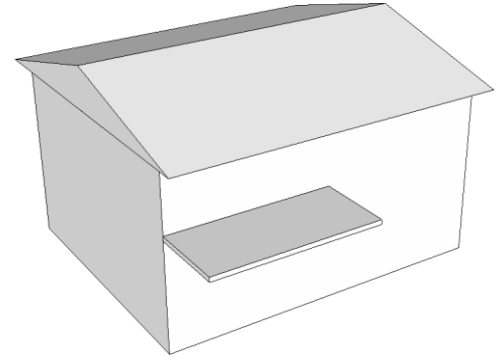
Configuration	Peak Net Pressure coefficient			
	Local		Area-avg.	
	Min.	Max.	Min.	Max.
1	-1.52	2.22	-0.61	0.82
2	-1.41	1.51	-0.82	0.4
3	-0.83	0.68	-0.49	0.37
4	-2.45	2.03	-1.38	0.7
5	-2.93	1.03	-2.34	0.37
6	-2.15	0.63	-1.38	0.35
7	-1.12	1.58	-0.37	0.63
8	-1	1.36	-0.54	0.73
9	-0.88	1.58	-0.51	0.77
10	-2.88	1.15	-1.8	0.42
11	-2.95	1.01	-2.36	0.42
12	-2.62	0.87	-2.01	0.44
13	-1.23	1.15	-0.42	0.4
14	-1.32	1.18	-0.75	0.47
15	-1.09	1.05	-0.49	0.68
16	-1.22	1.88	-0.26	0.49
17	-1.05	1.31	-0.3	0.54
18	-0.75	1.45	-0.4	0.84
19	-1.16	1.64	-0.42	0.73
20	-1.05	1.52	-0.56	0.82
21	-0.94	1.38	-0.47	0.89

CASE III-Upper surface pressure coefficients by region



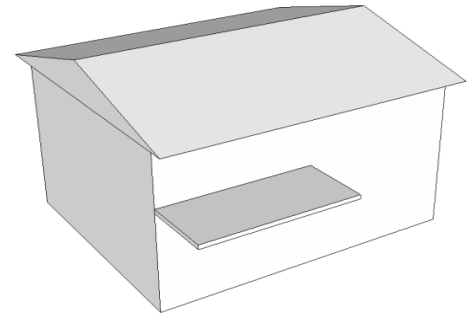
Config.	Peak local pressure coefficient at different regions						Area-Averaged	
	CORNER		EDGE		INTERIOR		ENTIRE SURFACE	
	Min.	Max.	Min.	Max.	Min.	Max.	Min.	Max.
1	-1.48	0.46	-1.64	1.27	-1.32	0.83	-1.07	0.38
2	-1.48	0.71	-1.38	1.23	-1.64	0.99	-1.16	0.48
3	-1.46	1.97	-1.42	1.50	0.00	0.00	-1.41	1.28
4	-1.85	0.53	-1.74	1.24	-1.81	0.70	-1.27	0.35
5	-1.69	0.88	-1.53	1.08	-1.70	0.74	-1.19	0.43
6	-1.54	1.35	-1.66	1.11	0.00	0.00	-1.46	0.87
7	-1.41	1.32	-1.49	1.65	-1.57	1.49	-1.22	1.03
8	-1.43	1.53	-1.47	1.71	-1.67	1.58	-1.16	1.06
9	-1.43	1.62	-1.49	1.60	0.00	0.00	-1.29	1.31
10	-1.83	0.41	-1.93	1.29	-1.78	0.61	-1.13	0.17
11	-1.87	0.48	-1.75	1.93	-1.66	0.34	-1.16	0.07
12	-1.53	1.09	-1.75	0.75	0.00	0.00	-1.54	0.63
13	-1.40	1.36	-1.45	1.63	-1.86	1.52	-1.10	0.95
14	-1.47	1.66	-1.65	1.59	-1.68	1.54	-1.13	1.12
15	-1.58	1.77	-1.68	1.76	0.00	0.00	-1.31	1.49
16	-1.33	1.55	-1.32	1.79	-1.42	1.55	-0.93	1.03
17	-1.32	1.64	-1.36	1.65	-1.57	1.78	-1.02	1.10
18	-1.96	1.74	-2.25	1.38	0.00	0.00	-1.70	1.17
19	-1.41	1.38	-1.41	1.85	-1.52	1.50	-0.97	0.92
20	-1.37	1.49	-1.42	1.63	-1.73	1.76	-1.04	1.11
21	-1.32	1.68	-1.38	1.65	0.00	0.00	-1.12	1.31

CASE III-Lower surface pressure coefficients by region



Config.	Peak local pressure coefficient at different regions						Area-Averaged	
	CORNER		EDGE		INTERIOR		ENTIRE SURFACE	
	Min.	Max.	Min.	Max.	Min.	Max.	Min.	Max.
1	-1.47	0.91	-1.48	1.34	-1.39	1.19	-1.22	0.74
2	-1.21	0.93	-1.22	1.23	-1.02	1.16	-0.99	0.80
3	-1.15	1.36	-1.08	1.31	0.00	0.00	-1.05	1.13
4	-1.58	1.24	-1.39	1.66	-1.59	1.50	-1.16	1.14
5	-1.25	1.69	-1.49	1.81	-1.31	1.79	-1.08	1.51
6	-1.23	1.88	-1.40	1.96	0.00	0.00	-1.18	1.69
7	-1.37	1.02	-1.39	1.19	-1.04	1.06	-1.05	0.81
8	-1.32	0.92	-1.26	1.00	-1.01	0.91	-1.02	0.66
9	-1.32	1.12	-1.17	1.01	0.00	0.00	-1.11	0.77
10	-1.40	1.53	-1.46	1.68	-1.37	1.71	-1.03	1.38
11	-1.42	1.23	-1.29	1.52	-1.28	1.56	-1.08	1.04
12	-1.59	1.84	-1.46	1.86	0.00	0.00	-1.39	1.54
13	-1.51	1.26	-1.64	1.54	-1.66	1.39	-1.26	1.15
14	-1.33	1.27	-1.42	1.45	-1.30	1.29	-1.14	1.10
15	-1.39	1.45	-1.46	1.49	0.00	0.00	-1.26	1.27
16	-1.25	0.86	-1.46	1.17	-1.01	1.17	-0.98	0.75
17	-1.25	0.97	-1.07	1.19	-0.97	1.04	-0.99	0.77
18	-1.48	0.99	-1.49	0.94	0.00	0.00	-1.41	0.75
19	-1.27	0.84	-1.21	0.99	-1.02	0.88	-1.03	0.70
20	-1.18	0.89	-1.07	1.04	-1.01	1.01	-1.03	0.68
21	-1.13	0.95	-1.07	0.72	0.00	0.00	-1.07	0.59

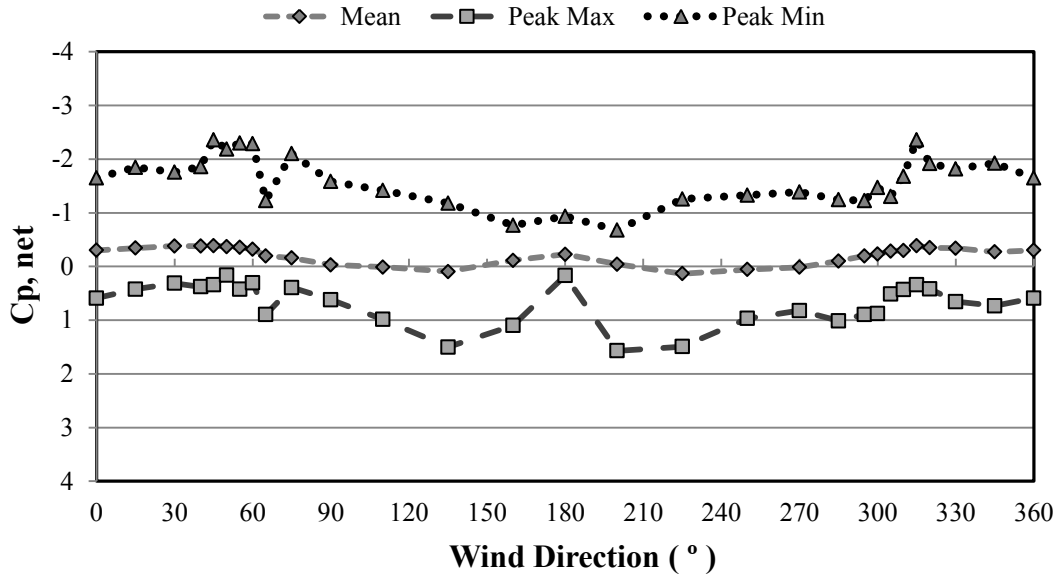
CASE III-Net Pressure coefficients



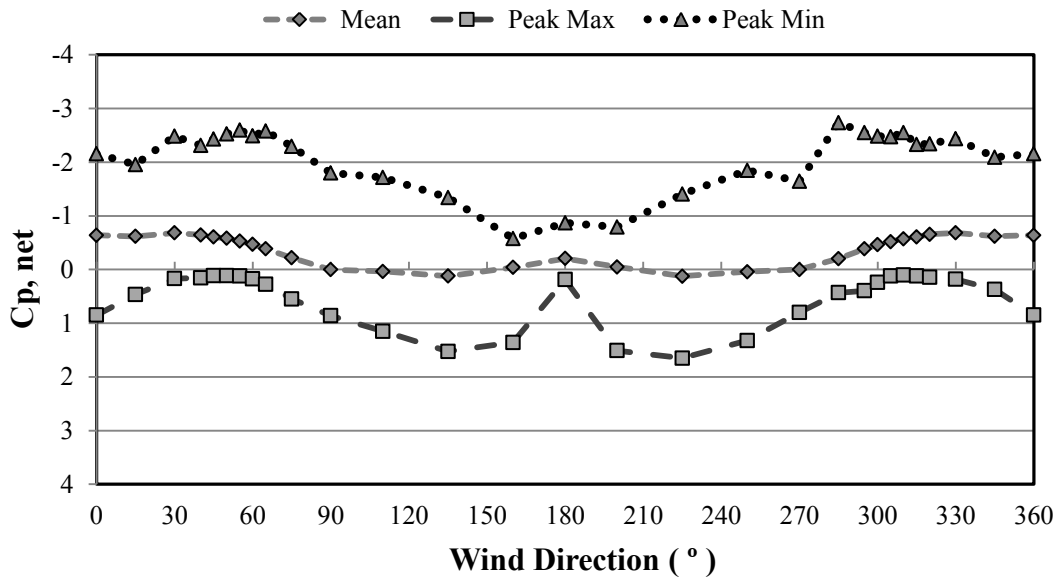
Configuration	Peak Net Pressure coefficient			
	Local		Area-avg.	
	Min.	Max.	Min.	Max.
1	-1.24	1.87	-0.63	0.87
2	-1.29	1.26	-0.8	0.42
3	-0.74	1.02	-0.49	0.84
4	-2.18	1.47	-1.22	0.61
5	-2.24	1.16	-1.54	0.42
6	-1.68	0.54	-1.22	0.26
7	-0.8	1.59	-0.3	0.61
8	-0.87	1.78	-0.37	0.82
9	-0.59	2.06	-0.42	1.08
10	-2.69	1.23	-1.71	0.56
11	-3.02	0.84	-1.9	0.35
12	-2.4	0.66	-1.73	0.23
13	-1.32	1.34	-0.49	0.47
14	-1.3	1.37	-0.54	0.59
15	-0.94	1.2	-0.49	0.8
16	-1.09	1.53	-0.28	0.61
17	-0.95	2.32	-0.33	1.05
18	-0.95	1.61	-0.68	1.36
19	-0.86	1.84	-0.21	0.73
20	-0.95	1.84	-0.26	0.98
21	-0.56	1.73	-0.33	1.15

Appendix B2 Local, mean, and area averaged net pressure coefficients as a function of the wind direction for configurations of each of the three cases (see Table 3.2). Pressure coefficients are referenced to the hourly mean speed at the mean roof height.

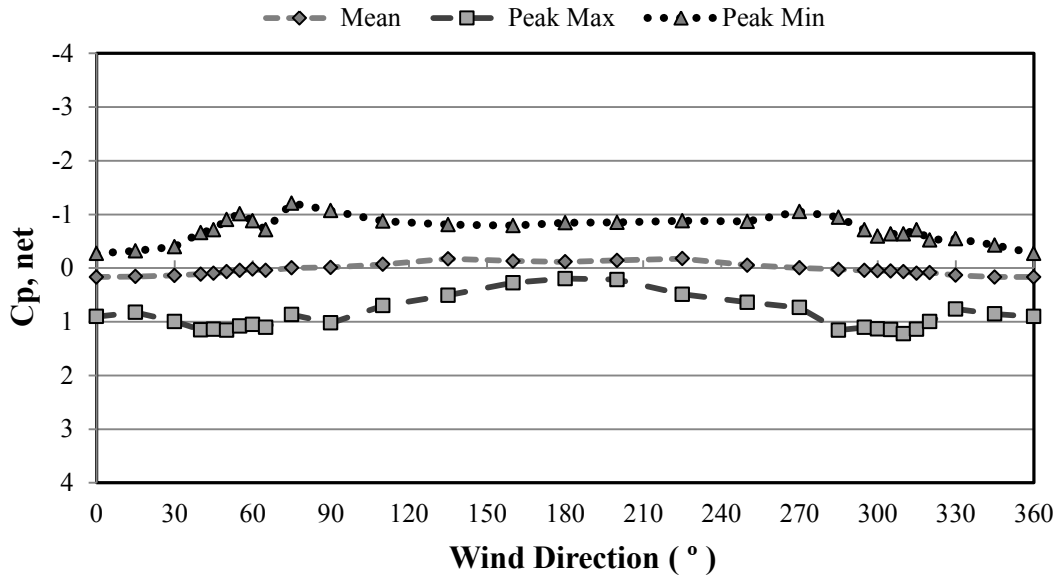
Configuration 1 – CASE I



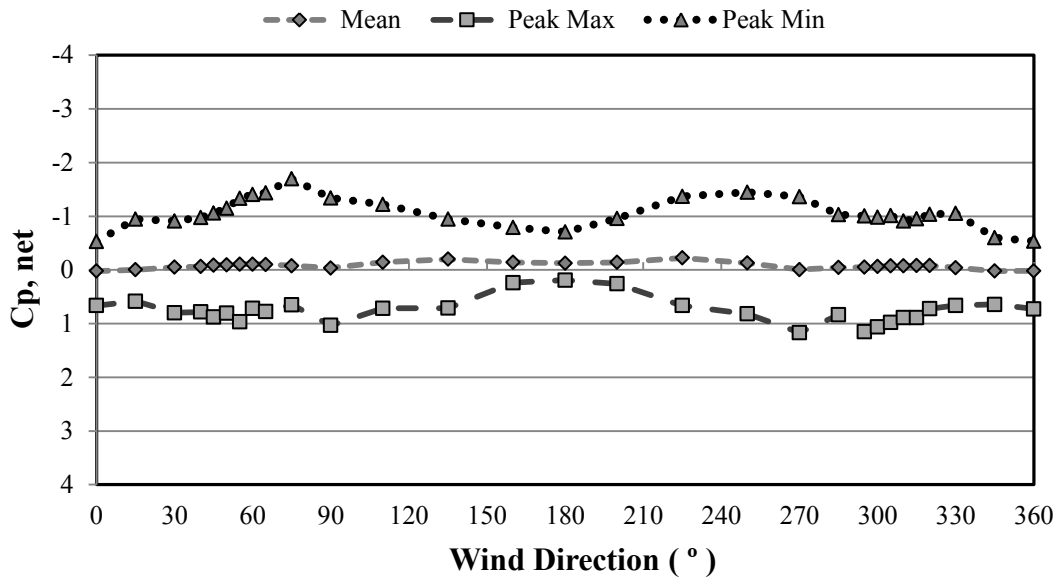
Configuration 4 – CASE I



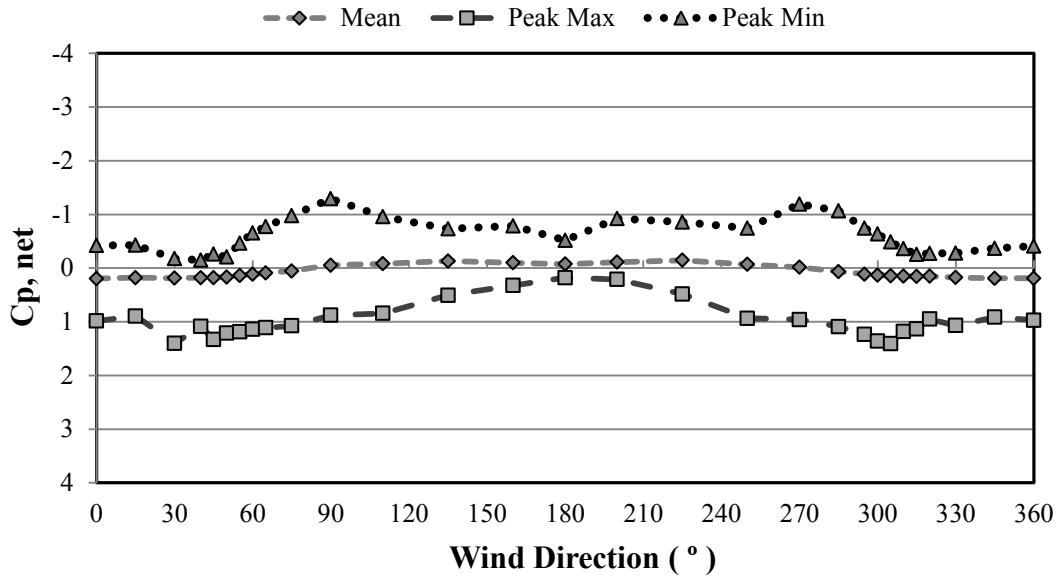
Configuration 7 – CASE I



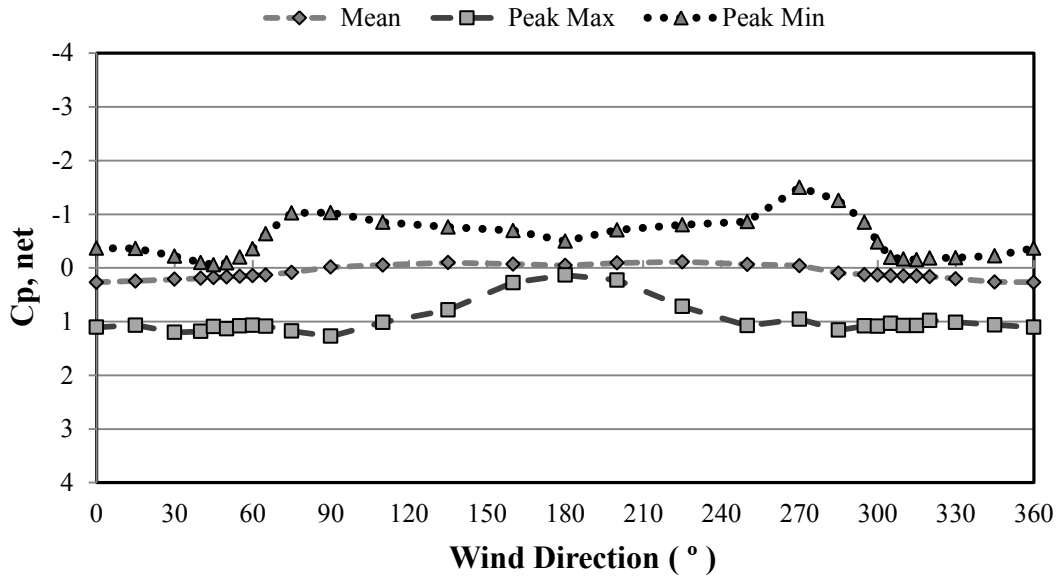
Configuration 13 – CASE I



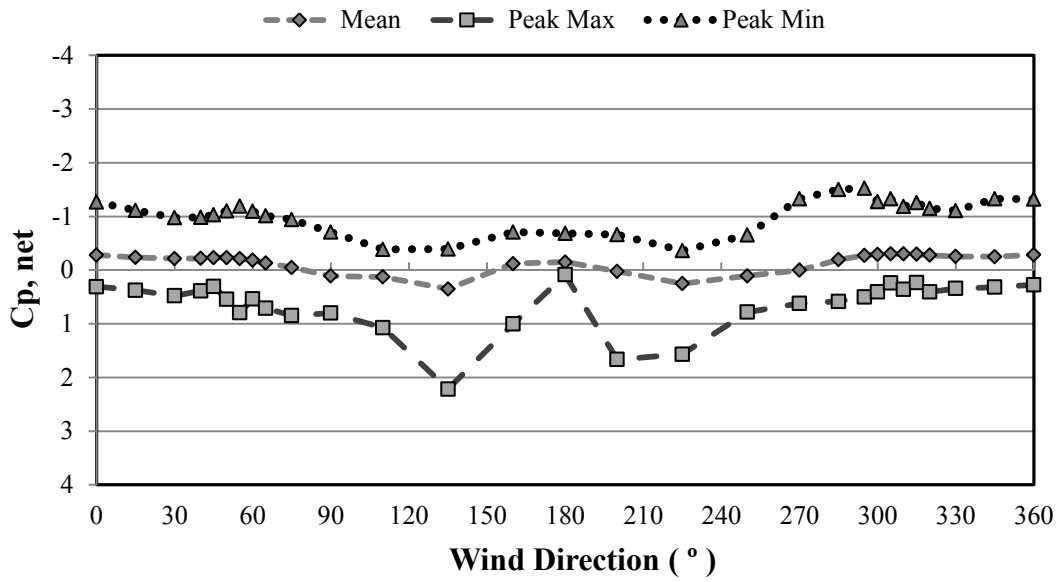
Configuration 16 – CASE I



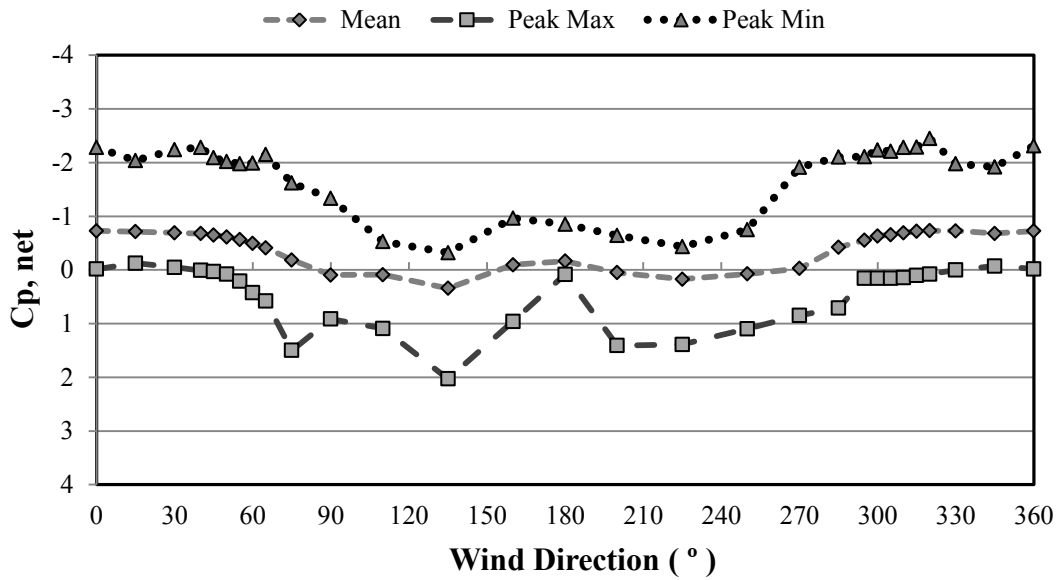
Configuration 19 – CASE I



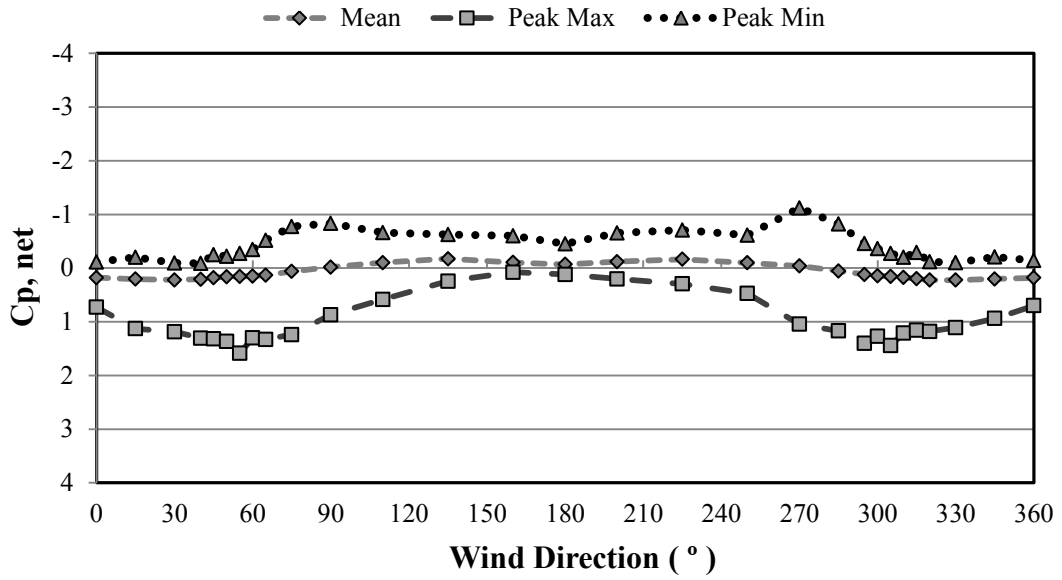
Configuration 1 – CASE II



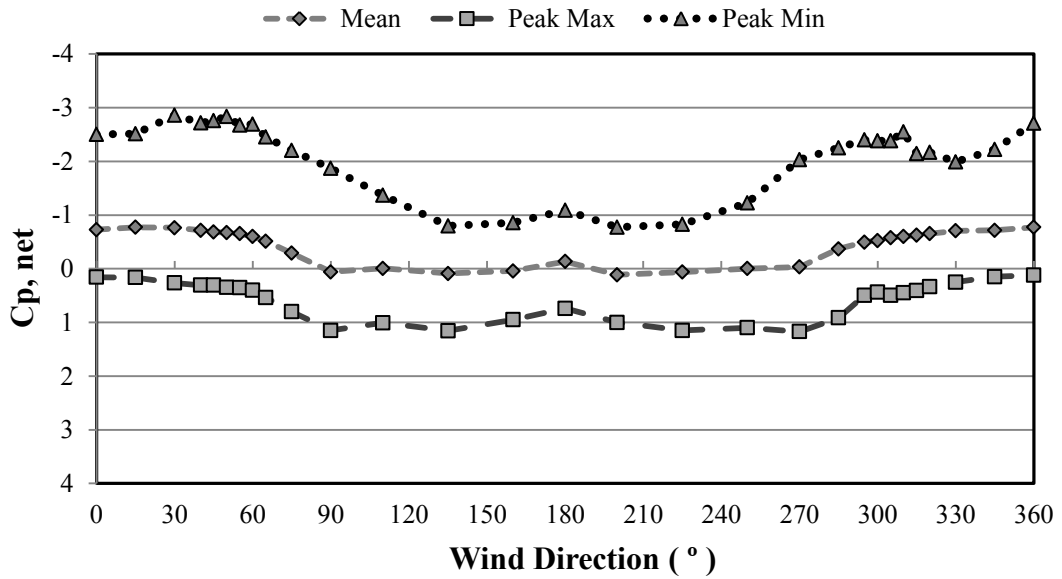
Configuration 4 – CASE II



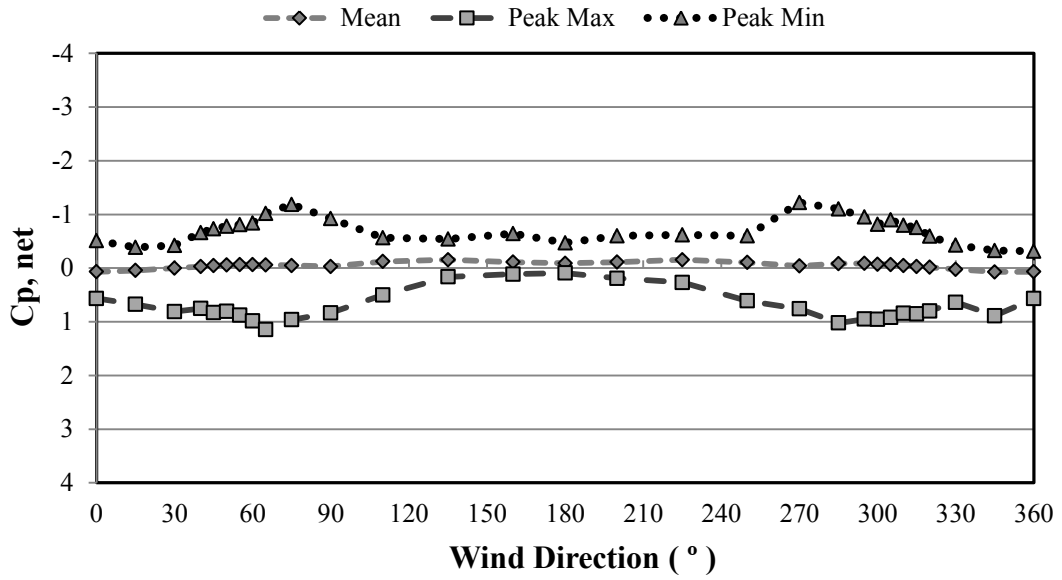
Configuration 7 – CASE II



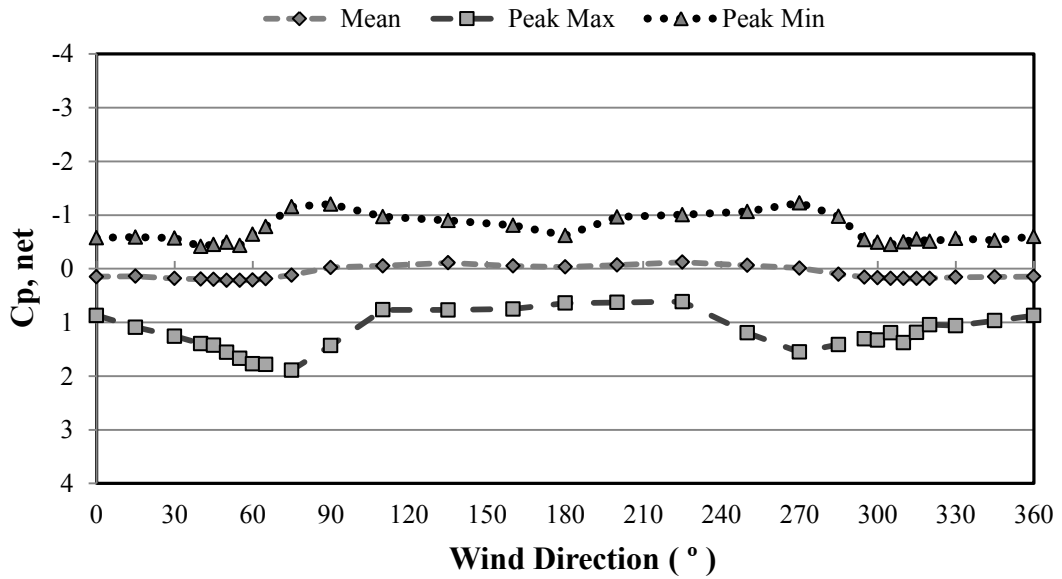
Configuration 10 – CASE II



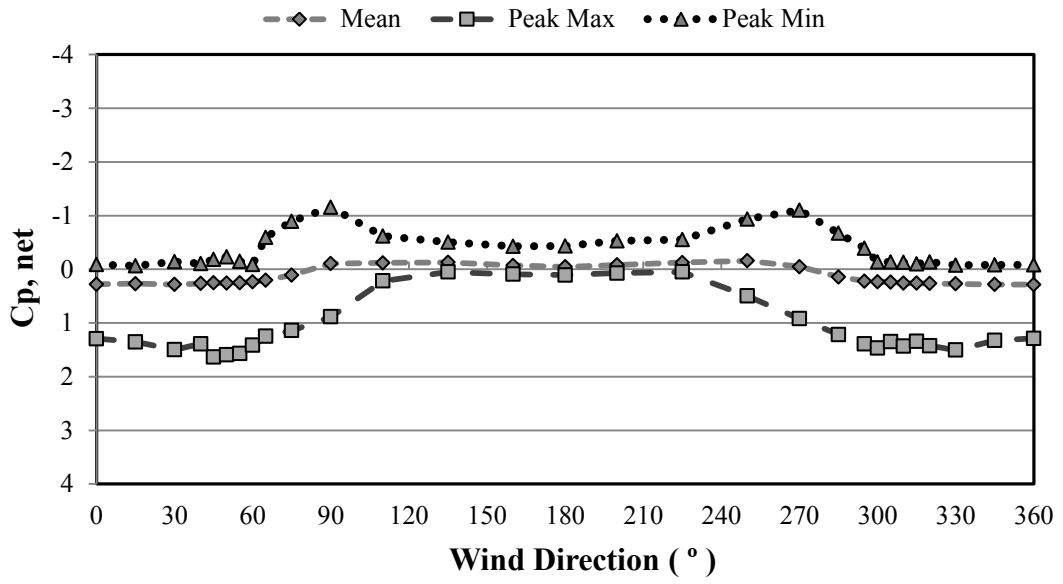
Configuration 13 – CASE II



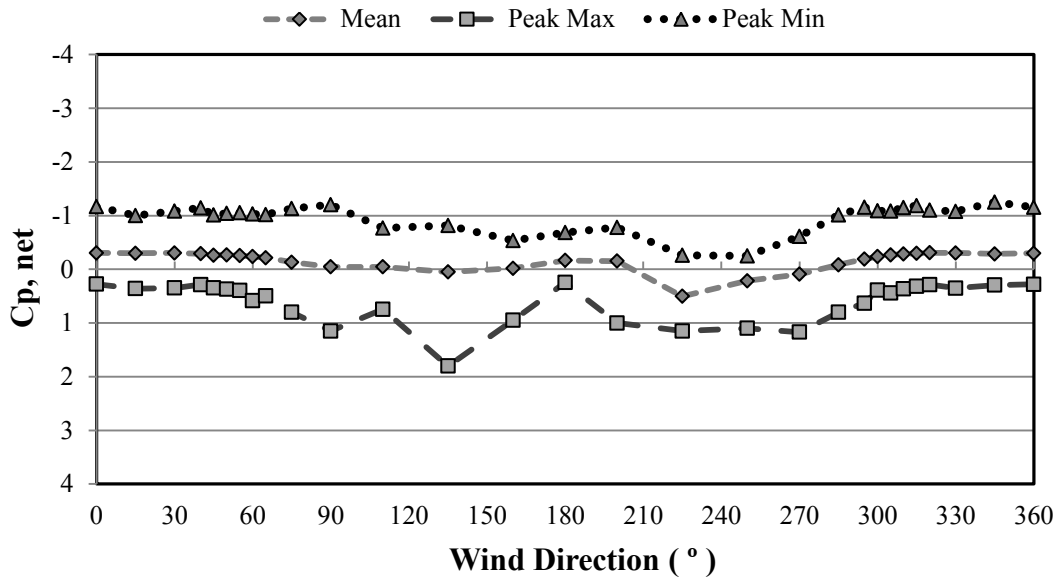
Configuration 16 – CASE II



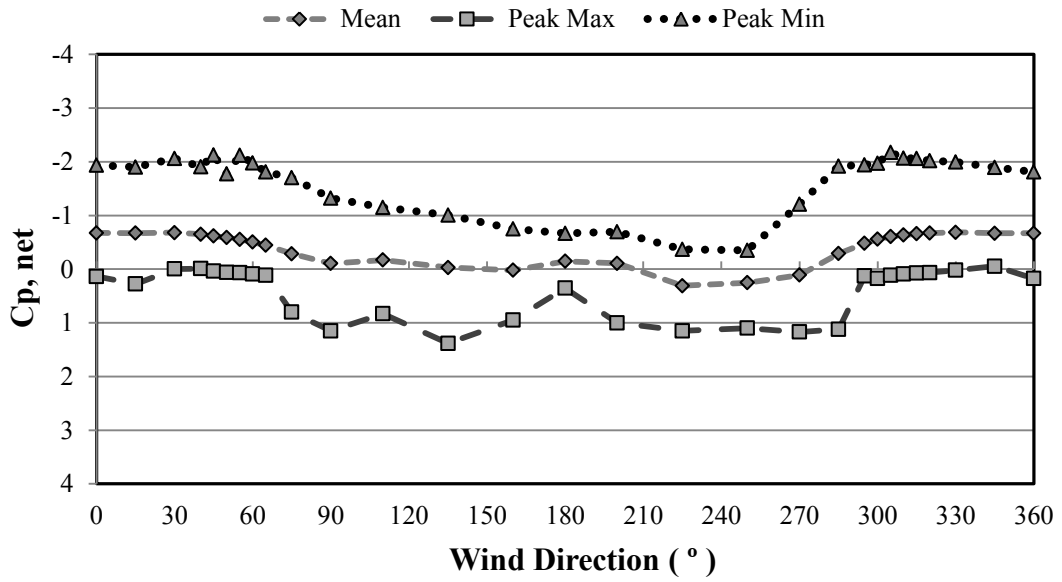
Configuration 19 – CASE II



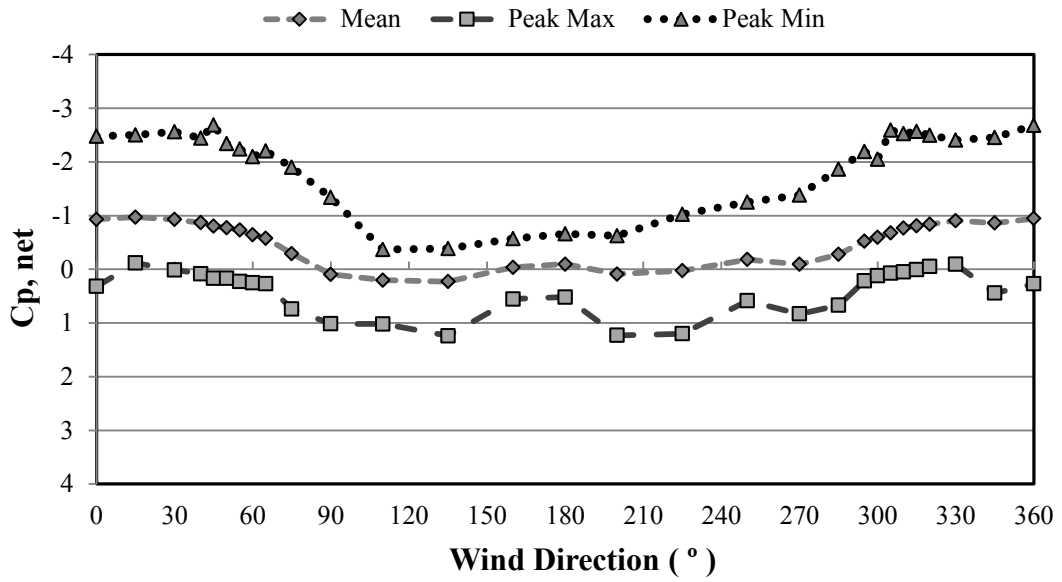
Configuration 1 - CASE III



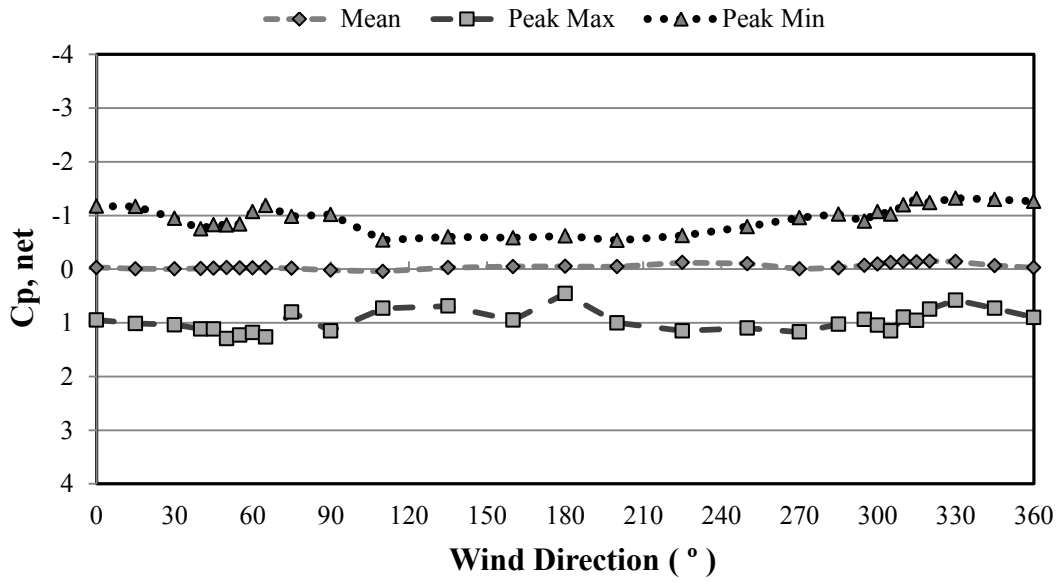
Configuration 4 - CASE III



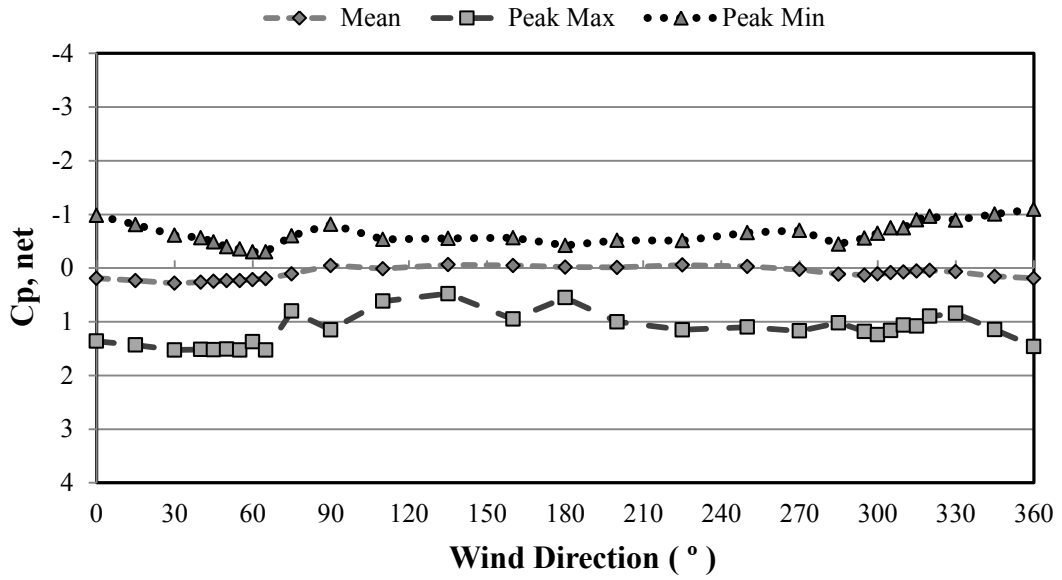
Configuration 10 – CASE III



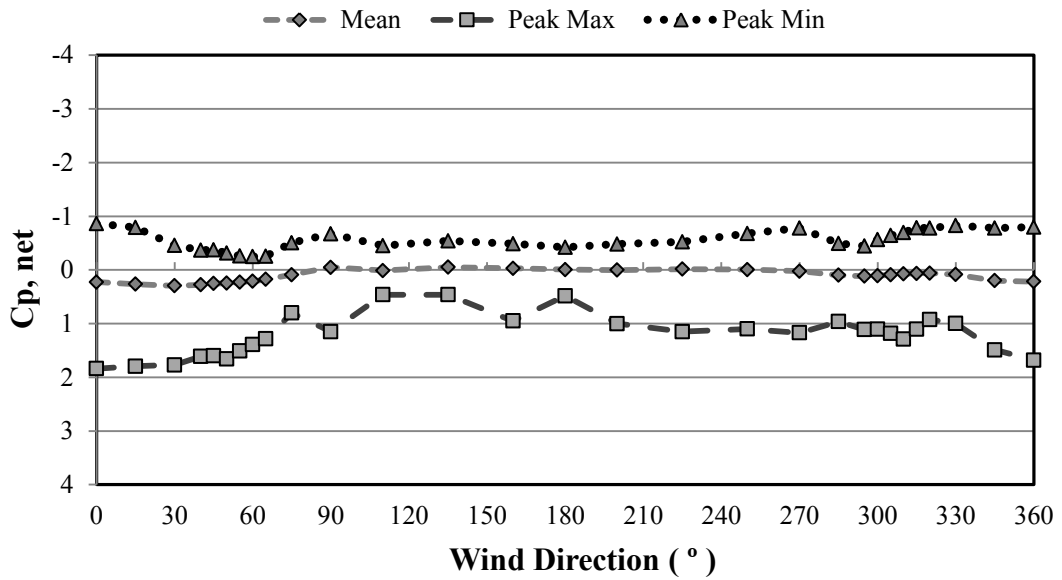
Configuration 13 – CASE III



Configuration 16 – CASE III

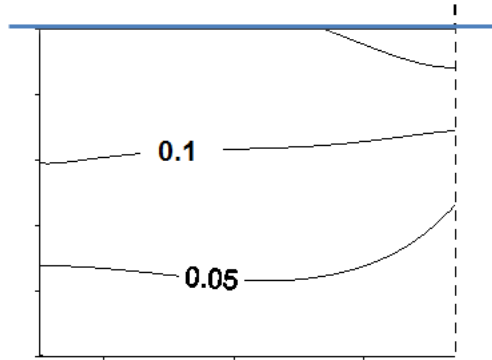


Configuration 19 – CASE III

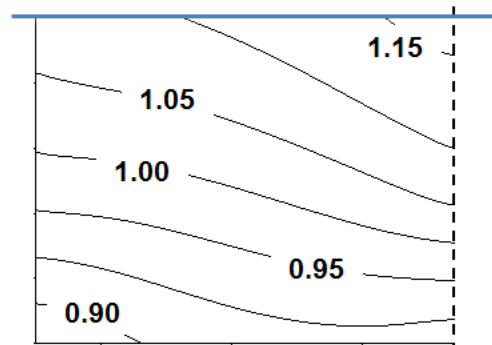


Appendix B3 Upper, lower and net pressure coefficients contour plots for low and intermediate hc/h ratios of Cases II and III (see Table 3.2). Pressure coefficients are referenced to the hourly mean speed at the mean roof height.

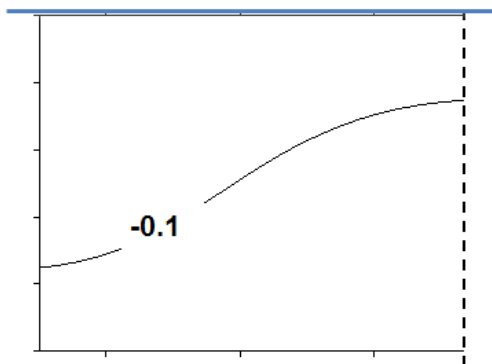
Configuration 7 Case 2 – Zero degree (\perp) wind direction



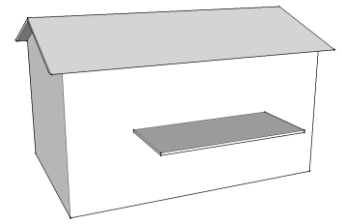
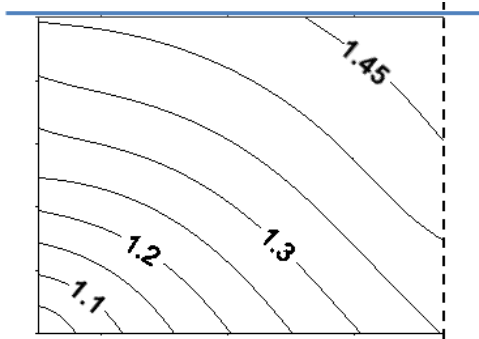
Upper Surface Min. Peaks - $C_{p,upper}$ (min)



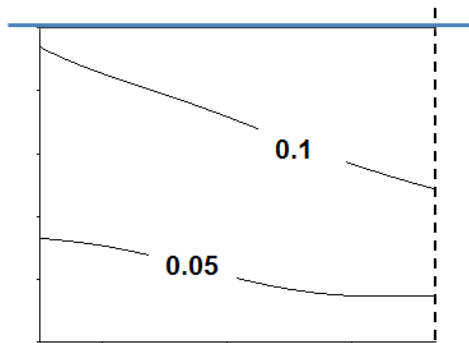
Lower Surface Max. Peaks - $C_{p,lower}$ (max)



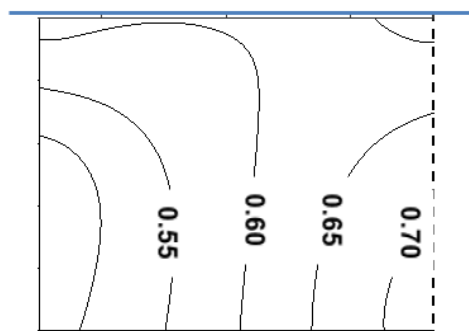
Net Min. Peaks - $C_{p,net}$ (min)



Upper Surface Max. Peaks - $C_{p,upper}$ (max)

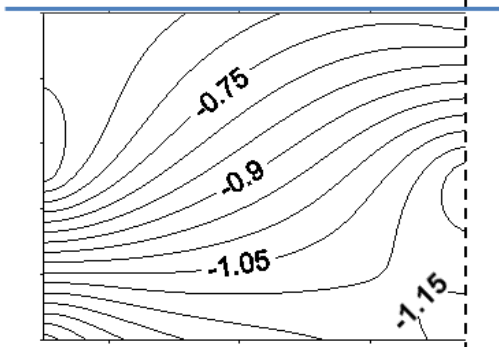
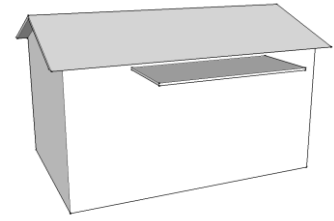


Lower Surface Min. Peaks - $C_{p,lower}$ (min)

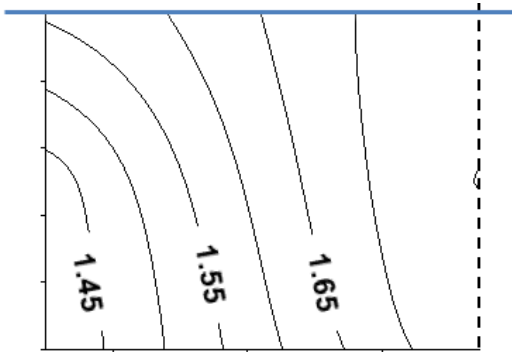


Net Max. Peaks - $C_{p,net}$ (max)

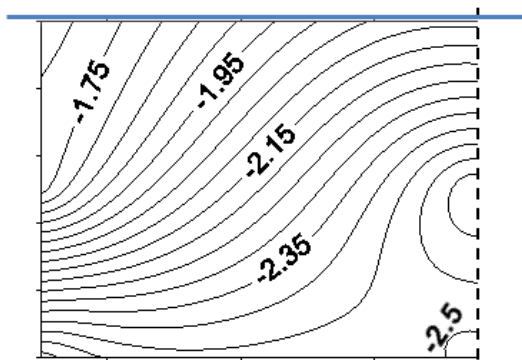
Configuration 10 Case 2 – Zero degree (\perp) wind direction



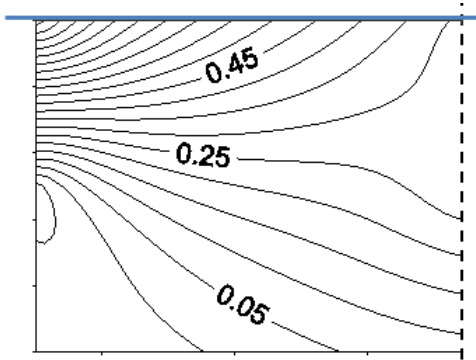
Upper Surface Min. Peaks - $C_{p,upper}$ (min)



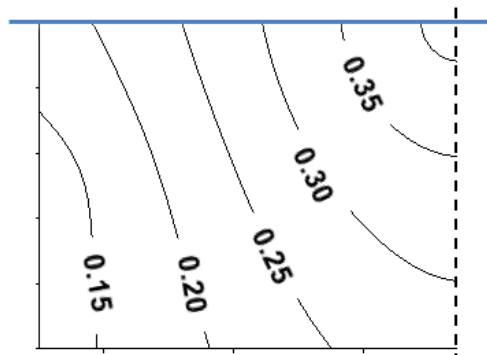
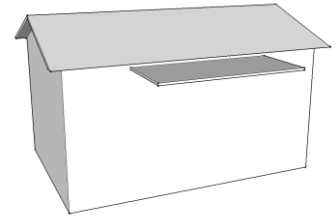
Lower Surface Max. Peaks - $C_{p,lower}$ (max)



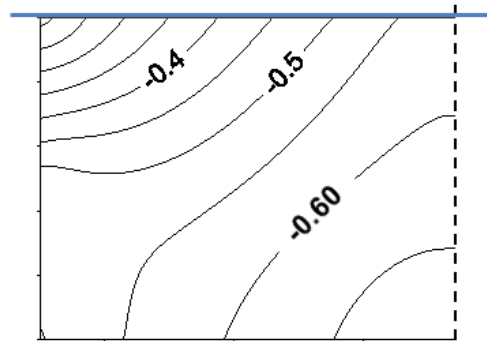
Net Min. Peaks - $C_{p,net}$ (min)



Upper Surface Max. Peaks - $C_{p,upper}$ (max)

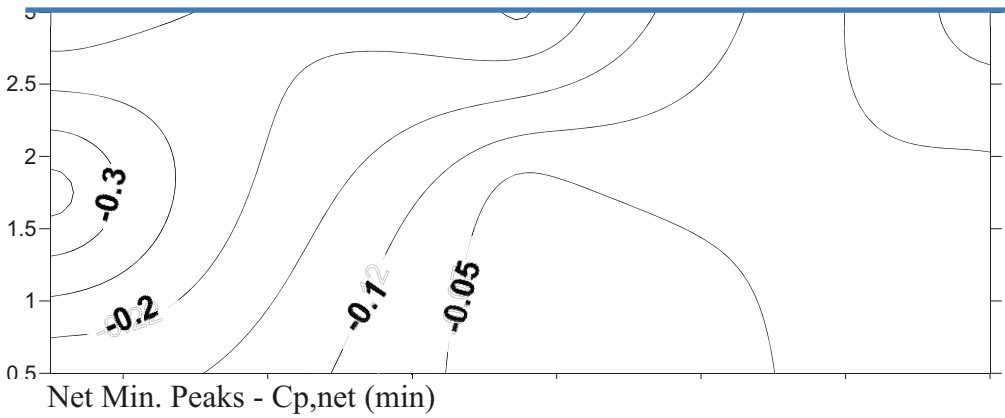
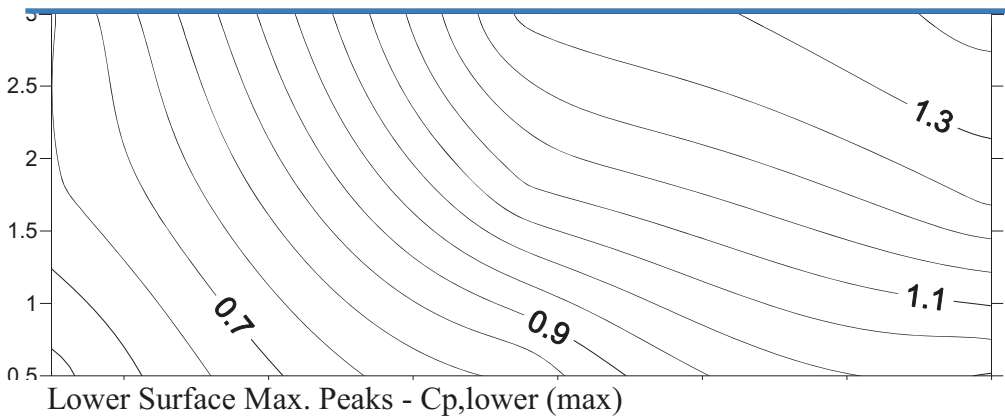
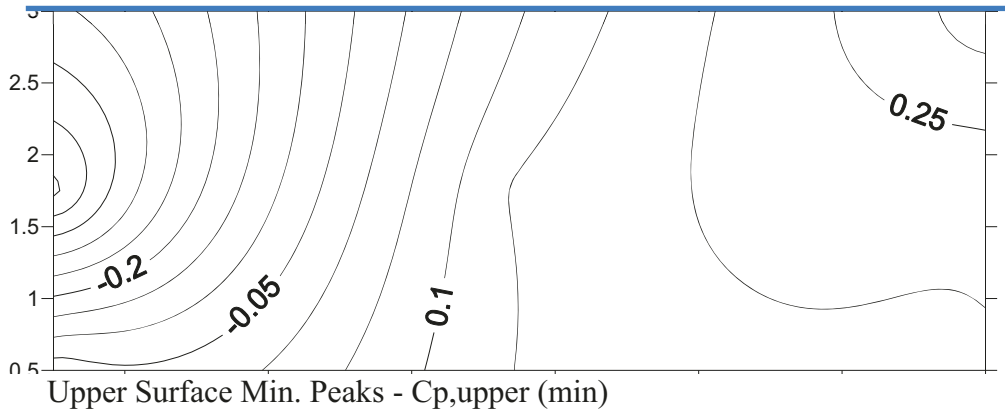
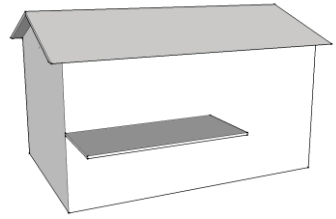


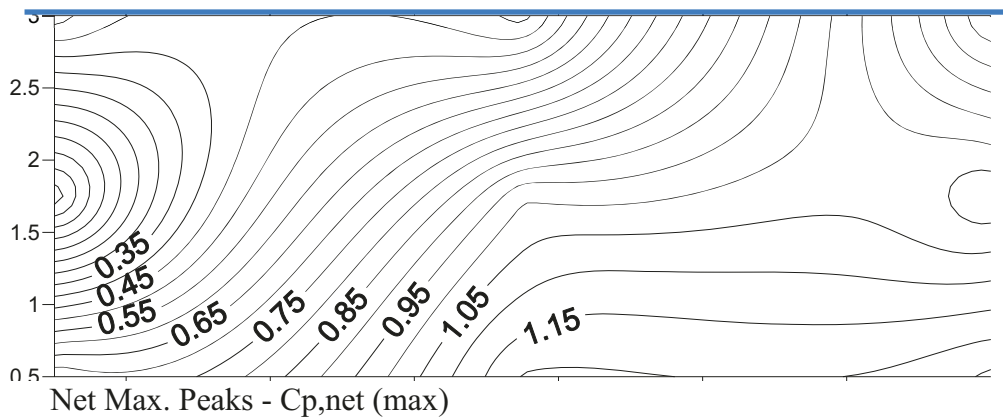
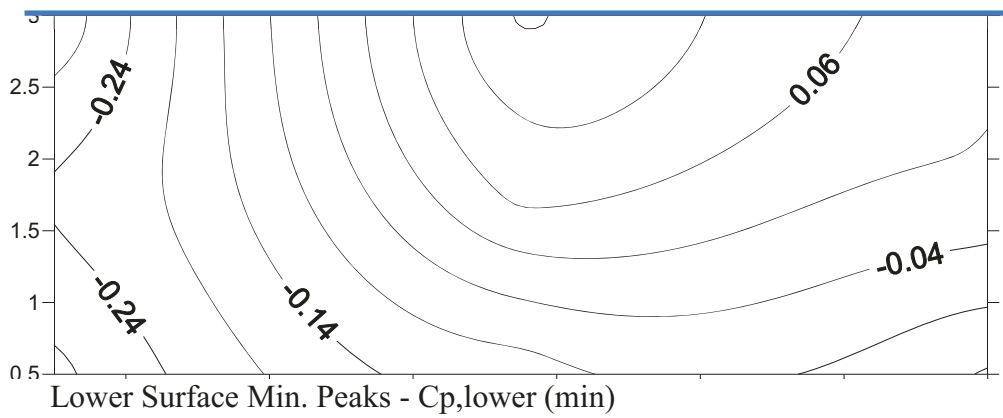
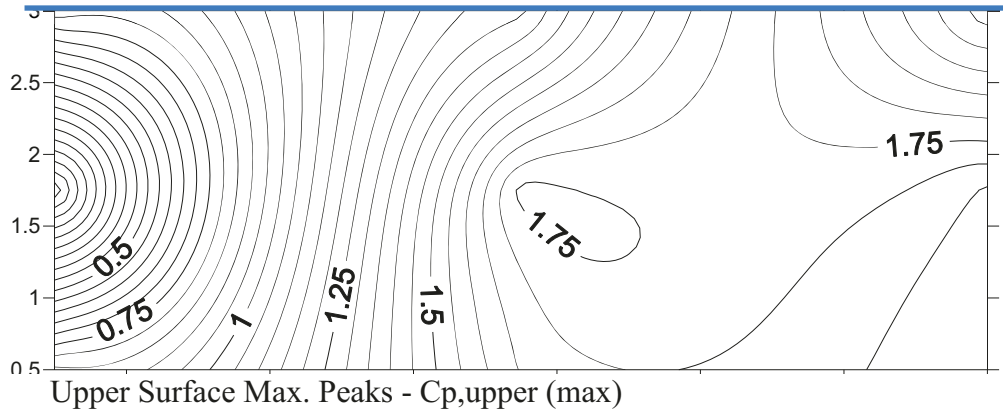
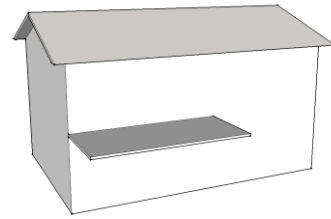
Lower Surface Min. Peaks - $C_{p,lower}$ (min)



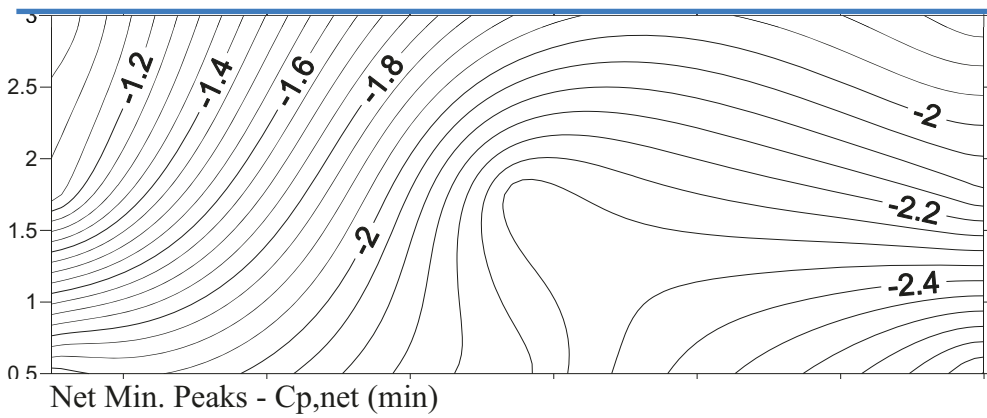
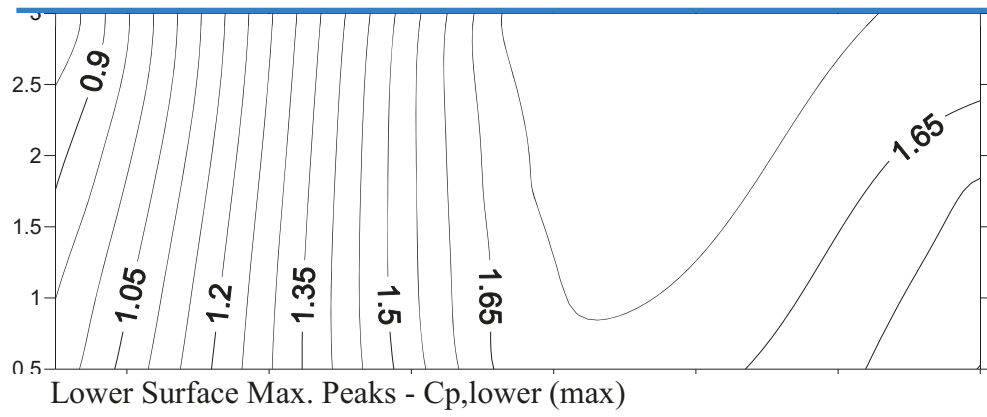
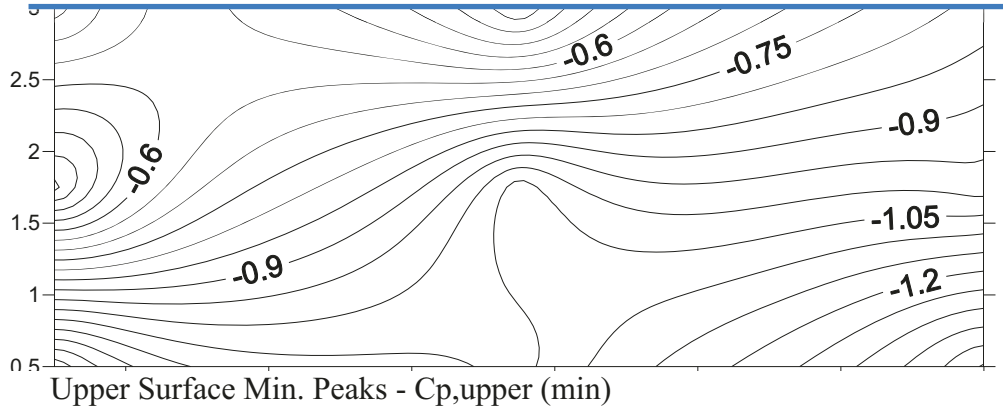
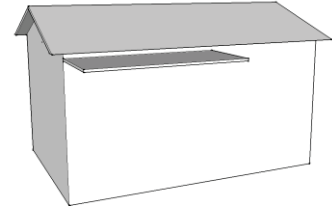
Net Max. Peaks - $C_{p,net}$ (max)

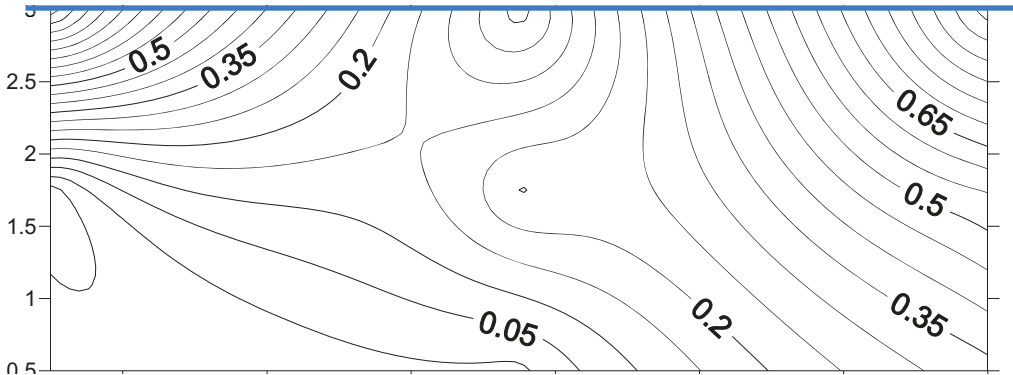
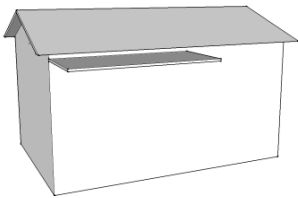
Configuration 7 Case 3 – Zero degree (\perp) wind direction



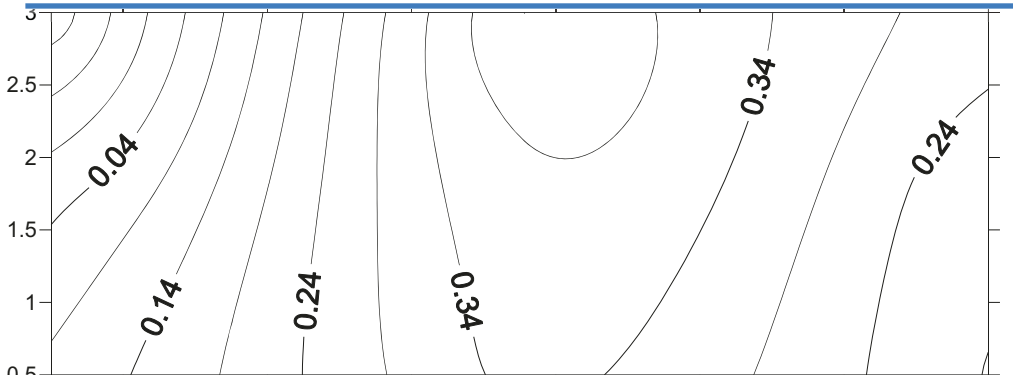


Configuration 10 Case 3 – Zero degree (\perp) wind direction





Upper Surface Max. Peaks - $C_{p,upper} (max)$



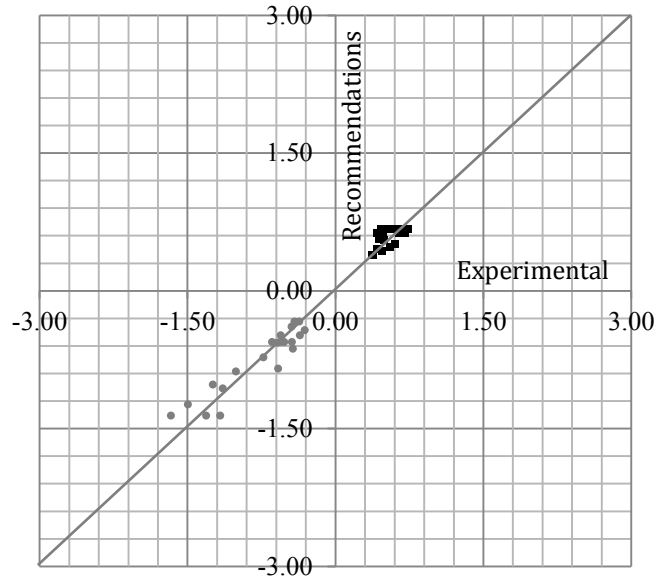
Lower Surface Min. Peaks - $C_{p,lower} (min)$



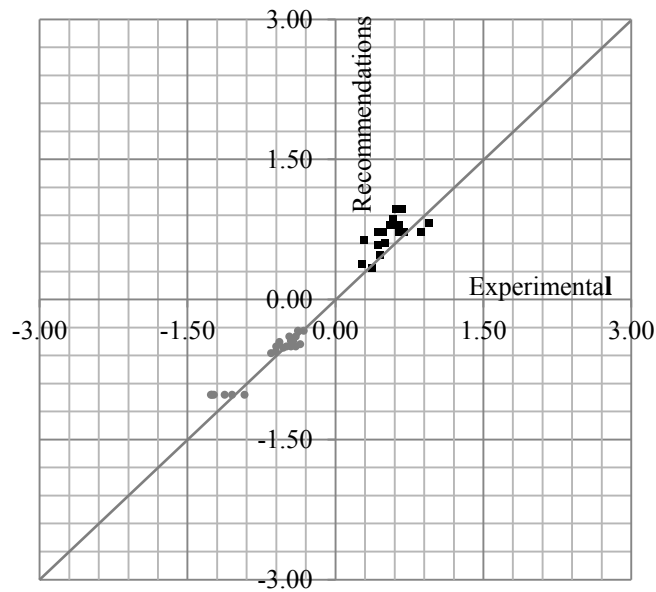
Net Max. Peaks - $C_{p,net} (max)$

APPENDIX C

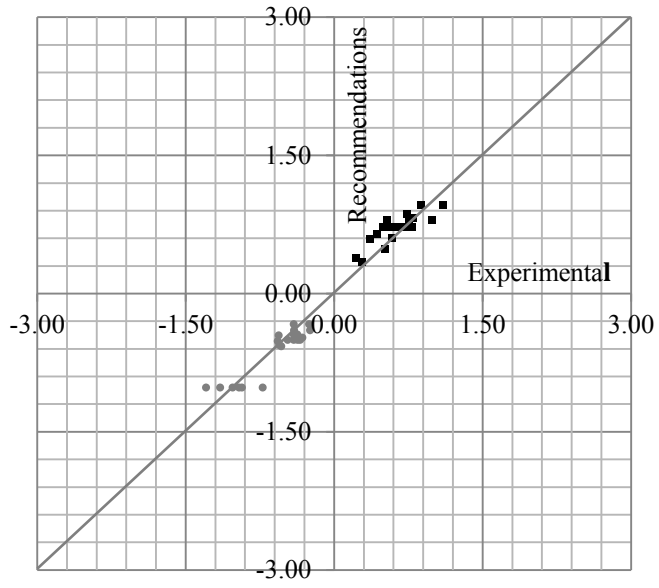
Appendix C1 Comparisons between the experimental results and the recommended design guidelines of the present study, pressure coefficients are referenced to the 3 second wind speed at the mean roof height.



Comparisons with the experimental results of CASE I

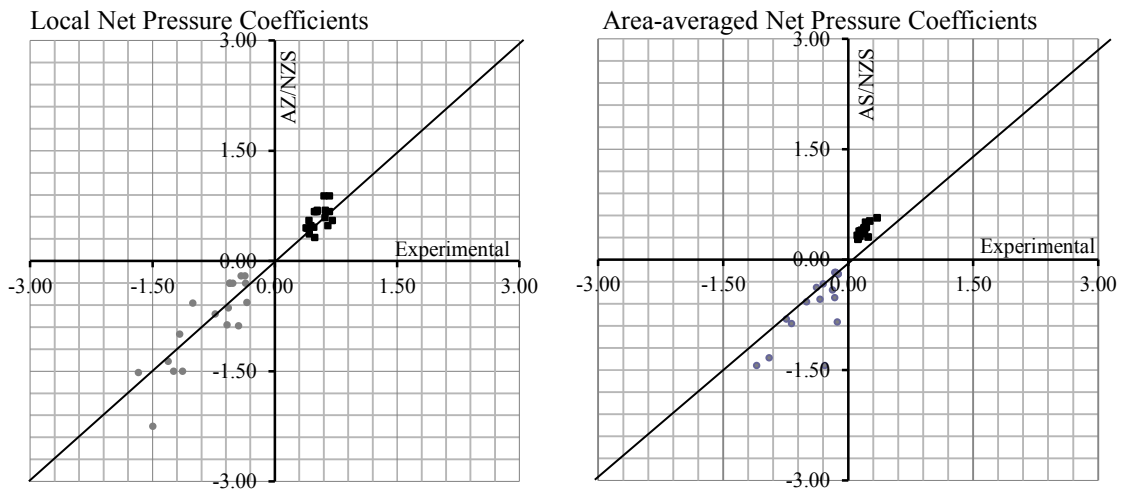


Comparisons with the experimental results of CASE II



Comparisons with the experimental results of CASE III

Appendix C2 Comparisons between the experimental results of the present study and the recommended values of the AS/NZS, pressure coefficients are referenced to the 3 second wind speed at the mean roof height.



Appendix C3 Comparisons between the experimental results of the present study and the recommended values of the DIN, pressure coefficients are referenced to the 3 second wind speed at the mean roof height.

